BOKU
University of Natural Resources & Life Sciences
Department of Chemistry
Division of Protein Biochemistry
Christian Doppler Laboratory for Antibody Engineering

Enlightening the Fcab-antigen interaction via X-ray crystallography and biochemical studies

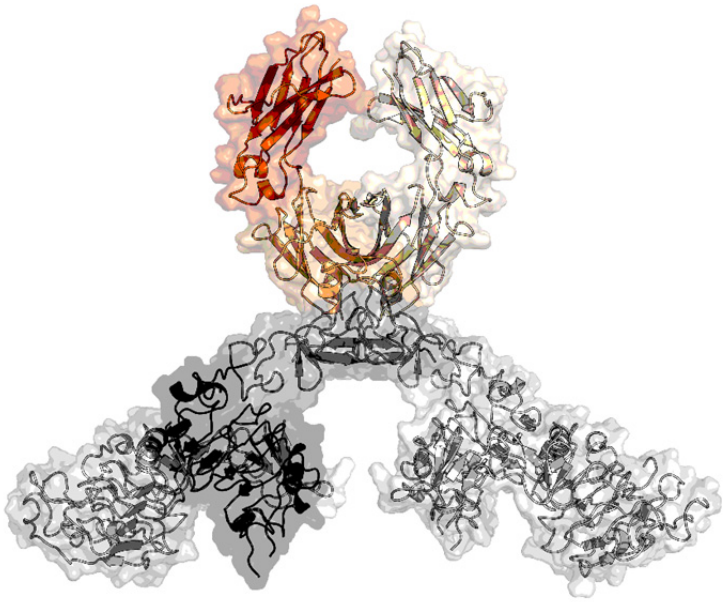

Ph.D. thesis

Dipl.-Ing. Elisabeth Lobner

Vienna, June 2017

Supervisor
Univ.Prof. Dr. Christian Obinger

I rarely plan my research; it plans me.

Max Ferdinand Perutz

ACKNOWLEDGEMENTS

I would like to express my deepest gratitude to the many people who have accompanied me on this 4-year journey. All of you greatly contributed to the completion of this thesis and I am very grateful for your many-faceted support during this challenging, educational and inspiring time. Many of my colleagues have become dear friends, above all Irene Schaffner, my "BOKU-twin"- I appreciate the time we spend together very much.

First and foremost, I would like to thank Christian Obinger for supervising my thesis and providing scientific input whenever needed – as well as fun and inspiration in my daily work at the institute. I also want to thank Christa Jakopitsch, my BioToP coordinator and travel buddy for all the inspiring moments we shared during our professional and private journies. Special thanks goes out to my three great students Kathrin Göritzer, Michael Kitzmüller and Konstantin Kubinger for their constant and committed support of my work. Michael's untimely passing away was a huge loss, both personal as well as professional, for everyone who knew him.

For the indispensable help in determination of the crystal structures I would like to thank Anne-Sophie Humm and Georg Mlynek from the Max F. Perutz Laboratories. Furthermore, I would like to acknowledge Michael Traxlmayr who has been a constant source of expertise and friendship during most of my study time.

Last but definitely not least I want to sincerely thank my family – my parents and my sister Eva-Maria – who have always supported me despite the fact that my career at the interface of biology and chemistry came as a surprise to them.

Thank you, Alex for your patience, inspiration and loving support.

ABSTRACT

To date, monoclonal antibodies have proven to be the most promising class of therapeutic molecules. An antibody can be dissected into its two Fab (fragment antigen binding) arms and the Fc (fragment crystallizable) part that activates the immune system and is responsible for the long *in vivo* half life. Besides a substantial amount of full-size immunoglobulin G molecules, various antibody fragments and Fc-fusion proteins have been approved for the biopharmaceutical market. Thus, the Fc protein represents an attractive scaffold for engineering therapeutic molecules as could be demonstrated in the generation of Fcabs (Fc domain with antigen-binding sites). By engineering of the C-terminal loops (AB, CD and EF loop) in the CH3 domains two antigen binding sites can be inserted in close proximity.

The present study determines the first X-ray structures of four Fcabs that differ in loop design, specificity, affinity and stability and reveals their overall structural integrity and native fold. The first Fcab-antigen pairs include the HER2-binding Fcab H10-03-6 and its stabilized version STAB19. Their diverging biophysical behavior can be attributed to differences in the EF loop conformations. Furthermore, the Fcab-HER2 complex structures give insights into the binding interface and together with analyses by ITC, SEC-MALS and FCS we could demonstrate that one homodimeric Fcab binds two HER2 molecules in a negative cooperative binding mode.

The second Fcab-antigen pairs encompass the VEGF-binding Fcab 448 and its affinity matured variant CT6. Just like the Fcab, VEGF is a homodimeric molecule, thus the interaction partners polymerize upon mixing in solution. Therefore, a heterodimeric Fcab (JanusFcab) consisting of one VEGF-binding Fcab chain and one non-binding Fc-wt chain was constructed resulting in distinct 2:1 (JanusFcab:VEGF) complexes. This heterodimeric format allowed the elucidation of the 2.2 Å complex structure and further biochemical investigations.

KURZFASSUNG

Bis heute zählen monoklonale Antiköper als die vielversprechendste Klasse von therapeutischen Molekülen. Das Immunoglobulin der Klasse G besteht aus zwei Fab (Antigen-bindendes Fragment) Armen sowie einem Fc (kristallisierbares Fragment) Teil, der die Fähigkeit zur Aktivierung des Immunsystems besitzt und für die lange *in vivo* Halbwertszeit verantwortlich ist. Der Fc Teil stellt somit einen interessanten Baustein dar, um therapeutische Moleküle zu engineeren wie am Bespiel von Fcabs (Antigen-bindendes Fc Fragment) gezeigt werden konnte. Durch Engineering der C-terminalen Loops (AB, CD und EF loop) in der CH3 Domäne können zwei nah beieinander liegende Antigen-Bindungsstellen erzeugt werden.

In der vorliegenden Arbeit wurden die ersten Röntgenkristallstrukturen von Fcabs, die sich hinsichtlich ihres Loop Designs, ihrer Spezifität und Affinität sowie ihrer Stabilität unterscheiden, aufgelöst und dadurch konnte gezeigt werden, dass die typische Immunglobulin-Domänenstruktur erhalten bleibt. Die ersten, untersuchten Fcab-Antigen Paare inkludieren den HER2-bindenden Fcab H10-03-6 und seine stabilisierte Version STAB19. Die unterschiedlichen biophysikalischen Eigenschaften konnten einer unterschiedlichen EF Loop Konformation zugeordnet werden. Darüber hinaus, konnte durch Aufklärung der Komplexkristallstrukturen und biochemischen Analysen mittels ITC, SEC-MALS und FCS ein negativ-kooperatives Bindungsverhalten gezeigt werden.

Die zweiten Fcab-Antigen Paare umfassen den VEGF-bindenden Fcab 448 und seine affinitätsgereifte Version CT6. VEGF ist, genauso wie das Fcab, ein homodimeres Molekül. Dadurch bilden die beiden Interaktionspartner Polymerketten. Deswegen wurde ein heterodimeres Fcab (JanusFcab) bestehend aus einer VEGF-bindenden Fcab Kette und einer nicht-bindenden Fc-wt Kette gebaut. Dies ermöglichte die Bestimmung der 2:1 (JanusFcab:VEGF) Komplexstruktur bei 2.2 Å und der Thermodynamik der Protein-Protein Interaktion.

TABLE OF CONTENTS

1 INTDRODUCTION

Getting the antibody into shape

The typical Y shape of antibodies is probably the most popular protein structure known to date. Already several decades ago, scientists were eager to gain structural information on these proteins recognizing unique patterns of antigens. From 1959 on, this problem was addressed by R. R. Porter and G. M. Edelman by just splitting the immunoglobulin (Ig). By means of chemical and enzymatic treatment they divided the antibody into smaller pieces followed by physicochemical characterization. These pieces were not only identified as light (L) and heavy (H) chains but also as Fab (fragment antigen-binding) due to its retained ability for antigen binding and Fc (crystallizable fragment) which was not able to bind antigens but readily crystallized to diamond-shaped plates (Edelman and Poulik, 1961; Porter, 1959). Ten years later Edelman succeeded in the accurate depiction of the chemical structure of antibodies only based on the amino acid sequence of human γG1 immunoglobulin and a large amount of biochemical data that were published by then (Figure 1) (Edelman et al., 1969). Finally, this model was fully validated by determination of the first crystal structure of a full-length human IgG1 at 6 Å resolution showing the typical shape through the molecular boundary (Sarma et al., 1971). In 1977, E. W. Silverton and colleagues used this low resolution electron density map together with a computational approach for generation of a quaternary structure of this antibody (Figure 1)

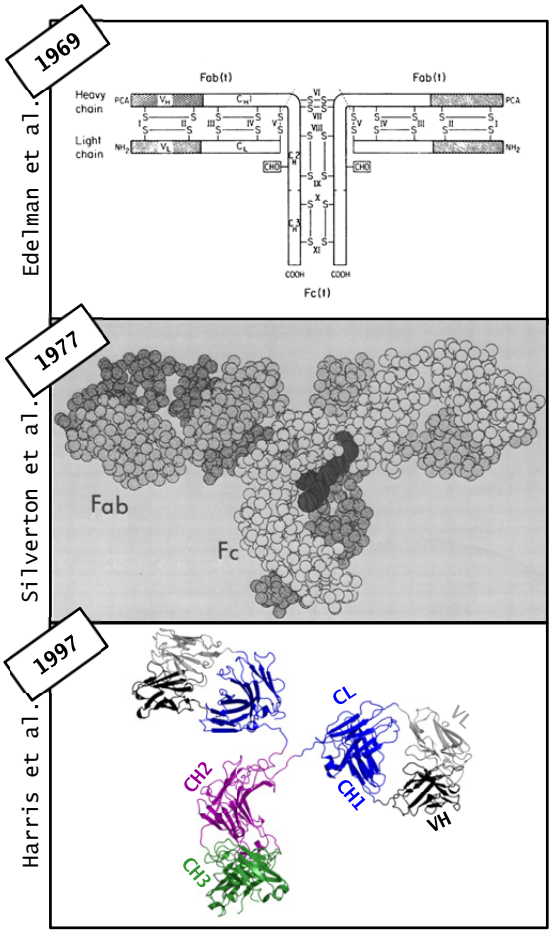

Figure 1. Investigation of the antibody structure over time.

(Silverton et al., 1977). Beside a wealth of 3D structures of different Fabs and Fcs, the first high resolution structure (2.8 Å) of an intact IgG2a antibody (PDB: 1IGT) was solved in 1996 and allows elucidation down to the atomic-level (Figure 1) (Harris et al., 1997). In 1972, Edelman and Porter were awarded with the Nobel Prize in Physiology or Medicine *"for their discoveries concerning the chemical structure of antibodies"* (Ribatti, 2015).

The rise of the antibody

Since then, the antibody made a rapid development towards therapeutic molecule. To date, more than 60 antibodies or antibody-based products including ADCs (antibody-drug conjugates), bispecific antibodies and Fabs for the treatment of various diseases such as cancer, infections and immune disorders, are approved for clinical use by the FDA (Food and Drug Administration). Especially, in the last six years the therapeutic antibody landscape got boosted with over 30 new approved drugs (antibodysociety.org) and there is no end to that boom in sight. As the INN (International Nonproprietary Names) names determined by the WHO (World Health Organization) already imply, there are mouse (-*o*-), rat/mouse (-*axo*-), chimeric (-*xi*-), chimeric/humanized (-*xizu*-), humanized (-*zu*-) and fully human (-*u*-) antibodies among the therapeutic products (Mallbris et al., 2016). Bestsellers include rituximab (Rituxan®, Roche), a CD20-specific antibody introduced for treatment of non-Hodgkin's lymphoma, infliximab (Remicade®, Janssen) and adalimumab (Humira®, AbbVie) both targeting the cytokine TNF (tumor necrosis factor) and used to treat Crohn's disease, rheumatoid arthritis and plaque psoriasis. Moreover, the VEGF-specific antibody bevacizumab (Avastin®, Roche) as well as the HER2-specific antibody trastuzumab (Herceptin®, Roche) are approved for the treatment of several types of cancer (Leavy, 2010).

Due to the progress in understanding tumor immunology the promising sector of immune-oncology has yielded in the approval of six immune checkpoint IgG inhibitors. Since tumor cells evading strategy include stimulation of immune T-cell inhibitory receptors such as CTLA-4 (cytotoxic T-lymphocyte-associated protein 4) or PD-1 (programmed cell death protein 1), blocking this interaction results in increased activation of the immune system. In 2011, the anti-CTLA-4 IgG1 ipilimumab gained approval as first checkpoint inhibitor. The other very promising, approved antibodies target either PD-1 or

its binding ligand PD-L1 (programmed cell death-ligand 1) overexpressed in several types of cancer.

The antibody and its derivatives

Although full-length antibodies are the primary format used, the modular nature of antibodies allows designing antibody-related formats with tailored characteristics (Figure 2). In general, immunoglobulin G consist of two identical heavy chains encompassing the VH, CH1, CH2 and CH3 domains and two identical light chains composed of the VL and CL domains. The antigen-binding sites are located on the two Fab arms. The recruitment of effector functions such as antibody-dependent cellular cytotoxicity (ADCC) or complement-dependent cytotoxicity (CDC) and the long *in vivo* half life is mediated by the Fc part. Customized formats can be generated through engineering desired properties such as affinity and avidity, valency, serum half-life, biodistribution and tissue penetration, effector functions and incorporation of multiple target specificities (Nelson, 2010).

Antibody fragmentation by papain or pepsin digestion yields in monovalent or bivalent Fab fragments (Figure 2) which can be desired to overcome unnecessary or unwanted effector functions (Labrijn et al., 2008). Four of such fragments, only consisting of the Fab region have already entered the clinic. Ranibizumab, for example, is an anti-VEGF Fab, derived through affinity-maturation of bevacizumab (Chen et al., 1999) and used for the treatment against wet age-related macular degeneration. However, Fab fragments can also be combined by genetic methods leading to bispecific (Fab_2) or even trispecific (Fab_3) formats (Holliger and Hudson, 2005). Shortened half life of such constructs lacking the Fc part can be counteracted by fusion to albumin or PEGylation as evidenced by the clinical anti-TNF-α Fab certolizumab pegol used for the treatment of Crohn's disease (Herrington-Symes et al., 2013; Kontermann, 2009).

An even smaller format at a size of about 28 kDa is the single-chain variable fragment (scFv) consisting of the antigen binding variable domains of heavy and light chain joint by a polypeptide linker (Figure 2) (Bird et al., 1988; Worn and Pluckthun, 2001). The scFv is easily expressible in various hosts and a perfect building block for further formats. Bivalent molecules can be achieved by fusing two scFvs to the CH3 domains (Minibody) or to the whole Fc part

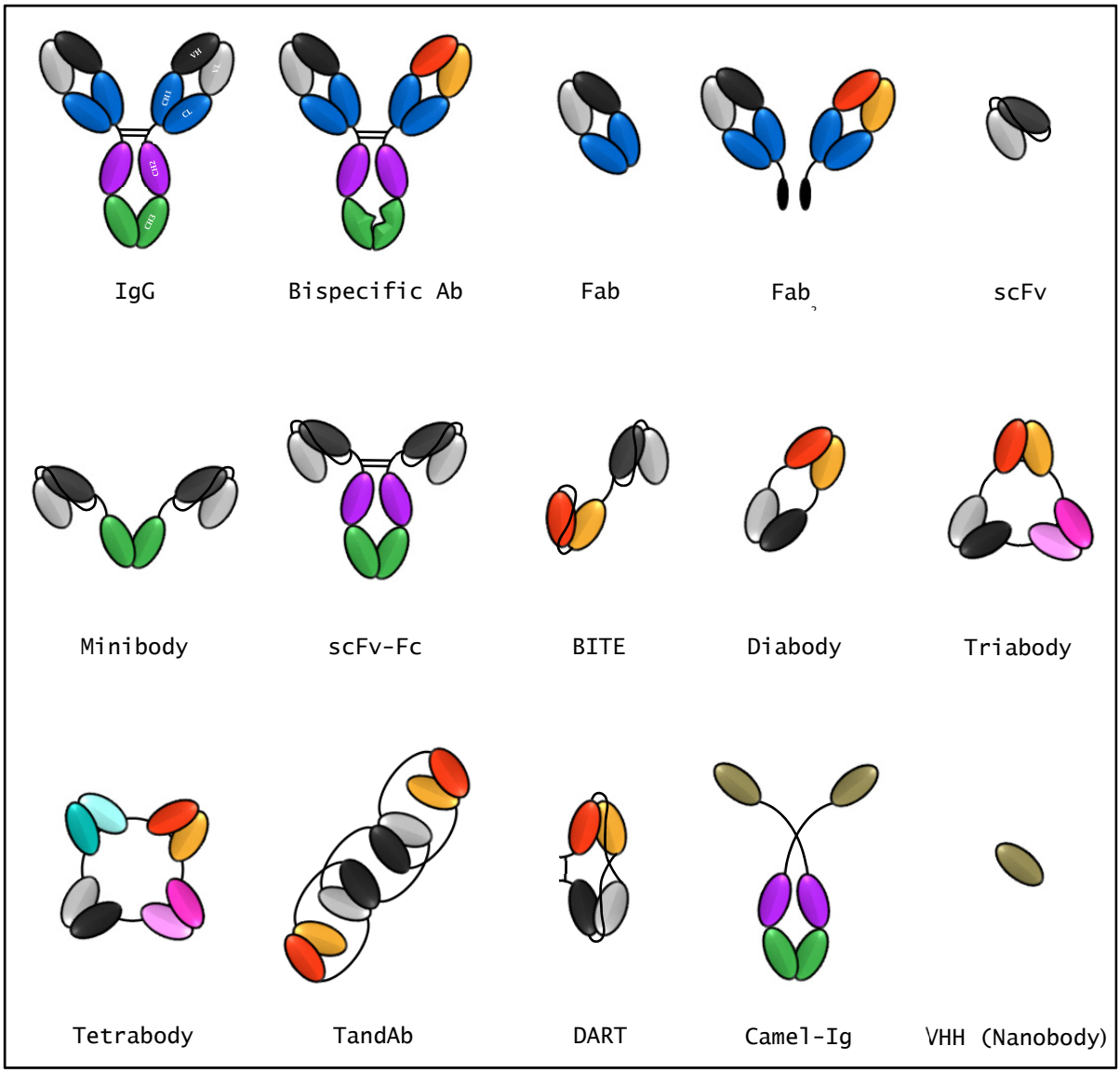

Figure 2. Schematic representation of IgG and various related formats.

(scFv-Fc) resulting in a pronounced total tumor uptake and long *in vivo* half life (Holliger and Hudson, 2005). An interesting advancement in immunotherapy was the engagement of two scFv, with one being antigen-specific and the other one directed against CD3 on T cells resulting in a bispecific T cell engager (BITE®, Figure 2) (Baeuerle and Reinhardt, 2009). Blinatumomab is the first clinical approved BITE targeting CD19 expressed on B cells and used for the treatment of acute lymphoblastic leukemia (Goebeler et al., 2016).

Another strategy includes the combination of two, three or four scFvs by using shorter linker length forcing the single domains to pair with the complementary domains of the other chain. The resulting formats (i.e. diabodies, triabodies and tetrabodies, Figure 2) can be designed either multivalent or multispecific (Holliger et al., 1993; Todorovska et al., 2001). A

further development of the diabody represents the tandem diabody (TandAb®) consisting of four variable domains resulting in increased valency and stability (Kipriyanov et al., 1999). The TandAb AFM11 equipped with the same target specificities as blinatumomab is currently evaluated in clinical phase I.

A diabody-like entity also developed for T cell recruitment represents the dual affinity re-targeting (DART®, Figure 2) format. The two chains building up the two binding Fv domains are additionally covalently linked via a disulfide bridge for stabilization (Moore et al., 2011).

Unique among mammals was the discovery of camelid antibodies (Heavy chain IgGs, Figure 2), which are solely composed of two identical heavy chains. The binding portion is formed by a single N-terminal domain (VHH) that is directly connected to the CH2 and CH3 domain. The VHH domain shows high structural identity to the human VH domain (Desmyter et al., 1996). Major differences include mutations within the framework regions that are conserved in human VH domains forming the hydrophobic interface with the VL domains. The single domain nature of the VHH fragment facilitates *in vitro* display methods as well as recombinant expression and forms the basis of the nanobody format (Harmsen and De Haard, 2007).

The above described formats reveal the importance of targeting different epitopes or antigens simultaneously. For this reason, a lot of effort has been invested towards the generation of recombinant bispecific full length IgGs that bear effector functions through an intact Fc region. In general, bispecific antibodies are composed of different heavy and light chains that are all expressed in the same producer cells resulting in a random assembly of the different chains and thus in a substantial amount of non-functional molecules. To tackle this chain association problem several strategies have been developed. A breakthrough for correct assembly of the heavy chains was the knobs-into-holes technology based on mutations within the CH3 domains interface. This strategy mimics a key-locks system by introducing a bulky residue in one CH3 domain that assemblies with a small residue introduced in the other CH3 domain (Ridgway et al., 1996). A substantial amount of advancements and variations of this technology has been established over the last years to improve the purity as well as the overall stability and yield of the heterodimer formats. By introduction of electrostatic steering effects heterodimer purity could be increased but with a drop in thermostability (Gunasekaran et al., 2010).

Another strategy represents the SEEDbody technology based upon the generation of hybrid CH3 domains derived from IgG and IgA (Davis et al., 2010). A very promising format was developed by Von Kreudenstein et al. by means of *in silico* design and *in vitro* evaluation (Spreter Von Kreudenstein et al., 2013). By combinations of mutations that prevent homodimerization with mutations that enhance stability a highly pure heterodimer variant with wild-type like thermostability was developed. However, finding a solution for the correct association of the heavy chains is just half of the story. For generation of a full-length bispecific antibody random pairing of the two different light chains with the two different heavy chains must be prevented. To address this "light-chain problem" Schaefer et al. introduced the CrossMab technology, where correct pairing of the light chains is achieved by exchanging the CH1 domain of one heavy chain with the CL domain of the corresponding light chain (Schaefer et al., 2011). Another strategy represents the introduction of mutations within the CH1-CL and the VH-VL interface enforcing correct assembly of the respective light and heavy chains (Lewis et al., 2014). Beside a wealth of bispecific antibodies under clinical evaluation, to date, catumaxomab, is the only market approved bispecific antibody targeting the anti-epithelial cell adhesion molecule (EpCAM) and CD3. This first generation bispecific antibody was produced by fusion of rat with mouse hybridomas resulting in increased incidence of the production of correctly assembled antibodies due to species restricted pairing of heavy and light chain (Heiss et al., 2010; Kontermann and Brinkmann, 2015; Lindhofer et al., 1995). The above described approaches for generation of heterodimeric antibodies capable of binding two adjacent targets or crosslinking two different antigens while maintaining Fc mediated effector functions show great promise as therapeutic agents for treatment of cancer and inflammatory diseases.

Engineered IgG1-Fc –The jack of all trades

The great advantage of having the Fc part included in antibody-derived constructs is its property to unify all essential antibody functions except of antibody recognition. The Fc part of IgG1 can interact with various natural binding partners (Figure 3) such as the neonatal Fc receptor (FcRn) responsible for the long *in vivo* half life (> 10 days). FcRn binds IgG in acidic vesicles

(pH ≤ 6.5) and releases it upon encountering the basic pH of 7.4 in the blood stream, thereby preventing IgG from lysosomal degradation (Martin et al., 2001). Three classes of Fcγ receptors (FcγRI [CD64], FcγRII [CD32] and FcγRI [CD16]) expressed on the surface of various immune cells bind to the lower hinge region of IgG and are responsible for induction of phagocytosis (Jefferis et al., 1990). Moreover, C1q, the recognition subunit of the C1 complex, binds to residues of the CH2 and CL domain, thereby triggering the activation of the classical pathway of the complement system (Gaboriaud et al., 2003).

The intracellular tripartite motif-containing 21 (TRIM21) is a cytosolic receptor that targets antibody-opsonized pathogens to the proteasome (James et al., 2007). Additionally, a major advantage for purification of recombinant Fc-containing formats is the ability of the Fc portion to bind to protein A of *Staphylococcus aureus*. For more details see chapter "Natural binding partners of IgG1-Fc" (Lobner et al., 2016).

Various clinical approved drugs have already proven the advantage of having the Fc part included in the respective construct. In most cases, the Fc portion is fused to an interaction protein of interest, such as a ligand that activates upon binding to a receptor or blocks receptor binding (Levin et al., 2015).The Modular Antibody Technology™ enables the introduction of novel binding sites in the C-terminal loops of the CH3 domain of human IgG1-Fc to generate an Fcab (Fc domain with engineered antigen binding sites). The CH3 domain encompasses three structural loop regions that can be engineered for antigen binding: AB loop (residues 355-362), CD loop (383-391) and EF loop (residues 413-422) (Eu numbering system (Edelman et al., 1969)). This topic is discussed in more detail in chapter "Generation of novel and improvement of existing functions in IgG1-Fc" (Lobner et al., 2016). In 2010, Wozniak-Knopp et al. reported the generation of the HER2 (human epidermal growth factor receptor 2) specific Fcab H10-03-6 by randomization of the AB and EF loop of human IgG1-Fc. To increase the available sequence and structure space five additional residues were inserted into the EF loops. The resulting library was displayed on yeast and selected for binding to HER2. After affinity-maturation the final best performing Fcab H10-03-6 revealed maintained binding to protein A and FcγRI as well as a K_D value of 23 nM for binding to HER2 (Traxlmayr et al., 2013; Wozniak-Knopp et al., 2010). Moreover, H10-03-6 exhibited an *in vivo* half life similar to Fc-wt and *in vitro* ADCC activity against the HER2-expressing SKBr3 cell line.

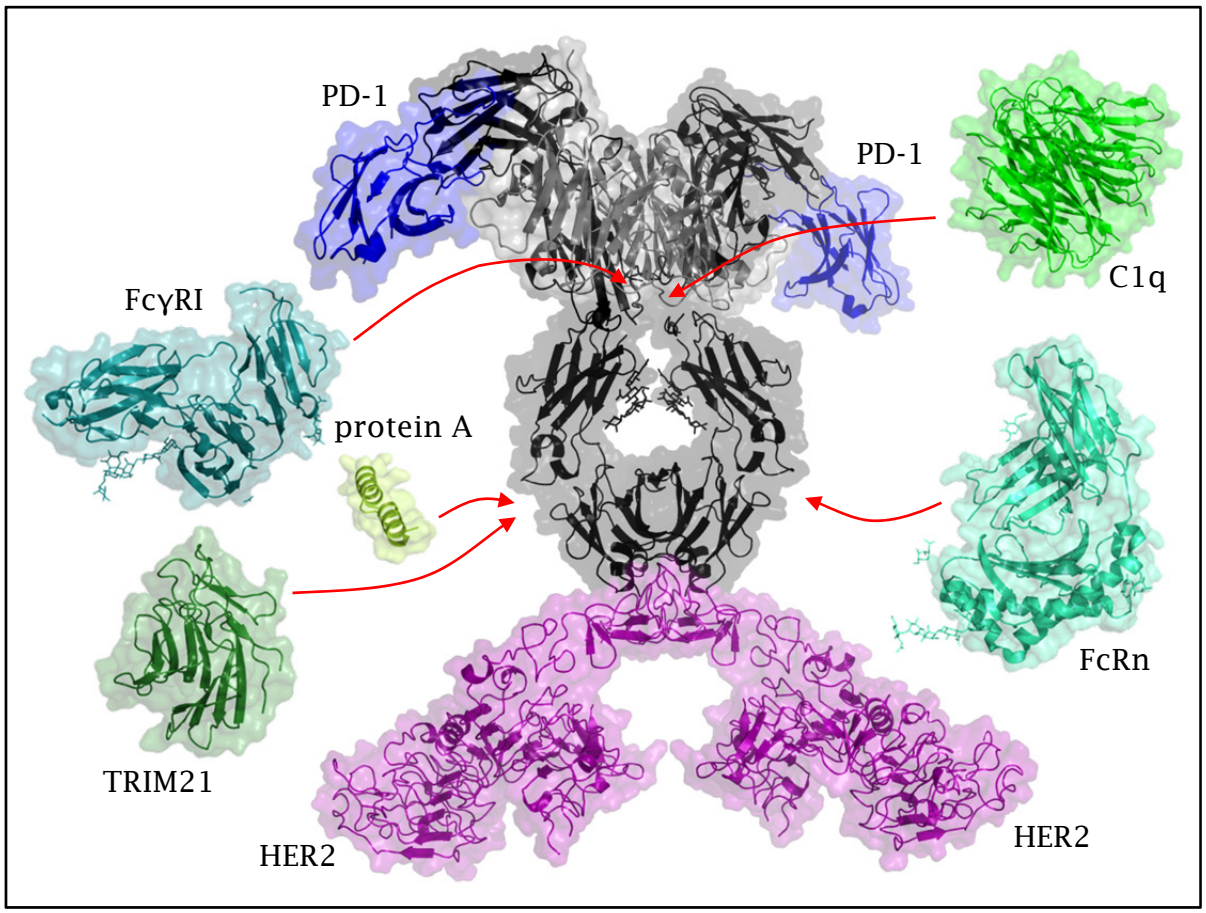

Figure 3. Schematic representation of a mAb² directed against PD-1 and HER2 and its binding ligands. The theroretical mAb² is composed of the Fcab-HER2 complex structure (PDB: 5K33) (Lobner et al., 2017), the nivolumab Fab-PD-1 complex structure (PDB: 5WT9) and the hinge region of the full-length structure of an IgG1 (PDB: 1HZH) (Saphire et al., 2001). The latter was used as structural template for the construction of the mAb². Red arrows mark the binding site of the complement system protein C1q (PDB: 1PK6) (Gaboriaud et al., 2003), the neonatal Fc receptor (PDB 1I1A) (Martin et al., 2001), the C-terminal PRYSPRY domain of TRIM21 (PDB: 2IWG) (James et al., 2007), the mini-Z domain of protein A (PDB: 1OQO) and the Fc gamma receptor I (PDB: 4W4O) (Kiyoshi et al., 2015). The epitope of C1q was evaluated by docking studies (Schneider and Zacharias, 2012).

However, due to extensive mutations in the CH3 domain biophysical properties developed detrimental. Therefore, Traxlmayr et al. developed a directed evolution protocol for improvement of the conformational stability of promising Fcab molecules. The strategy included soft randomization of the binding loop regions of the parental binder followed by heat incubation of the yeast displayed library. Moreover, the selection strategy encompassed simultaneous selection for binding to HER2 and to a structurally specific ligand such as FcγRI. The yielding Fcab molecules (STAB clones) revealed a substantial increase in thermostability by nearly retained affinity to HER2 (Traxlmayr et al., 2013).

Another approach for assessment of Fcab stability on a library scale was developed by Hasenhindl et al. This strategy included the construction of yeast surface display libraries of IgG1-Fc that carried mutations or insertions at distinct positions of the C-terminal loop regions. The libraries were incubated at increasing temperatures and probed for binding to Fc specific ligands. The calculated temperatures of half-maximal irreversible denaturation of each library revealed a clear tolerance hierarchy to randomization of the distinct loop positions and allowed for rapid comparison of the primary structural information and stability (Hasenhindl et al., 2013).

The great success of the Fcab format has been proven by the HER2-specific Fcab FS102 that entered clinical phase I. FS102 carries five mutations in the AB and EF loops and showed superior antitumor activity in HER2-high xenograft models. Moreover, in *in vitro* and *in vivo* studies this Fcab was shown to even surpass the activity of the clinical approved antibodies trastuzumab and pertuzumab (Leung et al., 2015).

Another very promising format of the Modular Antibody Technology™ platform is the generation of a bispecific antibody, a so-called mAb^2 (Figure 3), by just fusing any antigen-specific Fcab to Fab arms encompassing another antigen specificity (Lobner et al., 2016). The mAb^2 FS118 designed to block the immune checkpoint molecules LAG-3 (Lymphocyte-activation gene 3) and PD-L1 is currently in preclinical evaluation.

Beyond antibodies – Alternative formats

Although the market is dominated by full-size IgGs the first candidates of small non-Ig protein scaffolds for the treatment and diagnosis of cancer and inflammatory diseases have already entered clinical development. Most of these scaffolds are from human origin and thus reveal low immunogenic potential. A major advantage of these non-antibody scaffolds (Figure 4) are their small size, their high thermostability and their low demand to the expression host. Therefore, they can easily be produced in bacterial expression systems or even chemically synthesized. The paratope of the non-Ig scaffolds are either located on exposed loop regions or scattered in secondary structural motifs. In most cases the scaffolds have been engineered for antigen binding using multiple

display platforms. Multivalency and multispecificity can also be achieved by just assembling multiple non-Ig scaffolds (Skrlec et al., 2015).

A highly thermostable non-Ig protein (T_m > 80 °C) is represented by adnectin (Figure 4). It is based on the 10th fibronectin type III domain, a human extracellular matrix protein and structural similar to antibody variable domains. The molecule lacks disulfide bonds and free cysteine and can readily be produced with high yields in bacteria. Three flexible surface-exposed loops on one side of the protein have proven to be convenient for engineering the binding surface (Simeon and Chen, 2017). A prominent example for the therapeutic potential of adnectin molecules is BMS-986089 that targets myostatin with extremely high affinity (K_D < 0.5 nM) and used for the treatment of skeletal muscle diseases (Madireddi et al., 2016).

Anticalins (Figure 4) derived from lipocalins, a class of secreted proteins that transport or store hydrophobic compounds. The 20 kDa small anticalin scaffold adopts a typical β-barrel structure mounted with four loops that form the binding interface (Skerra, 2008). The anticalin PRS-050 selected against VEGF-A with picomolar affinity is currently evaluated in clinical phase I. In addition, the *in vivo* half life of PRS-050 was extended by site-directed PEGylation (Gille et al., 2016).

The scaffold of so-called fynomers (Figure 4) derived from the src-homology domain 3 (SH3) of the FYN tyrosine kinase. Interestingly, FYN-SH3 domains are fully conserved between mice, rats, gibbons and humans (Weidle et al., 2013). The very small fynomer (7 kDa) is composed of two anti-parallel β-sheets with two connecting loops that can be engineered for target interaction. A clinical phase I/II bispecific format is the FynomAb COVA322, consiting of an anti-IL-17A fynomer fused to the C-terminus of the light chain of the approved IgG1 adalimumab directed against TNF applied in the treatment of rheumatoid arthritis (Silacci et al., 2016; Simeon and Chen, 2017).

Kunitz domains (Figure 4) encompassing the same size as fynomers derive from the active motif of Kunitz-type protease inhibitors. Their structure is composed of a twisted two-stranded β-sheet and two α-helices stabilized by three disulfide bridges. The loop connecting the secondary structural motifs can be engineered for antigen binding. In 2012, the FDA approved the Kunitz domain-derived kallikrein inhibitor Ecallantide (DX-88) for treatment of hereditary angioedema, a disease caused by C1 inhibitor gene mutation that is

the primary inhibitor of kallikrein (Schneider et al., 2007; Simeon and Chen, 2017).

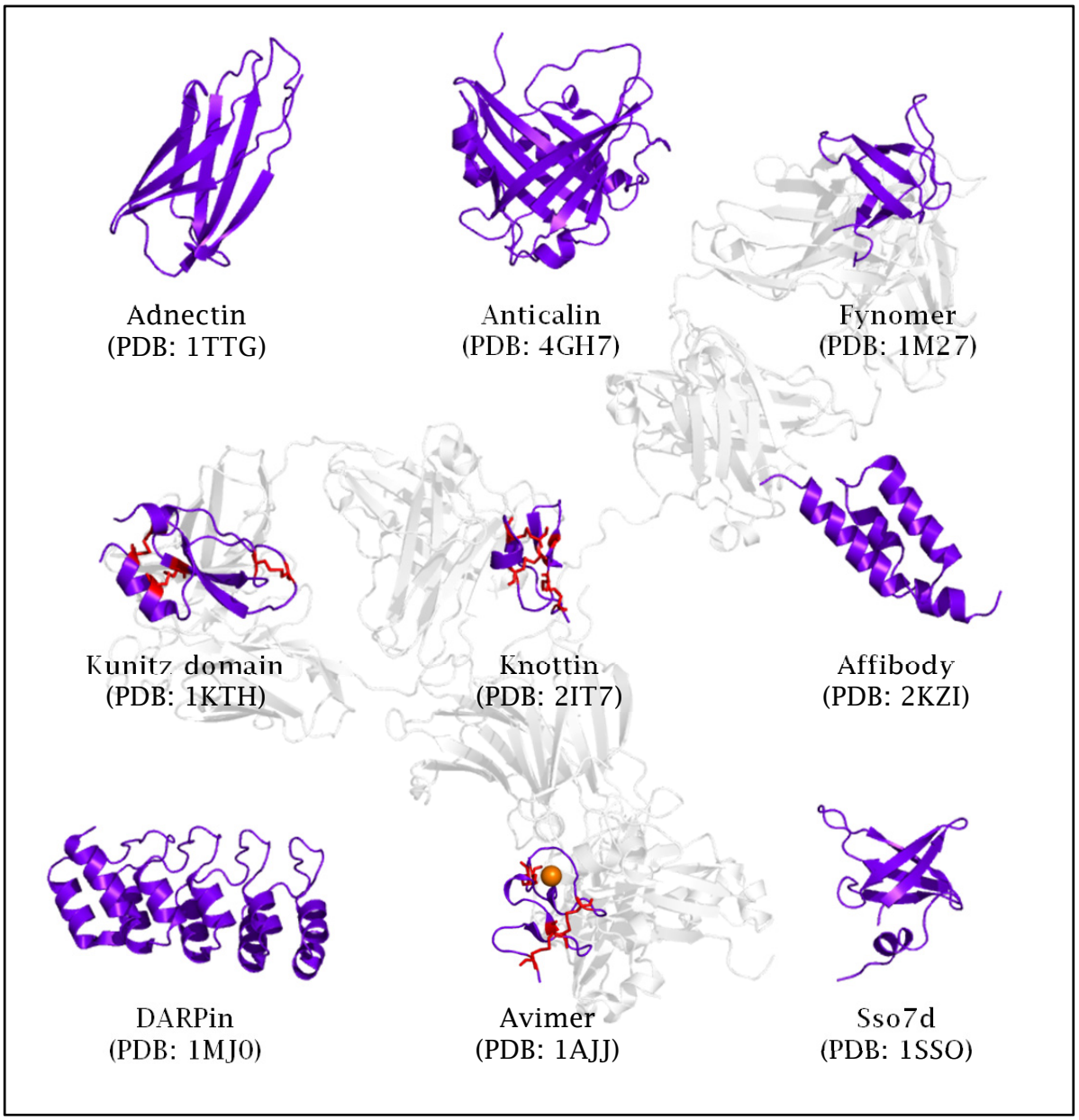

Figure 4. Selection of various protein scaffolds. The disulfide bridges are indicated as red sticks and the calcium as orange sphere. A full-size IgG (PDB: 1HZH) is depicted in gray for comparison of the size. The proportions regarding the size of the structures are true to scale.

Another class of highly thermostable non-Ig scaffolds is represented by knottins (Figure 4). Knottins are small cysteine-rich miniproteins found in a wide range of species such as plants, animals and fungi and include a broad range of functions such as protease inhibition, ion channel blockade and antimicrobial activity. Knottins reveal a cyclized structure that is cross-braced by a knotted arrangement of disulfide bonds. The surface-exposed loops can be engineered for ligand binding. Due to their high stability against proteolytic degradation

and thus resistance against the harsh conditions of the gut, knottins are feasible candidates for oral administration (Craik et al., 2010; Simeon and Chen, 2017; Thell et al., 2016). Linaclotide, a naturally-derived knottin, is an FDA approved oral drug used for the treatment of irritable bowel syndrome and chronic idiopathic constipation (Layer and Stanghellini, 2014).

Affibodies (Figure 4) are based on the Z domain of the Ig-binding *Staphylococcus aureus* protein A. Their structure adopts a three-helix bundle motif with a size of about 6 kDa. The solvent-accessible residues scattered around two of the three helices can be engineered for ligand binding ((Nygren, 2008; Simeon and Chen, 2017). The labelled affibody ABY-025 engineered to target HER2 has shown to accurately quantify the HER2-status in metastatic breast cancer in a phase I/II clinical trial (Sorensen et al., 2016).

DARPins (designed ankyrin repeat proteins, Figure 4) are artificial protein scaffolds built from tightly packed repeats of ankyrin proteins. Each repeat consists of a β-turn followed by two antiparallel α-helices. DARPins are usually designed with 4-6 repeats whereas the non-conserved, surface exposed residues can be engaged in target recognition. Most DARPins indicate high thermostability (up to above 85 °C), and can be brought to very high protein concentrations without aggregating. DARPins have also been established as intracellular biosensors of protein conformation and as crystallization chaperones (Binz et al., 2003; Pluckthun, 2015). Moreover, the PEGylated DARPin Abicipar targeting VEGF-A for the treatment of wet age-related macular degeneration is currently in phase III clinical trial (NCT02462928).

Avimers (Figure 4) derive from the A-domain of a large family of human extracellular receptor. They encompass a size of only 4 kDa and are stabilized by binding of a calcium ion and three disulfide bridges. The avimer scaffold consists of approximately 35 amino acids, 12 of them being conserved and thus the remaining residues can be randomized for ligand binding (Silverman et al., 2005). The trimeric avimer C326 engineered for binding to IL-6 for the treatment of Crohn's disease entered clinical development in 2007 but no further progress has been reported (Ranganath et al., 2015).

Another very promising scaffold is represented by DNA-binding protein Sso7d (Figure 4) derived from the hyperthermophilic archaeon *Sulfolobus solfataricus* (Gera et al., 2011). Sso7d indicates a high thermostability (T_m = 98 °C) and thus enables a high tolerance to mutations and protein evolvability. Due to its high positive charge nature the Sso7d scaffold was

recently engineered for charge-neutralization. Based on these charged-neutralized libraries binders against mouse serum albumin and different epitopes of human EGFR were selected. Remarkably, the paratope is located on the rigid β-sheet that is expected to reduce the entropic penalty upon antigen binding (Traxlmayr et al., 2016). The Sso7d scaffold was already applied for the development of highly efficient reagentless biosensors (de Picciotto et al., 2016) as well as for the immobilization on cellulose for paper-based diagnostic tests (Miller et al., 2016).

2 AIMS OF THE THESIS

The Modular Antibody Technology™ introduced by the company F-star enables the generation of novel Fc based molecules comprising the additional ability for antigen binding (i.e. Fcabs). Various Fcab molecules that differ in loop design, stability, affinity and specificity have previously been generated by different sorting strategies using yeast surface display. The selected Fcabs for the present study included the HER2-binding Fcabs H10-03-6 and its stabilized version STAB19, in addition to the highly mutated VEGF-A-binding Fcabs 448 and its affinity matured version CT6.

This thesis aimed at investigation of the structural basis of these selected Fcab molecules to enlighten the impact of structural properties of the respective Fcab molecule to its overall stability and biophysical properties. Moreover, the interaction of the Fcabs with their respective antigen should be investigated in detail with a broad set of biochemical and biophysical methods. Since the Fcab is a homodimeric molecule encompassing two potential binding sites in close proximity, the occupancy of each was so far elusive and had to be determined.

Therefore, suitable expression systems as well as purification strategies for all proteins under study had to be established. To determine and ensure highly pure and well-folded protein the quality had to be controlled by size exclusion chromatography combined with multi-angle light scattering (SEC-MALS), differential scanning calorimetry (DSC) and liquid chromatography-electrospray ionization-mass spectrometry (LC-ESI-MS). High quality proteins served as basis for the X-ray crystallography studies of unbound and antigen-bound Fcabs to elucidate the binding modes, binding stoichiometries and residues that are involved in the respective interaction.

To extend the picture of the respective Fcab-antigen interaction in solution, the binding stoichiometries as well as the thermodynamics and binding modes should further been investigated by means of SEC-MALS, isothermal titration calorimetry (ITC) and fluorescence correlation spectroscopy (FCS).

3 MANUSCRIPTS

Engineered IgG-Fc – one fragment to bind them all

Lobner E., Traxlmayr M.W., Obinger C. and Hasenhindl C.

Review article

Immunological Reviews (2016), 270(1): 113-131. doi: 10.1111/imr.12385.

Immunological Reviews

Elisabeth Lobner
Michael W. Traxlmayr
Christian Obinger
Christoph Hasenhindl

Engineered IgG1-Fc – one fragment to bind them all

Authors' addresses
Elisabeth Lobner[1], *Michael W. Traxlmayr*[1,*], *Christian Obinger*[1], *Christoph Hasenhindl*[1,†]
[1]Christian Doppler Laboratory for Antibody Engineering, Department of Chemistry, Vienna Institute of BioTechnology, BOKU – University of Natural Resources and Life Sciences, Vienna, Austria.

Correspondence to:
Christoph Hasenhindl
Austrianni GmbH
Campus Vienna Biocenter 5
A-1030 Vienna, Austria
Tel.: +43 1 2260075 20
e-mails: christoph.hasenhindl@austrianni.com or christoph.hasenhindl@boku.ac.at

Present addresses: *Koch Institute for Integrative Cancer Research and Department of Chemical Engineering, Massachusetts Institute of Technology, Cambridge, MA, USA.
†Austrianni GmbH, Vienna, Austria.

This article is part of a series of reviews covering Immunoglobulins: from genes to therapies appearing in Volume 270 of *Immunological Reviews*.

Summary: The crystallizable fragment (Fc) of the immunoglobulin class G (IgG) is a very attractive scaffold for the design of novel therapeutics due to its quality of uniting all essential antibody functions. This article reviews the functionalization of this homodimeric glycoprotein by diversification of structural loops of CH3 domains for the design of Fcabs, i.e. antigen-binding Fc proteins. It reports the design of libraries for the selection of nanomolar binders with wildtype-like *in vivo* half-life and correlation of Fc receptor binding and ADCC. The *in vitro* and preclinical biological activity of selected Fcabs is compared with that of clinically approved antibodies. Recently, the great potential of the scaffold for the development of therapeutics for clinical use has been shown when the HER2-binding Fcab FS102 entered clinical phase I. Furthermore, methods for the engineering of biophysical properties of Fcabs applicable to proteins in general are presented as well as the different approaches in the design of heterodimeric Fc-based scaffolds used in the generation of bispecific monoclonal antibodies. Finally, this work critically analyzes and compares the various efforts in the design of highly diverse and functional libraries that have been made in the engineering of IgG1-Fc and structurally similar scaffolds.

Keywords: *IgG1-Fc, Antibody engineering, Library design, Fcab*

Introduction

Monoclonal antibodies (mAbs) undoubtedly belong to the most prominent therapeutics of the last two decades. Since 1986, more than 40 mAbs have been approved by the Food and Drug Administration (FDA) for the use in various diseases, including cancer, immune disorders, and infectious diseases, and many more are in clinical trials, with full-size IgG still representing the majority of these approved mAbs. However, based on the success of these drugs, several different antigen-binding formats such as antibody fragments or domains (i.e. antibody-based scaffolds) and non-antibody protein scaffolds have been investigated for their potential as binding molecules. The postulated advantage of such molecules is the reduced size that potentially leads to enhanced tissue penetration and facilitated production.

For example, three full-size antigen-binding fragments (Fab) of IgG have been approved by the FDA for clinical use so far [certolizumab pegol (1), ranibizumab (2), and

Immunological Reviews 2016
Vol. 270: 113–131

Immunological Reviews
0105-2896

Acknowledgements
This work was supported by the Christian Doppler Research Association (Christian Doppler Laboratory for Antibody Engineering), the company F-star Biotechnology Ltd., as well as the Austrian Science Foundation (FWF W1224 – Doctoral Program on Biomolecular Technology of Proteins – BioToP). The authors declare no conflict of interest.

abciximab (3)]. At a considerable smaller size, single-chain variable fragments (scFv) comprise the variable domains of heavy and light chain connected by a polypeptide linker and therefore contain the complete binding sites of antibodies. It has been reported that scFvs can be readily expressed in various hosts like bacteria, yeasts, and plants (4–6). An advancement of this technology was the construction of bispecific T-cell engagers [BiTEs (7)], comprising two scFvs with specificities for CD3 and a target antigen expressed as one polypeptide chain. Dual-affinity re-targeting molecules (DARTs) follow a similar principle: As a further development of the diabody technology (8), a C-terminal disulfide bond covalently links two scFvs that are expressed as separate polypeptides to generate a more stable bispecific molecule (9). Xiao *et al.* reported the selection of molecules based on the isolated CH2 domain of IgG1 binding to the HIV-1 envelope glycoprotein (10). Another concept uses nanobodies, i.e. the single-domain antigen-binding fragments of camelid heavy chain antibodies, which, for example, have the potential for application in oral immunotherapy due to the increased resistance to extreme pH and proteolytic digest as compared to conventional antibodies (11, 12). Examples for non-antibody-binding scaffolds comprise, e.g. designed ankyrin repeat proteins (DARPins). DARPins are small, single-domain proteins derived from natural repeat proteins that can be engineered to bind diverse antigens (13). And finally, the immunoglobulin-like structure of the tenth type III unit of human fibronectin (^{10}Fn3) has served as the basis for the engineering of one further novel binding scaffold (14).

The potential therapeutic value of these formats is, however, largely reduced due to the absence of the crystallizable fragment (Fc) and the resulting inability to trigger effector functions such as antibody-dependent cellular cytotoxicity (ADCC) or complement-dependent cytotoxicity (CDC). Accordingly, the *in vivo* half-life is limited due to the absence of the Fc-located binding site of the neonatal Fc receptor FcRn, and a lot of effort is necessary to overcome these drawbacks, which to some degree outweighs the advantage of the smaller size.

In 2009, Rüker and Wozniak-Knopp (15) reported the engineering of the structural loops of immunoglobulin constant domains to generate novel binding sites (Modular Antibody Engineering). Based on the observation that immunoglobulin-like domains are structurally conserved in the β sandwich core regions while at the same time exhibiting high variability of the loops (16), the three C-terminal loops of the CH3 domain of IgG1-Fc were engineered to bind diverse antigens in initial studies, yielding antigen-binding Fc fragments termed 'Fcabs'. In this review, the therapeutic potential of such Fcabs and efforts in functional engineering as well as the engineering of biophysical properties will be discussed. There will be no focus on the engineering of individual antibody domains like monomeric CH2 or CH3 domains as scaffolds for the design of novel binders, as this topic has been reviewed recently (17).

Structure of IgG-Fc

The structure and function of human IgG-Fc has been described extensively. However, it is necessary to provide the background for discussion in the present review. Immunoglobulins of isotype G are the predominant antibody class in circulation and comprise two identical light (L) and heavy (H) chains forming a 'Y-shaped' structure (18). An IgG molecule can be dissected into two distinct fragments (Fab, Fc) that are responsible for the *in vivo* properties (*Fig. 1*): An antigen-binding fragment (Fab) is a heterodimeric protein composed of one light chain and the N-terminal half of one heavy chain. It encompasses two variable (V) domains (VH, VL) whose complementarity-determining regions (CDRs) form the antigen-binding site, and two constant (C) domains (CL, CH1) (*Fig. 1*). By contrast, the crystallizable fragment (Fc) is a homodimeric glycoprotein with one monomer consisting of two constant immunoglobulin domains (CH2, CH3) from the C-terminal half of one heavy chain (*Fig. 1*). Through interaction with its ligands [Fcγ receptors (FcγR), C1q and FcRn] it mediates various immune effector functions and increases the half-life of the antibody molecule (19). The Fc and the two Fab

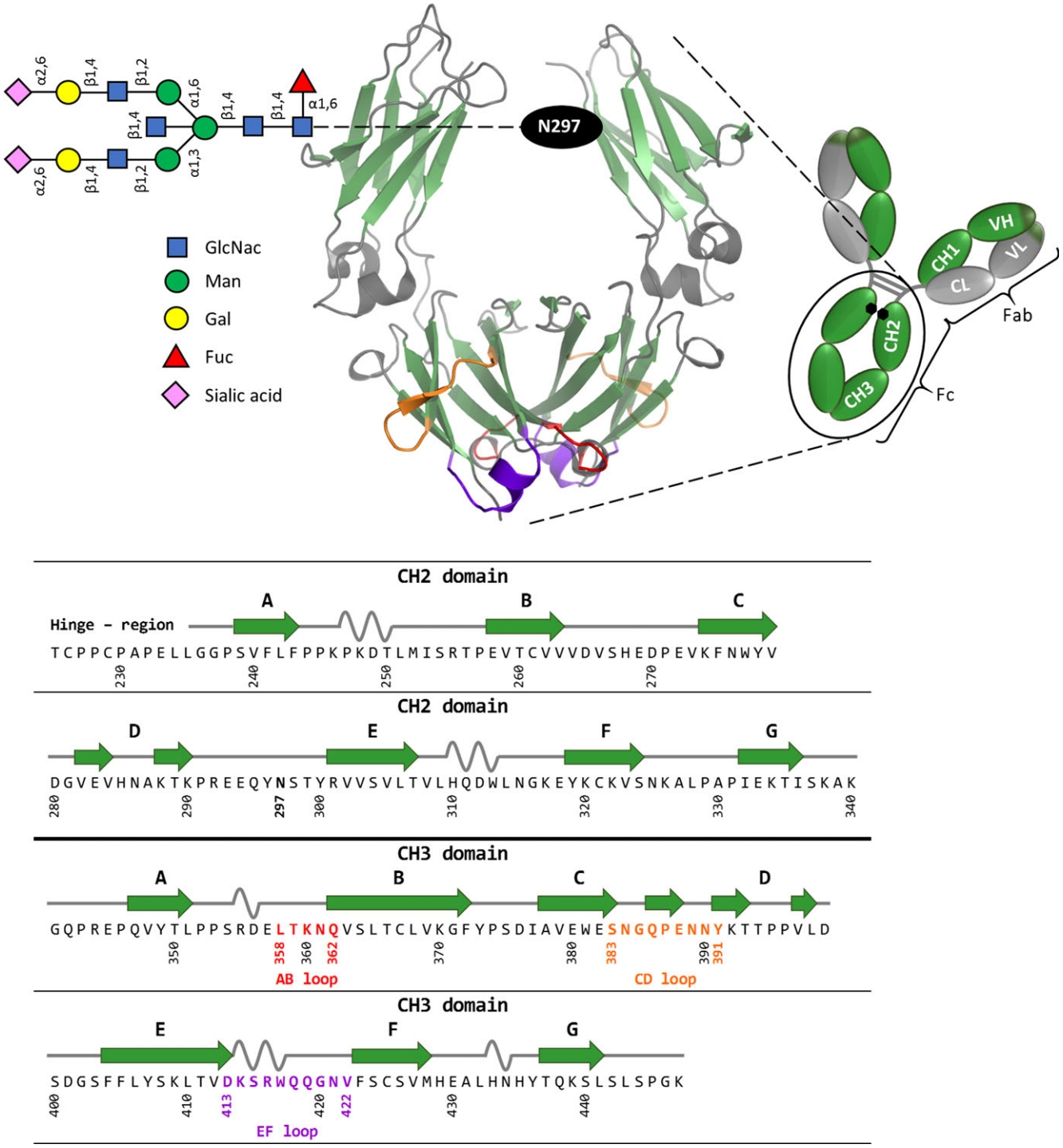

***Fig. 1.* Schematic representation of homodimeric human IgG1-Fc (PDB-ID 1OQO), generated using PyMOL, with the corresponding amino acid sequence.** IgG1 is composed of two heavy and two light chains, with the Fab region carrying the antigen-binding sites and the Fc part mediating various effector functions. The homodimeric Fc part comprises the CH2 and CH3 domains, where β strands are depicted in green, and α helices and random coils are shown in gray. The C-terminal loops of the CH3 domain are colored in red (AB loop), orange (CD loop), and purple (EF loop). The asparagine at position 297 carries the glycan (NaNaFbi), graphically represented according to Anthony *et al.* (44). The amino acid sequence of the CH2 and CH3 domain of wildtype IgG1-Fc is shown and numbered according to Eu numbering system (20). On top of the sequence, the secondary structure elements of CH2 and CH3 according to the crystal structure (PDB-ID 1OQO) are shown.

fragments meet at a central flexible segment, the hinge region, which plays an important role in the mediation between antigen recognition and effector functions and forms interchain disulfide bonds between the two heavy chains. X-ray crystallography of IgG1-Fc comprising amino acids 216–446 (20) (*Fig.* 1) normally reveals structure for

residues 238–443, underlining that the hinge region is highly flexible (21–24). In addition, the conformation of the hinge proximal region of the CH2 domain is shown to be 'soft', i.e. to be relatively mobile in comparison to the more defined structure observed at the CH2–CH3 interface.

Four distinct IgG subclasses differing in their heavy chains (and consequently in their Fc), exist in humans (hIgG1-4), and in mice (mIgG1, 2a, 2b, 3). This review will mainly focus on the structure–function relationships of the Fc of human IgG1 as a basis for engineering strategies for the design of novel therapeutic proteins. In the following, IgG-Fc and IgG1-Fc will always mean the basic homodimeric scaffold including two monomers, each being composed of the N-terminal hinge region followed by CH2 and CH3 domains (i.e. Thr225 to Lys446; for amino acid numbering and assignment of secondary structures, see *Fig. 1*).

A single N-linked glycan is attached to asparagine 297 (CH2 domain) of each heavy chain. The glycan has a complex biantennary structure (*Fig. 1*) and can vary by the addition of sugar residues to specific parts of the core structure. The latter is composed of N-acetylglucosamine and mannose and can be modified by the addition of fucose, bisecting N-acetylglucosamine, and two arms defined by α1,3 and α1,6 mannose linkages (*Fig. 1*). The arms can be extended by the addition of galactose and sialic acid. There is a tremendous heterogeneity in the IgG-Fc glycan, with over 30 distinct glycans detected on circulating IgG in healthy individuals (25). The two Fc glycans are essential for the structural integrity of Fc (and IgG) by contributing mainly to the interface of the CH2 domains, where they face the center of the Fc with the α1,3 arm protruding into the cavity between the heavy chains and the α1,6 arm extending along the heavy chain backbone (26, 27). Crystal structures of IgG-Fc reveal a distinct conformation for the oligosaccharide resulting from multiple non-covalent interactions with the protein (23). This was confirmed by molecular dynamics (MD) simulations demonstrating that the glycans form more hydrogen bonds with the individual protein chains at the cost of glycan–glycan interactions (28).

The thermodynamic parameters (obtained by differential scanning calorimetry) describing the unfolding of IgG1-Fc reflect these interactions, with the thermal unfolding of the CH2 domains showing a progressive reduction in stability with loss of sugar interactions while the unfolding of the CH3 domain is unaffected (29). Typically, IgG1-Fc exhibits two thermal transitions (best modeled using two sequential two-state transitions) with the lower temperature transition (T_{m1} approximately 71°C) reflecting unfolding of the CH2 domain and the second transition (T_{m2} approximately 82°C) unfolding of the CH3 domain at pH 7.4 (30). The latter underlines the importance of the extensive hydrophobic CH3–CH3 interface for the stabilization of IgG1-Fc. During unfolding, the CH2 domains behave as a single cooperative unit, and unfolding is reversible as long as the protein sample is taken to approximately 75°C at maximum, whereas unfolding of the CH3 domains is irreversible. Typically, the thermal stability of the Fc fragment decreases with decreasing pH as demonstrated experimentally (31) and by computational means (28).

Based on the importance of glycosylation for the conformational and thermal stability of IgG1-Fc, yeast surface display has been the method of choice to screen IgG1-Fc libraries for variants with desired properties (32). The advantage of yeast display over phage, bacterial, and ribosome display is the existence of a eukaryotic protein production machinery that is necessary for post-translational modifications (including glycosylation) and quality control of expressed proteins in the endoplasmic reticulum (ER) and the Golgi complex of eukaryotes (33). Also, in contrast to phage and ribosome display, yeast display selections usually include one or more flow cytometric sorting steps, facilitating quantitative analysis during selection. In addition, normalization for protein expression is possible by including expression tags (34).

Natural binding partners of IgG1-Fc

The most obvious advantage of IgG-Fc over other antibody-derived or non-antibody binding scaffolds is its quality of combining all essential antibody functions except for antigen recognition, including binding to FcγRs. These may be expressed constitutively on hematopoietic cells (e.g. macrophages, eosinophils, neutrophils, natural killer cells, lymphocytes) and other tissues and may be induced or upregulated, differentially, on each cell type when exposed to cytokines or other activating agents (21). Stimulation of cells through FcγRs may result in the activation or deactivation of one or more of a variety of effector functions, including ADCC, CDC, phagocytosis, oxidative burst, release of inflammatory mediators, etc. (35). Due to the high sequence homology between the FcγR types and between the subclasses of IgG, spatial homology for interaction sites is found. In general, binding sites are located at the lower hinge and adjacent regions in the CH2 domain (36, 37) (*Fig. 2*).

A dynamic model of Fc–FcγR recognition was proposed in which oligosaccharide/protein interactions within the Fc

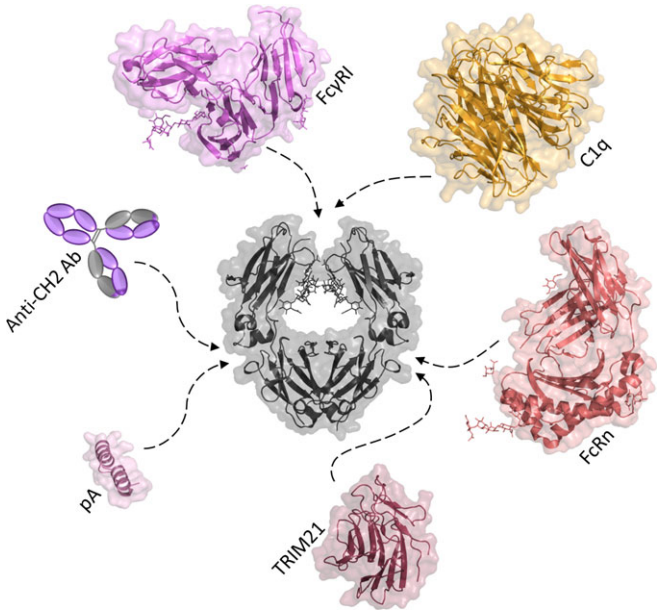

***Fig.* 2. Representation of secondary structural elements with transparent molecular surface of IgG1-Fc and its binding ligands.** IgG1-Fc (PDB-ID 1OQO) is colored in gray. Glycan structures are depicted as lines. Dashed arrows mark the binding site of the neonatal Fc receptor [PDB-ID 1I1A (50)]; Fc gamma receptor I [PDB-ID 4W4O (119)]; the mini-Z domain of protein A (PDB-ID 1OQO); a globular head of the complement system protein C1q [PDB-ID 1PK6 (47)]; the C-terminal PRYSPRY domain of TRIM21 [PDB-ID 2IWG (120)]; and the anti-CH2 antibody (clone MK 1 A6, AbD Serotec). The epitope of C1q was obtained by docking studies combined with MD simulations by Schneider *et al.* (121). Traxlmayr *et al.* (86) defined the binding site of the anti-CH2 antibody to be located at the C-terminal part of the CH2 domain. The proportions regarding size of all shown crystal structures are true to scale.

protein generate an equilibrium population of conformers, with distinct structures that recognize and bind individual ligands (21). Besides contribution to the conformational and thermal stability, the two glycan chains of Fc are an absolute requirement for binding of Fc (and IgG) to FcγRs, as this interaction is lost after deglycosylation (27). The Fc glycan apparently maintains an open conformation of the Fc heavy chains required for interaction with FcγRs as supported by the structure of aglycosylated Fc (38). In the latter, the two heavy chains arrange in a closed conformation and therefore lack the FcγR-binding pocket. However, it was demonstrated that mutations in the Fc backbone can alter the overall structure of aglycosylated Fc and restore binding to FcγRs to some extent, suggesting that the Fc glycan chains primarily affect protein–protein interactions by altering the Fc backbone conformation (39). The interplay between the primary and secondary N-acetylglucosamine residues with the protein structure seems to be particularly critical for FcγR recognition (40).

The human FcγRI (CD64) is expressed on monocytes and macrophages and a number of myeloid cell lines and binds to IgG1 and IgG3 with similar affinity at the lower hinge region around residues 234–238 and residues in the hinge proximal region of the CH2 domain (41, 42). In humans, two forms of FcγRII (CD32) are found, namely FcγRIIa and FcγRIIb. Both are widely expressed on multiple cell types, constitutively and/or following induction or upregulation (43) and bind to IgG1 and IgG3 with similar affinity. While their external domains are highly homologous they transduce opposite signals (activating versus inhibitory) via their intracytoplasmatic domains. The binding site at the Fc is similar to that of FcγRI (21). Finally, FcγRIII (CD16) is a low-affinity receptor either expressed as an intrinsic (FcγRIIIa) or glycosphingolipid-linked protein (FcγRIIIb). Binding of natural killer (NK) cell-expressed FcγRIIIa to the lower hinge region activates ADCC (37).

As mentioned above there is some variation in composition of IgG-Fc glycans *in vivo* and this may directly contribute to modulation of interaction (and affinity) with individual FcγRs classes, thereby mediating activating, inhibitory, or anti-inflammatory processes. Specific glycan forms have been associated with distinct immunological milieus (44). For example, increase in fucosylation and decrease in sialylation and galactosylation on the Fc glycan were observed during inflammatory conditions (45). There is an ongoing discussion whether these modifications are related to the expression of glycan-modifying enzymes like glycosyltransferases or whether other regulatory mechanisms are involved. Further studies are necessary to dissect the regulation of antibodies *in vivo* and this knowledge will also lead to the design and production of more efficient (glycoengineered) therapeutics, i.e. full-size mAbs or Fcabs, respectively.

Fig. 2 illustrates that C1q, the recognition subunit of C1 (i.e. the complex triggering activation of the classical pathway of complement) also binds at the N-termini of the CH2 domains. Similar to FcγRs, binding depends on the presence and mode of glycosylation at Asn297. It includes acidic and basic residues at CH2 but might also involve *in vivo* interaction with the CL domains of the Fab arms (46, 47). There are six heads on C1q, connected by collagen-like stems to a central stalk, and the isolated heads bind to the Fc rather weakly. Recently, it has been shown that antigen-binding on cell surfaces can facilitate the formation of IgG-hexamers and that these IgG-hexamers engage the headgroups of C1q (48). The resulting avidity effect increases the apparent affinity for C1q and triggers complement lysis. The IgG-hex-

amers are formed by non-covalent Fc–Fc interactions involving residues I253, H433, and N434. Mutation of these residues strongly reduces complement activation. Moreover, the authors also defined mutations in the IgG-Fc molecule that increased the formation of hexamers and thus resulted in improved activation of CDC. Thus, this study not only defined the molecular mechanism that triggers the classical pathway of complement but it also enabled the construction of Fc-mutants that activate the complement system more potently.

As mentioned above, one of the advantages of IgG-Fc-based therapeutic antibody fragments is the presence of a natural binding site for the neonatal Fc receptor FcRn (*Fig.* 2). FcRn mediates the transport of maternal IgG across the placenta in humans, thereby conferring humoral immunity to the fetus against antigens encountered by the mother (49). In addition, FcRn binds IgG with nanomolar affinity at acidic pH (≤6.5) in intracellular vesicles and releases it upon encountering the basic pH of the bloodstream (7.4). This recycling process prevents lysosomal degradation, ultimately resulting in prolonged serum half-life. The FcRn/Fc-binding interface spans a large surface area at the CH2–CH3 interdomain region. The center of the FcRn/Fc interface includes a hydrophobic core with surrounding salt bridges. At the Fc, the interface encompasses residues in the AB loop and the EF loop of the CH2 domain, as well as the G-strand of the CH3 domain (50).

Another highly specific receptor binding to the IgG-Fc region via its C-terminal PRYSPRY domain (*Fig.* 2) is the tripartite motif-containing 21 (TRIM21) protein. This cytosolic receptor recognizes antibody-opsonized pathogens and targets them to the proteasome through auto-ubiquitylation of E3 ubiquitin ligase. The neutralization mechanism of TRIM21 is thought to link the adaptive immune system with intracellular defense (51, 52).

Numerous other ligands bind to IgG-Fc, including proteins produced by microorganisms. The most prominent example is *Staphylococcus aureus* Protein A that binds with high affinity at the CH2–CH3 interface of IgG1 and IgG2 and is used for purification of mAb formats containing Fc (e.g. Fcabs).

Generation of novel and improvement of existing functions in IgG1-Fc

As outlined above, binding of ligands to IgG-Fc involves the N-termini of the CH2 domains as well as the CH2-CH3 interface (*Fig.* 2), whereas the C-termini of the CH3 domains are not affected. Each CH3 domain provides three C-terminal (structural) loops that can be diversified for the generation of novel antigen-binding sites: residues 358 to 362 (AB loop), residues 383 to 391 (CD loop) and residues 413 to 422 (EF loop) (*Fig.* 1). These loops correspond to regions with the most pronounced flexibility within IgG1-Fc (28). Upon engineering the loops, Fcabs, homodimeric Fc proteins with two potential antigen-binding sites in close vicinity, can be generated.

Wozniak-Knopp *et al.* (53) were the first to report the incorporation of antigen-binding properties in human IgG1-Fc. Five residues in each the AB loop (358–362) and the EF loop (413–415, 418–419) of the CH3 domain (compare with *Fig.* 1) were randomized using NNB degenerate codons and five additional random residues were inserted at position 415 to enlarge the potential binding surface. A 7.4×10^7 yeast surface display library was constructed and probed for binding to Protein A and FcγRI for comparison with surface-displayed wildtype IgG1-Fc. It was shown that a considerable amount of clones retained the binding to these proteins, suggesting structural integrity of the displayed molecules. Fc fragments binding to the extracellular domain of HER2 (an oncoprotein of the ERBB receptor family) were selected by fluorescence-activated cell sorting (FACS) using decreasing concentrations of the antigen. Next, the Fcab exhibiting the highest binding affinity was matured, yielding the final clone H10-03-6, for which specific binding to HER2 at a K_D value of 8.6 nM could be determined by surface plasmon resonance (SPR) spectroscopy. Moreover, H10-03-6 was shown to elicit ADCC in an experiment involving a HER2-expressing cell line and primary human NK cells to an extent that was approximately 20-fold lower than for trastuzumab, a monoclonal antibody binding to HER2 which is applied in the treatment of certain breast cancers (54). Importantly, no adverse effect of loop engineering on the *in vivo* half-life of the molecule could be determined after injection of H10-03-6 or wild-type IgG1-Fc in BALB/c mice.

The correlation of FcγRIIIa-binding affinity and ADCC in Fcabs was further investigated by Kainer *et al.*, who performed mutational studies to modulate ADCC potency. In a similar experiment as described above, HER2 overexpressing cells and NK cells were mixed and treated with variants of a HER2-binding Fc fragment carrying mutations that were previously reported to affect the affinity for FcγRIIIa. The authors concluded that known effects of the affinity-potency correlation can be assumed for the Fcab format (55).

A recently published study describes a more elaborate investigation of the *in vivo* and *in vitro* activity of H10-03-6

with a special emphasis on the comparison with the clinically approved anti-HER2 antibody trastuzumab (56). Complementing the work described above, the authors demonstrated the simultaneous binding of FcγRIIIa and HER2 to H10-03-6 in an SPR-spectroscopic experiment as well as binding of FcγRIIIa to H10-03-6 on the surface of HER2-expressing SKBr3 cells. It was demonstrated that the epitopes that are recognized by trastuzumab and H10-03-6 overlap. Interestingly, a human tumor cell proliferation assay revealed that, in contrast to trastuzumab, H10-03-6 is not able to inhibit proliferation in a dose-dependent manner. However, when a preclinical *in vivo* tumor xenotransplant model using human HER2 expressing BT-474 cells was used to confirm tumor-killing via ADCC, a significant retardation of tumor growth could be determined which provided proof of the biological activity of the Fcab despite its obvious differences in functionality compared to trastuzumab.

A complementary study on the ADCC potency of H10-03-6 was published by Jez *et al.* (57), who expressed the Fcab in human cells as well as wildtype and glycoengineered plants to generate four different glycoforms of H10-03-6. The authors describe the crucial importance of the glycosylation pattern on ADCC activity, thereby confirming the applicability of concepts reported for full-size IgG to the Fcab format.

Recently, the discovery and preclinical activity of a novel HER2-targeting Fcab, FS102, was reported (58). Residues 358–362 and 413–419 in the AB and EF loops, respectively, were randomized to construct a yeast surface display library, which was screened for binding to the extracellular domain of HER2. The structural integrity of specific clones was confirmed by their uncompromised binding to anti-CH2, FcγRI, and Protein A. One resulting Fcab, FS102, contained a total of nine amino acid substitutions in both loops (compared to wildtype IgG1-Fc) but exhibited similar biophysical properties, meaning no major structural deviation between the two molecules. FS102 binds HER2 with high affinity comparable to that of trastuzumab and pertuzumab, but does not compete with either mAb in binding to the receptor, suggesting that it is targeting a different epitope. Interestingly, FS102 induces profound HER2 internalization and degradation and, finally, tumor cell apoptosis, which is an important mode of action for antibody therapeutics. The antitumor effect of FS102 in patient-derived xenografts correlated strongly with the HER2 amplification status of the tumors. At gene copy numbers of >10 HER2 per cell, superior activity of FS102 over trastuzumab or the combination of trastuzumab and pertuzumab was observed both *in vitro* and *in vivo*, and FS102 induced complete and sustained tumor regression in a significant portion of HER2-high patient-derived xenograft tumor models. The mode of action of FS102 is still under discussion but might be related to the structure of the Fcab and its two potential HER2-binding sites that are close together (20–40 Å) and relatively inflexible compared to the two typical IgG antigen-binding sites (120–170 Å). It is possible that the Fcab favors a more ordered and tightly packed interaction with the antigen and thereby initiates pronounced aggregation and internalization of the Fcab/antigen complexes. Binding of the Fcab might also favor a conformation of HER2 that is more susceptible to degradation.

Aside from the successful introduction of novel binding sites into IgG1-Fc, it was demonstrated that the C-terminal loops in the CH3 domains can also be engineered to generate pH-dependent binding between the Fcab and the respective antigen. As serum half-life controlled by FcRn is a major parameter to be considered for the applicability of therapeutic antibodies, engineering pH-sensitivity into the interaction of antibodies with their targets may also increase the clinical potential of these molecules. Increasing the affinity to the antigen in the plasma (pH 7.4) while simultaneously decreasing the interactions at acidic pH potentially reduces antigen-mediated clearance in the lysosome and therefore allows for administration of therapeutic antibodies at lower frequencies and doses. It was demonstrated that prolonged half-life of tocilizumab, a humanized antibody against IL-6 receptor, and antibodies binding to proprotein convertase subtilisin kexin type 9 can be engineered by subjecting several residues within the CDR loops to histidine scanning. The authors suggested that the antibody–antigen complex dissociates at endosomal pH and the antibody is salvaged from degradation by binding to FcRn which recycles it back to the cell surface (59, 60).

To apply this concept to IgG1-Fc, the HER2-binding variant H10-03-6 was used as model Fcab and a library was constructed by applying parsimonious mutagenesis to the regions coding for the binding loops of H10-03-6 in order to generate pH-dependent binding sites. The resulting yeast surface display library was subjected to alternating selections for binding at pH 7.4 and non-binding at pH 6.0 (61). Fcab variants could be selected whose interaction with HER2 was pH-dependent not only in the yeast display format but also when HER2-positive SKBr3 cells were titrated with soluble Fcabs. Importantly, this effect was not caused by conformational changes, as shown by DSC and MD simulations. Only one variant contained a single His-substitution, but all

selected mutations were in the close proximity of existing histidines. The application of a surface display method for selections of pH-dependent binders in order to circumvent the labor-intensive histidine scanning approach was also demonstrated in a very recent study by Bonvin *et al.* (62). Here, scFv variants binding to the chemokine CXCL10 and enriched in histidine residues in the CDR-H3 were selected *de novo* from a phage library. Based on the selected lead clone, optimized libraries were constructed. When reformatted into human IgG1, the isolated antibody 1A4 inhibited CXCL10-induced chemotaxis with an IC50 of 1.6 nM. In addition, the strong pH-dependency was evidenced by performing a dose–response ELISA, where 1A4 exhibited a 167-fold lower affinity to CXCL10 at pH 6.0 than at pH 7.4.

Of course, not only can IgG1-Fc be engineered to obtain novel functionalities but also to improve existing functions. One example is the enhancement of the intrinsic property of ADCC elicitation. For instance, Lazar *et al.* (63) combined algorithms for computational prediction and high throughput screening methods to selectively optimize the affinity and specificity for FcγRs. Designed Fc variants of the HER2-binding monoclonal antibody trastuzumab exhibited ADCC enhancements over wildtype with the enhancement levels being proportional to the increase in affinity for FcγIIIa. Importantly, ADCC was observed for the engineered variants even with a cell line whose low surface levels of HER2 did not allow for ADCC detection after using wildtype trastuzumab. The authors concluded that especially for antibodies that fail in inhibiting proliferation, enhanced engagement of the immune system by Fc engineering and thus mediated killing, i.e. by ADCC and CDC, could prove to be important.

Another very promising and constantly growing field in which the engineering of IgG1-Fc plays an important role is the generation of bispecific antibodies (bsAbs), which are able to simultaneously target two different antigens while at the same time maintaining important functions of a mAb. A number of different bispecific formats are currently in clinical trials or already approved for cancer therapy, with catumaxomab (Fresenius Biotech), a mouse IgG2a and rat IgG2b hybrid antibody combining binding to CD3 and EpCAM that was approved in 2009, being a prominent example (64). Two other bsAbs include RG7221 (Roche, Basel, Switzerland), a clinical phase II bsAb designed to bind Angiopoietin 2 and VEGF-A, and LY3164530 bsAb (Eli Lilly, Indianapolis, IN, USA), currently being evaluated in clinical phase I and comprising binding sites for HER1 and c-Met (65–68).

The technologies proposed for the construction of the latter two molecules use different strategies to solve the light chain association problem. The CrossMAbCH1-CL technology from Roche ensures correct pairing of the light chains by rearranging the CH1 domain of one heavy chain with the CL domains of the corresponding light chain (69), while bispecificity of the LY3164530 antibody is partly achieved by creating an orthogonal interface through mutations in V and L domains for the correct assembly of the different Fab domains.

The second prerequisite for the generation of bispecific antibodies is the enforcement of the correct heavy chain heterodimerization over wrong homodimerization, which requires modification of the Fc fragment. The knob-into-holes (KiH) approach mimics a key-locks system by introducing a bulky residue in one CH3 domain that favors binding to a small residue in the other CH3 domain (70). Atwell *et al.* (71) extended the KiH technology by construction of a phage library of CH3 'hole' mutants which were tested for binding to the T366W knob mutant and were able to select a heterodimer variant with improved thermal stability. To further stabilize and increase the purity of the heterodimeric Fc, an artificial disulfide bond was introduced by Merchant *et al.* (72). The latter development was exploited for the production of the above-mentioned bsAb RG7221.

Another approach represents the SEEDbody technology, which is based on the fact that the CH3 domains of human IgG and IgA do not dimerize (73). By using molecular modeling, the authors investigated interdigitating β-strand segments of IgG and IgA CH3 domains for the generation of complementary heterodimer contact surfaces.

One further technology to enforce correct dimerization includes mutations at the interface of the CH3 domains altering charge polarity of the heavy chain monomers. Two negatively charged residues in chain A pair with two positively charged residues that were introduced in chain B (DD-KK variant) resulting in a high degree of heterodimer purity, but also a decrease in thermal stability of the CH3 domain (66, 74). Similarly, Strop *et al.* (75) identified mutations in the hinge region of human IgG1 and IgG2 that produce stabilizing ionic interactions. By combining these changes of the amino acid sequence with an additional mutation at the canonical position 409 in the CH3 domain, bispecificity was further enhanced. However, in this case both homodimers were first produced separately and then purified by affinity chromatography using protein A. Formation of heterodimers was induced by mixing both samples at equimolar ratios and

incubating them under reducing conditions at 37°C for 24 h, resulting in the most stably paired variant EEE-RRR for hIgG1. Moore *et al.* (76) identified residues in the CH3 interface promoting Fc heterodimerization by combining structural considerations with sequence information. Several variants were screened for the highest degree of heterodimerization, and an HA-TF variant was identified, where His and Thr are stabilized through a hydrogen bond and Ala and Phe act as key and lock.

Von Kreudenstein *et al.* described the heterodimer format ZW1 providing high thermal stability and 95% purity, with the residual 5% being present as monomeric, but not homodimeric CH2–CH3 subunits. By combination of *in silico* design and experimental screening, variants with high degrees of heterodimerization but low thermal stabilities were selected. Based on these initial results, modifications of the selected heterodimeric variants were designed toward increasing purity and stability. The leading format ZW1 carries four mutations on each CH3 domain located in the CH3–CH3 interface and exhibits wildtype-like Tm values (77).

In a very recent study, Choi *et al.* (78) combined electrostatic with asymmetric hydrophobic interactions and generated the EW-RVT Fc heterodimer. By introducing a disulfide bond between the CH3 domains they could further improve purity and thermal stability (79).

All of the above-mentioned approaches to the heterodimerization of heavy chains and the correct pairing of light chains aim at the production of full-size bsAbs providing one distinct specificity at each of the two Fab fragments. By contrast, application of the modular antibody technology would allow for the combination of these Fab-located binding sites with novel, artificial antigen-binding sites in the structural loops of constant domains. For example, the Fc of an existing mAb could be replaced with an Fcab to generate a so-called mAb^2 that bivalently binds to one antigen via its Fab fragments and mono- or bivalently to a second antigen via the Fcab portion (*Fig.* 3).

Engineering of the biophysical properties of IgG1-Fc

The correctness of the overall fold of IgG1-Fc variants was confirmed in many cases. Under some circumstances it was necessary to improve the biophysical properties of Fcabs, either in advance by including stabilizing measures in the construction of libraries to make use of the full versatility of the scaffold or by 'repairing' functionalized, yet impaired, Fc fragments, which were mainly selected from early generation combinatorial libraries. Also, even though the Fc fragment is an intrinsically stable protein, the engineering of its properties could further accentuate the advantages over other non-antibody-based protein therapeutics.

A detailed systematic study on the effect that the engineering of the C-terminal structural loops of the CH3 domain of IgG1-Fc has on the biophysical properties of the Fc fragment was published by Traxlmayr *et al.* (80), who inserted the αvβ3 integrin-binding RGD motif in the respective loops. This motif, in the context of the heptapeptide

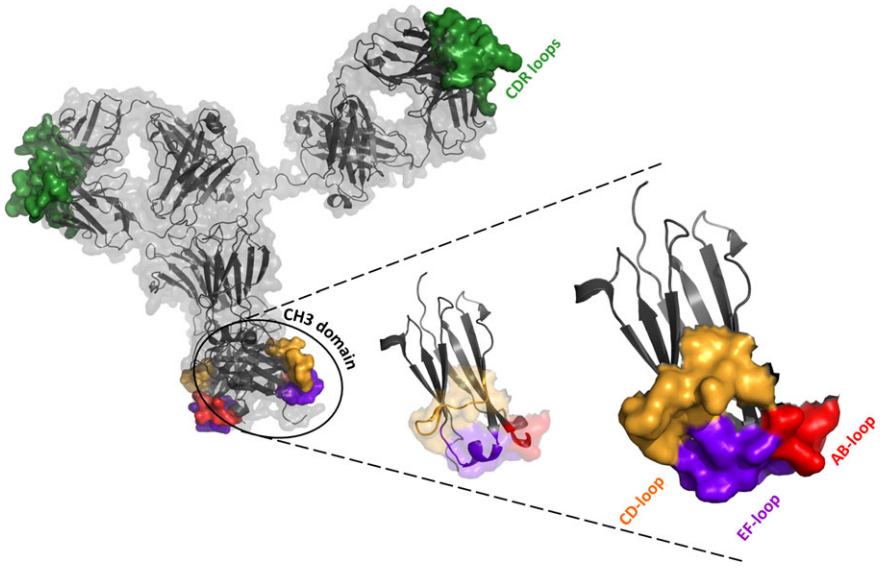

***Fig.* 3. Schematic representation of a hypothetical mAb2 [based on PDB-ID 1HZH (122)] and one isolated CH3 domain thereof.** Secondary structure elements of the antibody are colored in gray with the molecular surface of the CDR loops shown in green. Loop areas in the CH3 domains are displayed in red (AB loop), orange (CD loop), and purple (EF loop). The surface approximations of the three loops indicate the putative region for the generation of binding sites.

GCRGDCL, forms a cyclic and rather rigid structure as a consequence of disulfide bond formation by the flanking cysteines, resulting in increased interaction with integrins. Single-, double-, and triple-insertion variants (i.e. grafting of GCRGDCL into AB loop, CD loop, EF loop, AB+CD, AB+EF, or CD+EF) were expressed in *Pichia pastoris* and evaluated for the binding to soluble or cell surface-expressed αvβ3 integrin as well as for the effect of the engineering efforts on the overall fold and the structural integrity of the protein. Expression levels determined for the variants did not differ significantly from those determined for the wild-type protein, except for the heavily mutated triple-variant, where grafting of the rigid circular motif into each of the C-terminal loops apparently resulted in severe misfolding and degradation. Aside from wildtype-like expression levels, all other constructs exhibited high purity and homogeneity and eluted as single peaks and at defined elution volumes in size-exclusion chromatography, suggesting the correct folding of the proteins and the absence of aggregates. Also, using electronic circular dichroism spectroscopy, the overall secondary structure content was determined for each variant. No significant changes were observed for AB- and CD loop variants, whereas engineering of the EF loop apparently affected the helical content of the protein. This effect was also reflected in the strongly decreased stability of EF loop variants as determined by DSC. In contrast to that, manipulation of AB and CD loop destabilized the protein to a lesser degree. As expected, simultaneous insertion in two loops had a more pronounced effect on protein stability than single insertions. Furthermore, the interaction with natural ligands was analyzed by SPR spectroscopy and biolayer interferometry: FcRn-, Protein A-, and FcγRIIIa-binding revealed to be wildtype-like, which again confirmed the structural integrity of the recombinant proteins.

The importance of biophysical properties of antibody fragments for large-scale production and/or therapeutic efficacy has been demonstrated in various studies. Willuda *et al.* (81) described the correction of an anti-EGP-2 scFv fragment which, despite its high affinity, did not enrich at tumor xenografts. By grafting the binding residues of this scFv onto the framework of a more stable fragment and identification and introduction of stabilizing mutations, a functionally improved variant could be generated for which tumor localization was observed.

In a different study, antibodies directed against the chemokine CCL17 were selected from a Fab phage library designed by Shi *et al.* (82), many of them raised from the VH1-69 germline gene family abundant in the human immune repertoire (83). Sub-nanomolar binders could be isolated, which, however, exhibited strong non-specific protein–protein interaction and low solubility. The authors suggested that the high hydrophobicity of the germline CDR-H2 leads to these unfavorable properties. By generating a library with randomized surface-exposed residues within CDR-H1 and CDR-H2 to a group of biochemically distinct amino acids, a panel of novel clones could be isolated comprising both high affinity and reduced non-specific interactions. Surprisingly, the overall hydrophobicity of the selected clones was not significantly reduced, but three residues turned out to be critical in terms of undesired protein–protein interaction. Clones exhibiting a mutation at position I51 to polar or charged residues as well as at position F54 to small polar residues demonstrated higher solubility. Furthermore, mutation of P52 suggested a structural change to the loop associated with higher stability. This study reveals the challenge in selecting for high affinity and good biophysical properties and demonstrates the importance of combinatorial library design, which we will discuss later in this review.

One further study describes a monoclonal antibody that neutralizes binding of angiopoietin 2 to its receptor *in vitro* and inhibits tumor growth *in vivo* (84). Even though the pharmacological activity could be demonstrated, production of the antibody coincided with heterogeneity of the preparations, rapid aggregation, and poor expression yields. Exchange of a susceptible surface-exposed cysteine by all other 19 amino acids yielded a threonine-variant that exhibited reduced proneness to aggregation, improved homogeneity, largely increased expression levels, retained activity and, interestingly, the midpoint of denaturation shifted by 11°C, corresponding to a strongly improved thermal stability. The authors stated that the engineering process resulted in the fulfillment of requirements necessary for large-scale production in order to provide amounts of material sufficient for clinical trials.

Considering the conclusions from the above-mentioned work, comparable efforts proved to be beneficial for the Fc scaffold. One successful attempt to contribute to the development of a 'tool box' that would help the correction of impaired Fc fragments was published recently (85). In this work, IgG1-Fc scaffolds with increased thermal stabilities were constructed by following a directed evolution approach. The authors implemented a novel method that allows screening for stabilizing mutations in proteins that exhibit an already high thermal stability and T_m values of up to 85°C. Two libraries of IgG1-Fc variants differing in their

mutation rates were constructed by error-prone PCR targeting the entire gene. These libraries were then expressed in the yeast surface display format and incubated at 79°C in order to denature those variants displayed on yeast that were not stabilized by mutation. Variants that were still conformationally intact were stained with fluorescently labeled structure-specific markers, either FcγRI or anti-CH2 antibody, and thereby tagged for sorting of the displaying yeast cell by FACS. As a consequence of heat denaturation of the yeast cells, plasmid DNA coding for the stabilized variants had to be isolated, followed by re-transformation of *S. cerevisiae* and construction of novel libraries, now being enriched in variants carrying favorable mutations. A total of four sorting rounds were performed to select for the most stabilized variants in the libraries which were eventually identified by sequencing of the isolated plasmid DNA. Biophysical characterization of 17 single, double, and triple mutants expressed in *P. pastoris* revealed that all of the variants exhibited increased thermal stabilities and wildtype-like binding to relevant ligands, i.e. FcRn, FcγRIIIa, and Protein A. It was concluded that possible adverse effects of the artificial amino acid composition in the engineered loops might be counteracted by the introduction of the identified stabilizing mutations without negatively affecting the intrinsic functionality of the Fc fragment.

In addition, this original IgG1-Fc library pool generated by error-prone PCR and the selected libraries after one round of FACS were analyzed by high-throughput sequencing (86). For each amino acid position, the change in the mutation rate during selection was determined, indicating the tolerance to mutation at the respective position. As expected, selection for binding either to FcγRI or the anti-CH2 antibody resulted in reduced mutation rates. This was more pronounced in the CH3 domain reflecting the thermal denaturation pathway of IgG1-Fc with the reversibility of unfolding of the CH2 domain, as long as the CH3 domain remains natively folded. These data indicate a lower selection pressure for the CH2 domain, as only mutations either located in the binding site of the structure-specific markers or impeding the correct folding of the CH2 domain were eliminated. As both ligands that were used in this study bind to the CH2 domain, the changes in the mutation rates at positions in the CH3 domain were solely dependent on the impact of the respective side chain on foldability and/or stability, enabling the generation of a stability landscape of the CH3 domain. Importantly, positions that are evolutionarily conserved among different species were significantly less tolerant to mutation in these *in vitro* selections, validating the quality of the stability landscape. Furthermore, the experimentally derived tolerances to mutation correlated with the changes in the free energy of unfolding determined *in silico*. The results of this study not only revealed the sequence-stability relationship of an entire protein at single residue resolution but also proved to be an important tool for protein engineering, because library randomizations can be focused on mutation-tolerant regions of the protein. In addition, comparison of two selection experiments with different ligands (FcγRI and an anti-CH2 antibody) enabled the identification of their epitopes on IgG1-Fc.

In a follow-up project, this directed evolution protocol was applied to improve the biophysical properties of the HER2-binding Fcab H10-03-6 (87), which, even though the interaction with important effector molecules was wildtype-like, exhibited impaired biophysical properties in an initial characterization. In contrast to the method described above, mutagenesis was directed to the engineered loops only in order to minimize the overall changes the Fc fragment. An initial experiment revealed that the binding of H10-03-6 to HER2 was decreased after heat incubation, leading to the assumption that a correct fold is necessary for molecular recognition and that combination of heat shock and selection for ligand binding could be applied to simultaneously screen for improved thermal stability and retained affinity to the antigen. After heat incubation, the yeast displayed-library was either sorted for (i) binding to the antigen and to structurally specific ligands or (ii) binding to the antigen only. Enriched clones were expressed in *P. pastoris* and HEK293 cells and their biophysical properties were analyzed by SEC, ECD spectroscopy, and DSC. Stabilized variants resulting from the combined staining strategy (antigen and structurally specific ligand) exhibited higher thermal stabilities, which led to the assumption that this selection strategy should be favored. Importantly, all selected mutants were more stable than their parental clone H10-03-6. In addition, some stabilized Fcabs were less prone to aggregation after long term storage, showed more wildtype-like SEC elution profiles and the solubility of the Fcab exhibiting the highest thermal stability was largely increased when compared to the parental clone H10-03-6. The general applicability of this method to improve the biophysical properties of suitable proteins was concluded.

In addition, the differences in thermal stability of IgG1-Fc and Fcabs between the two expression systems, *P. pastoris* and HEK293, were analyzed. Generally, the high mannose glycan structures attached to Asn297 of the *P. pastoris*-produced Fc variants destabilizes the interface of the CH2

domains and therefore leads to lower T_m values. In a study by Schaefer and Pluckthun (88), significant differences between full-size IgGs produced in both expression systems revealed not only different temperatures of unfolding but also indicated differences in terms of aggregation susceptibility. Antibodies produced in *P. pastoris* were less prone to aggregate formation due their mannose-rich glycan structure and the N-terminal residual EAEA extension, remaining from the α-factor pre-pro secretion sequence. Although the thermal stability of *P. pastoris*-produced Fc variants was lower, the corresponding SEC elution profiles were highly comparable with the HEK-produced counterparts (87), as was the stability-ranking of Fcabs in both expression systems. This clearly underlined that *P. pastoris*-produced Fc variants can be used to investigate the biophysical properties and binding characteristics of a panel of selected Fcabs.

A different approach to stabilize IgG1-Fc in order to provide a stable scaffold for the engineering of antigen-binding sites or other novel functionalities is based on the insertion of artificial disulfide bonds based on computational prediction (89). Selected cysteine-variants were expressed in *P. pastoris* and their biophysical properties were characterized, revealing that the thermal stabilities of two variants bearing novel intradomain disulfide bonds were largely increased while the overall structure remained wildtype-like. Combination of both novel disulfide bonds resulted in even higher thermal stabilities. Moreover, stabilization of the HER2-binding Fcab H10-03-6 could be achieved by the introduction of only one of the disulfide bonds.

In a second study, the observation that the C-terminus of the CH3-dimer closely resembles the C-terminus of the CH1-CL-dimer of the Fab fragment led to the assumption that the three C-terminal amino acids of the CH3 domains could be replaced by those of the CL domain (90). The resulting variant exhibited a wildtype-like elution profile in SEC, leading to the assumption that specific disulfide bonding was accomplished and no incorrect cross-bridging occurred. Thermal denaturation of the protein occurred at significantly higher temperatures compared to wildtype IgG1-Fc and this effect was observed to be further pronounced in a variant carrying both the stabilizing inter- and intradomain disulfides. Interestingly, more detailed analysis by DSC revealed a strong stabilizing cooperative effect that the CH3-located alterations had on the CH2 domain. The introduction of both the computationally and rationally selected mutants into H10-03-6 increased the thermal stability of the protein to be approximately wildtype-like while antigen-binding was retained. Those identified mutations could serve as a valuable tool for stabilization of single proteins or entire libraries.

In a similar study, Gong *et al.* (91) described the stabilization of a monomeric human IgG1-CH2 domain by the introduction of artificial, rationally designed disulfide bonds. For two variants whose expression levels were comparable to the wildtype domain and which were highly soluble, increased thermal and conformational stabilities were determined in heat and chemical denaturation experiments. However, only for the more stable variant a monomeric state was determined. Structural changes in this variant as a consequence of the cysteine mutations were analyzed by NMR, once again confirming the correct formation of the novel disulfide bond. Nuclear Overhauser effect spectra were recorded and showed that the flexibility of both the wildtype CH2 domain and the stabilized variant were rigid in the framework but highly flexible in the loop regions. Based on these findings, it was suggested that the CH2 domain as well as its stabilized variant can be applied as scaffolds for engineering antigen binders.

In summary, the methods described in this section can be applied in several ways: One possibility is the introduction of thus identified stabilizing mutations in naïve libraries in order to 'prestabilize' the scaffold and thereby minimize the risk of selecting an Fcab with impaired biophysical properties. The combination of several beneficial mutations exhibiting additive stabilizing effects could not only compensate for destabilization upon mutation of the structural loops but also further improve the characteristics of the resulting binders. Moreover, starting from a stabilized protein scaffold has been shown to promote evolvability by tolerating a wider range of mutations (92). In other words, a library based on a stabilized protein contains a higher fraction of correctly folded and therefore functional protein mutants. A more elaborate way of exploiting stabilizing effects of single or multiple point mutations would be the 'repairing' of existing binders as a reaction to negative effects of loop mutations, as was shown for the HER2 binding Fcab H10-03-6.

Optimization of library design

The previous chapters have clearly shown that IgG1-Fc is a very attractive scaffold for the design of novel binding molecules that possess all antibody functions at only one-third of the size of a full-size IgG1 molecule. Like many other therapeutic antibodies, antibody-based and non-antibody-based molecules, Fcabs are selected from combinatorial libraries that became an alternative to conventional

methods, i.e. the hybridoma technology. The selection of proteins with the desired binding properties from these libraries is in many cases accomplished by the application of various display technologies such as phage, ribosome or yeast surface display (93). Therapeutic IgG1 molecules are generated by selecting either scFv or Fab from combinatorial phage libraries, or full-size IgG from yeast or mammalian display libraries. The three main aspects of such libraries that are known to impact library quality are (i) design, (ii) the origin of sequence diversity, and (iii) the method of library generation, while library quality can be assigned to the library size, diversity, and the developability of the selected molecules, i.e. high affinity and good biophysical properties. Maximization of library diversity can be accomplished by increasing the functional size and improving the resulting molecules' developability, which for example is achieved by restriction to one stable framework or a limited number of consensus frameworks. The issue of immunogenicity is met by choosing framework and CDR compositions as close to the human germline as possible (93).

The introduction of novel binding sites into non-complementarity-determing-region (CDR) loops in immunoglobulin-like domains of non-Ig proteins as well as immunoglobulin constant domains as already demonstrated in the context of Fcabs requires more elaborate considerations with respect to library design. While the lack of somatic hypermutation is, as is the case for CDR sequences of scFv or Fab fragments selected from combinatorial libraries, met by different affinity maturation strategies, the design of libraries for naïve selections is more challenging than in scFv or Fab libraries. First of all, there is little or no natural variation in the amino acid sequences of non-CDR loops and loop lengths are, in contrast to some CDR loops, mostly conserved. Information on typical amino acid compositions that can be drawn from the large pool of existing CDR sequences is not available for alternative scaffolds. And lastly, the knowledge of canonical CDR loop conformations is a design advantage that cannot be exploited in non-CDR loops as yet. Therefore, these favorable properties that are intrinsic to CDR loops have to be systematically investigated for non-CDR loops of Ig-derived and alternative binding scaffolds.

As the term 'antibody-based' is commonly used to describe formats that exploit the original binding site formed by the CDRs of either both or only one of the variable domains, antigen-binding IgG1-Fc, albeit derived from IgG1, will be classified as an 'alternative binding scaffold'. In this respect, the initial strategies that are pursued in order to provide a high degree of diversity, but also functionality, in libraries of different alternative binding scaffolds, are consistent. In this section, we will focus on these strategies and compare the library design efforts that have been made in the engineering of IgG1-Fc and other formats, especially the fibronectin type III scaffold, which, due to its immunoglobulin-like fold, is particularly interesting for comparison.

As mentioned above, the generation of diversity in alternative binding scaffolds cannot rely on the natural variation that is present in antibodies through somatic recombination and hypermutation during B-cell development. While in the course of this maturation process stable frameworks supporting diversity in variable domains are selected for, it is highly probable that diversification of one or several amino acid positions in alternative binding scaffolds impairs the overall protein fold to a certain degree. As mentioned above, in the case of Fcabs, it was shown that the introduction of an integrin-binding motif into each of the three C-terminal loops of IgG1-CH3 is possible while retaining the binding to generic ligands (80). However, overall folds of the proteins as well as thermal stabilities were impaired to some degree. The design of the first combinatorial libraries, i.e. the choice of amino acid positions in the C-terminal loops to be randomized, was based on the degree of evolutionary conservation and visual evaluation of the crystal structure of IgG1-Fc according to several criteria (solvent accessibility and structural independence of the respective amino acid side chains; generation of a coherent-binding surface) (15), and the applicability of this IgG1-Fc variant library was proved by isolating Fcabs binding to hen eggwhite lysozyme and CD20. Later, using an advanced library, it was shown that randomization of five positions in each the AB loop and the EF loop of IgG1-CH3 as well as insertion of five additional random amino acids in the EF loop, construction of a yeast surface display library and selection of IgG1-Fc variants binding to HER2 yielded well-expressing and biologically functional, yet slightly destabilized proteins (53). To circumvent this minor drawback already on the level of naïve libraries, two approaches have successfully been followed, which resulted in the construction of superior next generation libraries: First, prior to selections, naïve libraries can potentially be cleaned by isolating yeast cells that display IgG1-Fc still binding to conformationally specific ligands (e.g. Protein A or FcγRI) after diversification. Depending on the applied threshold of residual binding to these ligands, this cleaning step decreases the library size significantly. As an alternative, optimized regions of diversification were

identified for the generation of libraries of IgG1-Fc in order to minimize detrimental effects on the CH3 framework and increase the number of productive clones in the library (94). For this purpose, yeast surface display model libraries were constructed with distinct or overlapping regions randomized in the AB, CD, or EF loop of IgG1-CH3 and subjected to a protocol that involves the incubation at increasing temperatures of yeast suspensions induced for surface display and subsequent flow cytometric recording of the residual binding to conformationally specific ligands. Library denaturation curves were derived from the resulting mean fluorescent intensities and used for the determination of temperatures of half-maximal irreversible denaturation ($T_{1/2}$) of entire yeast libraries, yielding a clear hierarchy of the distinct loop regions' tolerance to randomization. IgG1-Fc libraries were re-designed based on these findings and are currently evaluated for their potential in the selection of Fcabs.

An approach to library design similar to the basic strategy pursued for Fcabs was published by Koide *et al.* (14), who identified the tenth type III unit of human fibronectin (^{10}Fn3), an immunoglobulin-like β-sandwich protein, as a potent binding scaffold. Similar to the involvement of the N-terminal loops BC, FG, and C'E of IgG1-CH2 in the binding of the Fcγ receptors (39), ^{10}Fn3 binds to integrin via the RGD motif in its FG loop. Initially, ^{10}Fn3 library design was based on sequence analyses of several fibronectin type III domains as well as structural evaluation of the loop architectures. Selections using a library with five residues randomized in each the BC and the FG loop yielded a ^{10}Fn3 variant binding to ubiquitin with an IC50 of 5 μM. However, this variant was less soluble at neutral pH than the wildtype ^{10}Fn3 protein and interacted with the column material in size-exclusion chromatography. In a follow-up study, it was suggested though that this negative side effect of mutation could be counteracted by the removal of unfavorable electrostatic interactions on the protein surface (95). Xu *et al.* (96) reported selections of ^{10}Fn3 variants binding to TNF-α. The 'master library' applied in these selections consisted of an equimolar mixture of three sublibraries having either one, two, or all three of the N-terminal ^{10}Fn3 loops randomized. Interestingly, all but one of the resulting TNF-α-binding ^{10}Fn3 variants stemmed from the sublibrary having all three loops randomized, indicating the importance of diversity for the isolation of high-affinity binders. Again, the stabilities reported for two representative variants were decreased. In a follow-up study, Parker *et al.* (97) reported the significant loss of stability and solubility of VEGF-R2-binding ^{10}Fn3 variants during affinity maturation, once more suggesting a trade-off between stability and affinity. The authors counteracted destabilization by structure-based site-directed mutagenesis, which also included the systematic reversion of randomized positions to their respective wildtype amino acids. Also, it was suggested to apply alternative designs of the apparently crucial DE loop of ^{10}Fn3. All of these findings were based on the biophysical characterization of a limited set of ^{10}Fn3 variants, which leads to the assumption that it would be possible to further enhance ^{10}Fn3 library design (i.e. at which positions the N-terminal loops can be randomized) by applying the flow cytometry-based method developed for libraries of IgG1-Fc to this scaffold as described above, even though it is focused on stability and does not take into account the effects library design will have on affinity (94). If, on the other hand, results from one further study on the ^{10}Fn3 scaffold by Lipovsek *et al.* (98) are taken into consideration, it can be expected that a higher number of randomized residues will increase the affinity of selected ^{10}Fn3 variants while, as mentioned above, stability and solubility will be impaired. Consequently, if information on the importance of distinct regions for the overall fold and stability of the scaffold is made available in a systematic manner, as was done for IgG1-Fc, desired affinities can be approached by manipulating increasing numbers of distinct loop positions while at the same time being aware of the effect this will have on the biophysical properties of the scaffold.

Besides the application of modular antibody engineering to the C-terminal loops of IgG1-Fc-CH3, various other studies have described the introduction of novel binding sites to immunoglobulin constant domains: Xiao *et al.* (10) identified HIV-1 inhibitors based on isolated IgG1-CH2 by randomizing the longest N-terminal loops in the domain, i.e. BC and FG. An interesting design feature was the addition of a glycine residue at the C-terminal end of each loop to provide flexibility and favor the accommodation of amino acid alterations necessary for stability and antigen recognition. However, as the stability of native CH2 is relatively low, the solubilities of three HIV-1-binding 'nanoantibodies' selected from this library were reported to be poor. To overcome these issues, the isolated CH2 domain was stabilized by introducing an additional disulfide bond and removing seven N-terminal residues (91, 99, 100). Starting from this scaffold, a library was constructed that comprised randomized BC and DE loops and a CDR-H3 from the HIV-1 gp120-binding VH m36 grafted in place of the FG loop (101). While one of two clones selected from this library

interacted non-competitively with an HIV-1 neutralizing epitope and FcRn, the second was not further characterized due to its aggregation proneness, leading to the authors' conclusion that further improvements to the library design would be necessary to develop IgG1-CH2 as a scaffold for the development of novel therapeutics.

Length variation of CDR loops is another important factor in the natural generation of diversity. Among the six CDR loops, H3 is the most diverse, both in terms of sequence and length. In a study on the clustering of antibody CDR loop confirmations, North *et al.* (102) assigned between two and eight different loop lengths to L1, L2, L3, H1, and H2, and 20 different lengths to H3, ranging from 5 to 26 residues. This length variability is introduced by imprecise joining during the combinatorial rearrangement of VH, DH, and JH genes in the course of B-cell maturation (103) and is considered to be a main contributor to the recognition of diverse antigens, as H3, given by its location in the center of the antigen-binding site, potentially controls the relative positions of VH and VL and affects the flexibility and cavity size of the paratope (104).

Consequently, in order to mimic this crucial aspect of the development of antigen specificity by the immune system, loop length variation in the antigen-binding sites of alternative scaffolds is an important factor in the generation of specific, high-affinity interactions. In the process of development of the Fcab scaffold, several steps have been made toward a loop elongation strategy that would allow for the selection of variants binding to diverse antigens while at the same time the intrinsic stability can be retained to a satisfactory degree. As mentioned above, the initial design for variant libraries of IgG1-Fc included the insertion of five additional residues at the N-terminal part of the EF loop, with this loop elongation aiding in the selection of an Fcab binding to HER2 with a K_D value of 8.6 nM (53). However, mutation and insertion negatively affected the biophysical properties of this Fcab (87). Therefore, one further aspect of the detailed analysis of the C-terminal loops of IgG1-CH3 was the systematic insertion of five additional random residues at different loop positions according to a sliding window (94). $T_{1/2}$ values were determined for the resulting yeast surface display libraries as described above and used for the comparison of the tolerance of different loop positions to insertion. The results from this study, as well as the identification of sites of natural insertion from phylogenetic analysis of IgG1-CH3 from different species, were also considered for the design of novel variant libraries of IgG1-Fc. As mentioned above, the evaluation of the effect of these design features is part of current investigations. Furthermore, findings from a study that dealt with the identification of stabilizing point mutations in IgG1-CH3 by using a directed evolution approach were combined with rational considerations (85, 105). In order to generate stabilizing stem regions that would allow for loop elongation, point mutations were introduced at two intrinsically stable motifs in the EF loop. The central part of this loop is constituted by an arginine residue forming a salt bridge with a glutamic acid in the CD loop, and a tryptophan residue that has been shown to be crucial for protein stability by contributing to the packing of the hydrophobic core. At the C-terminus of this RW motif, a glutamine residue was replaced by a stabilizing leucin residue. At the N-terminus of the adjacent F-strand, a serine between a phenylalanine also contributing to hydrophobic packing and a cysteine forming the intradomain disulfide bond was replaced by a stabilizing threonine. Yeast surface display libraries including or not including these stabilizing stem regions and carrying increasing numbers of additional residues in between them were constructed, and their stabilities were evaluated by using the yeast surface display-based method described above (94), showing that, indeed, a largely increased tolerance to loop elongation was achieved by this stabilization approach, with the potential of such libraries for the selection of Fcabs binding to diverse antigens being yet to be looked into.

While the work on the design of libraries of IgG1-Fc to date has focused on the question of how enhanced diversification, both in terms of site- or region-specific randomization and loop elongation, affects the overall fold and the biophysical properties of the scaffold, the trade-off between this focus and its effect on Fcab affinity is still under investigation. However, this has been addressed for other alternative formats, including the above-mentioned immunoglobulin-like ^{10}Fn3 scaffold, which is why the results of the underlying studies should be of interest in this context and a link can be made to ongoing and future projects dealing with IgG1-Fc. Koide *et al.* (106) performed basic experiments on the potential for elongation of all the loops in the ^{10}Fn3 domain, thereby providing some first information on the tolerance to insertion of alanines, which, of course, does not reveal the effect of full randomization. This was further investigated by Hackel *et al.* (107), who diversified all three N-terminal loops of ^{10}Fn3 both in length and composition. Four different lengths were chosen for each loop based on sequence analysis of ^{10}Fn3 from different species, and NNB degenerate codons were used to incorporate all 20 amino acids. Three FACS sortings of the

naïve library against lysozyme were performed. The output of this naïve selection was diversified by loop shuffling and error-prone PCR and sorted twice, followed by another four rounds of this procedure, yielding ^{10}Fn3 variants of single digit picomolar affinity and high sequence diversity, having accumulated a considerable number of beneficial framework mutations. Interestingly, further mutational studies on the DE loop of one particular high-affinity ^{10}Fn3 variant revealed that this loop can be either engineered to improve affinity or stability to a considerable degree. These results underline once more that library design for scaffolds based on immunoglobulin and immunoglobulin-like domains must undergo adjustments based both on the systematic evaluation of naïve libraries and selection outputs in order to efficiently approach an optimum balance of stability and affinity of relevant variant proteins.

The degree of CDR sequence diversification in combinatorial libraries of antibody-based alternative scaffolds, i.e. the usage of the amino acid repertoire, follows various different strategies. While naïve libraries provide natural diversity by combination of functional V-gene segments isolated from the lymphoid tissues of non-immunized donors [e.g. CAT 1.0 and CAT 2.0 libraries of Cambridge Antibody Technology (108, 109)], synthetic libraries such as the HuCALs (Morphosys) offer any desired amino acid compositions in the CDRs (110, 111). In general, it was observed that, despite the hypervariability of CDR sequences, there is a bias of functional CDRs to certain amino acid types, most of all tyrosine, glycine, and serine (112). Fellouse *et al.* showed that while scFv variants binding to some antigens at nanomolar affinities were selected from phage display libraries providing only a binary amino acid repertoire (i.e. tyrosine and serine), selections of binders from the same libraries to other antigens yielded affinities only in the micromolar range (113–115). Modifications of these libraries included an increased chemical diversity in CDR-H3 and the consideration of non-paratope residues potentially important for CDR conformation (116).

As mentioned above, Morphosys' HuCAL Fab libraries are fully synthetic, and they were developed over the course of several years (110, 111). The latest version, named HuCAL PLATINUM, offers, among other features, length variation in CDR-H2 and CDR-H3, and length-dependent amino acid frequencies as observed in the analysis of rearranged sequences, which was realized by using a large set of different trinucleotide mixtures. In principle, a similar approach is potentially valid for the construction of variant libraries of IgG1-Fc. Naturally, while the alignment of thousands of VH and VL sequences was used to generate information on the amino acid distributions in CDR loops, it cannot be estimated how, for example, binary codes or natural distributions in CDRs would influence the efficient isolation of well-developable Fcabs binding to diverse antigens at high affinities. Nevertheless, Hackel *et al.* investigated the effect of full or restricted diversity in ^{10}Fn3, which, again, can be a valuable source of information for the engineering of IgG1-Fc due to its immunoglobulin-like fold (117, 118). In these studies, the sequence-function landscape of the ^{10}Fn3 scaffold was approached by comparing various amino acid compositions in the N-terminal loops, leading to important conclusions: First, it was shown that maximal amino acid diversity is more beneficial for the selection of antigen-binding ^{10}Fn3 variants than a binary tyrosine/serine code as described above. And second, wildtype conservation at positions potentially important for structural integrity, as well as amino acid distribution biases toward the natural occurrence in CDRs made clear that both strategies were valuable for an efficient selection of binding ^{10}Fn3 variants. Consequently, while the identification of positions in IgG1-Fc-CH3 at which conservation of wildtype amino acids improves the biophysical properties of selected variants has been accomplished (86, 94), the application of tailored amino acid distributions as described above is a promising approach to be investigated in the future.

Conclusion

Over the past 30 years, therapeutic monoclonal antibodies and antibody-based alternative formats have been successfully developed, first by using the hybridoma technology and later by selection from combinatorial libraries. In this review, we introduced the potential of IgG1-Fc as a promising scaffold for the generation of alternative protein therapeutics. By applying the modular antibody engineering technology, novel binding sites for theoretically any desired antigen can be introduced in the C-terminal loops of the CH3 domains to create Fcabs, antigen-binding Fcs. In this way, the Fc is engineered to unite all important functions normally conveyed by full-size IgGs, i.e. (i) the mediation of effector functions through binding to FcγRs; (ii) contribution to a long half-life in serum through binding to FcRn, and (iii) (novel) binding to an antigen. FS102, a HER2-binding Fcab that has recently entered the clinic, is believed to accelerate aggregation and internalization of the antigen/

Fcab complexes as a consequence of the distinct Fcab structure, with pharmacokinetics not being impaired by the sequence changes in the CH3 domain.

In some cases, as has been described for other alternative scaffolds, the engineering process might negatively affect the biophysical properties of IgG1-Fc. The current article summarizes a set of methods, mostly based on directed evolution and yeast surface display, which provide a 'toolbox' for the correction of impaired biophysical properties of proteins in general. We also reviewed the various approaches to modifying IgG-Fc for the production of bispecific antibodies and described the highly promising concept of constructing mAb^2s, monoclonal antibodies with one specificity in the two antigen-binding sites of the Fabs and one additional specificity at the C-terminus of the Fc, which again can be accomplished by modular antibody engineering.

Finally, this review provides comments on potential further developments of libraries of IgG1-Fc. Loop position- and loop region-specific information has been obtained that will aid in the construction of libraries of high quality, and studies dealing with the modification of the architecture of the putative Fcab binding sites by loop elongation have been performed. Many approaches that have proved successful in the context of other alternative scaffolds, especially those targeting tailored amino acid distributions, can be used as models for the future investigation of libraries of IgG1-Fc, which will ultimately lead to a further accentuation of the intrinsically favorable properties of Fcabs.

References

1. Melmed GY, Targan SR, Yasothan U, Hanicq D, Kirkpatrick P. Certolizumab pegol. Nat Rev Drug Discov 2008;**7**:641–642.
2. Pieramici DJ, Avery RL. Ranibizumab: treatment in patients with neovascular age-related macular degeneration. Expert Opin Biol Ther 2006;**6**:1237–1245.
3. Genetta TB, Mauro VF. ABCIXIMAB: a new antiaggregant used in angioplasty. Ann Pharmacother 1996;**30**:251–257.
4. Bird RE, et al. Single-chain antigen-binding proteins. Science 1988;**242**:423–426.
5. Worn A, Pluckthun A. Stability engineering of antibody single-chain Fv fragments. J Mol Biol 2001;**305**:989–1010.
6. Raag R, Whitlow M. Single-chain Fvs. FASEB J 1995;**9**:73–80.
7. Baeuerle PA, Reinhardt C. Bispecific T-cell engaging antibodies for cancer therapy. Cancer Res 2009;**69**:4941–4944.
8. Holliger P, Prospero T, Winter G. Diabodies – small bivalent and bispecific antibody fragments. Proc Natl Acad Sci USA 1993;**90**:6444–6448.
9. Johnson S, et al. Effector cell recruitment with novel Fv-based dual-affinity re-targeting protein leads to potent tumor cytolysis and in vivo B-cell depletion. J Mol Biol 2010;**399**:436–449.
10. Xiao X, Feng Y, Vu BK, Ishima R, Dimitrov DS. A large library based on a novel (CH2) scaffold: identification of HIV-1 inhibitors. Biochem Biophys Res Commun 2009;**387**:387–392.
11. De Meyer T, Muyldermans S, Depicker A. Nanobody-based products as research and diagnostic tools. Trends Biotechnol 2014;**32**:263–270.
12. Harmsen MM, De Haard HJ. Properties, production, and applications of camelid single-domain antibody fragments. Appl Microbiol Biotechnol 2007;**77**:13–22.
13. Stumpp MT, Binz HK, Amstutz P. DARPins: a new generation of protein therapeutics. Drug Discovery Today 2008;**13**:695–701.
14. Koide A, Bailey CW, Huang X, Koide S. The fibronectin type III domain as a scaffold for novel binding proteins. J Mol Biol 1998;**284**:1141–1151.
15. Rüker F, Wozniak-Knopp G. Engineering of non-CDR loops in immunoglobulin domains. In: Little M ed. *Recombinant Antibodies for Immunotherapy*. New York: Cambridge University Press, 2009:231–242.
16. Halaby DM, Poupon A, Mornon J. The immunoglobulin fold family: sequence analysis and 3D structure comparisons. Protein Eng 1999;**12**:563–571.
17. Ying T, Gong R, Ju TW, Prabakaran P, Dimitrov DS. Engineered Fc based antibody domains and fragments as novel scaffolds. Biochim Biophys Acta 2014;**1844**:1977–1982.
18. Huber R, Deisenhofer J, Colman PM, Matsushima M, Palm W. Crystallographic structure studies of an IgG molecule and an Fc fragment. Nature 1976;**264**:415–420.
19. Hogarth PM, Pietersz GA. Fc receptor-targeted therapies for the treatment of inflammation, cancer and beyond. Nat Rev Drug Discov 2012;**11**:311–331.
20. Kabat EA, Wu TT, Perry HM, Gottesman KS, Foeller C. *Sequences of Proteins of Immunological Interest*. 5th edn. Bethesda, MD: National Institutes of Health, 1991:688–696.
21. Jefferis R, Lund J. Interaction sites on human IgG-Fc for FcgammaR: current models. Immunol Lett 2002;**82**:57–65.
22. Burton DR, Woof JM. Human antibody effector function. Adv Immunol 1992;**51**:1–84.
23. Deisenhofer J. Crystallographic refinement and atomic models of a human Fc fragment and its complex with fragment B of protein A from *Staphylococcus aureus* at 2.9- and 2.8-A resolution. Biochemistry 1981;**20**: 2361–2370.
24. Padlan EA. Anatomy of the antibody molecule. Mol Immunol 1994;**31**:169–217.
25. Kaneko Y, Nimmerjahn F, Ravetch JV. Anti-inflammatory activity of immunoglobulin G resulting from Fc sialylation. Science 2006;**313**:670–673.
26. Nimmerjahn F, Ravetch JV. Fcgamma receptors as regulators of immune responses. Nat Rev Immunol 2008;**8**:34–47.
27. Arnold JN, Wormald MR, Sim RB, Rudd PM, Dwek RA. The impact of glycosylation on the biological function and structure of human immunoglobulins. Annu Rev Immunol 2007;**25**:21–50.
28. Lai B, Hasenhindl C, Obinger C, Oostenbrink C. Molecular dynamics simulation of the crystallizable fragment of IgG1-insights for the design of Fcabs. Int J Mol Sci 2014;**15**:438–455.
29. Mimura Y, et al. The influence of glycosylation on the thermal stability and effector function expression of human IgG1-Fc: properties of a series of truncated glycoforms. Mol Immunol 2000;**37**:697–706.
30. Ghirlando R, Lund J, Goodall M, Jefferis R. Glycosylation of human IgG-Fc: influences on structure revealed by differential scanning micro-calorimetry. Immunol Lett 1999;**68**:47–52.
31. Vermeer AW, Norde W. The thermal stability of immunoglobulin: unfolding and aggregation of a multi-domain protein. Biophys J 2000;**78**:394–404.
32. Traxlmayr MW, Obinger C. Directed evolution of proteins for increased stability and expression using yeast display. Arch Biochem Biophys 2012;**526**:174–180.
33. Shusta EV, Holler PD, Kieke MC, Kranz DM, Wittrup KD. Directed evolution of a stable scaffold for T-cell receptor engineering. Nat Biotechnol 2000;**18**:754–759.
34. Boder ET, Wittrup KD. Yeast surface display for screening combinatorial polypeptide libraries. Nat Biotechnol 1997;**15**:553–557.
35. Hulett MD, Hogarth PM. Molecular basis of Fc receptor function. Adv Immunol 1994;**57**:1–127.
36. Fridman WH. Fc receptors and immunoglobulin binding factors. FASEB J 1991;**5**:2684–2690.
37. Wines BD, Powell MS, Parren PW, Barnes N, Hogarth PM. The IgG Fc contains distinct Fc receptor (FcR) binding sites: the leukocyte receptors Fc gamma RI and Fc gamma RIIa bind

to a region in the Fc distinct from that recognized by neonatal FcR and protein A. J Immunol 2000;**164**:5313–5318.
38. Feige MJ, Nath S, Catharino SR, Weinfurtner D, Steinbacher S, Buchner J. Structure of the murine unglycosylated IgG1 Fc fragment. J Mol Biol 2009;**391**:599–608.
39. Sazinsky SL, Ott RG, Silver NW, Tidor B, Ravetch JV, Wittrup KD. Aglycosylated immunoglobulin G1 variants productively engage activating Fc receptors. Proc Natl Acad Sci USA 2008;**105**:20167–20172.
40. Lund J, Takahashi N, Pound JD, Goodall M, Jefferis R. Multiple interactions of IgG with its core oligosaccharide can modulate recognition by complement and human Fc gamma receptor I and influence the synthesis of its oligosaccharide chains. J Immunol 1996;**157**:4963–4969.
41. Jefferis R, Lund J, Pound J. Molecular definition of interaction sites on human IgG for Fc receptors (huFc gamma R). Mol Immunol 1990;**27**:1237–1240.
42. Shields RL, et al. High resolution mapping of the binding site on human IgG1 for Fc gamma RI, Fc gamma RII, Fc gamma RIII, and FcRn and design of IgG1 variants with improved binding to the Fc gamma R. J Biol Chem 2001;**276**:6591–6604.
43. Ravetch JV, Bolland S. IgG Fc receptors. Annu Rev Immunol 2001;**19**:275–290.
44. Anthony RM, Wermeling F, Ravetch JV. Novel roles for the IgG Fc glycan. Ann N Y Acad Sci 2012;**1253**:170–180.
45. Gornik I, Maravic G, Dumic J, Flogel M, Lauc G. Fucosylation of IgG heavy chains is increased in rheumatoid arthritis. Clin Biochem 1999;**32**:605–608.
46. Duncan AR, Winter G. The binding site for C1q on IgG. Nature 1988;**332**:738–740.
47. Gaboriaud C, et al. The crystal structure of the globular head of complement protein C1q provides a basis for its versatile recognition properties. J Biol Chem 2003;**278**:46974–46982.
48. Diebolder CA, et al. Complement is activated by IgG hexamers assembled at the cell surface. Science 2014;**343**:1260–1263.
49. Ghetie V, Ward ES. Multiple roles for the major histocompatibility complex class I- related receptor FcRn. Annu Rev Immunol 2000;**18**:739–766.
50. Martin WL, West AP Jr, Gan L, Bjorkman PJ. Crystal structure at 2.8 A of an FcRn/heterodimeric Fc complex: mechanism of pH-dependent binding. Mol Cell 2001;**7**:867–877.
51. Mallery DL, McEwan WA, Bidgood SR, Towers GJ, Johnson CM, James LC. Antibodies mediate intracellular immunity through tripartite motif-containing 21 (TRIM21). Proc Natl Acad Sci USA 2010;**107**:19985–19990.
52. Randow F, MacMicking JD, James LC. Cellular self-defense: how cell-autonomous immunity protects against pathogens. Science 2013;**340**:701–706.
53. Wozniak-Knopp G, et al. Introducing antigen-binding sites in structural loops of immunoglobulin constant domains: Fc fragments with engineered HER2/neu-binding sites and antibody properties. Protein Eng Des Sel 2010;**23**:289–297.
54. Chernajovsky Y, et al. *Herceptin. Therapeutic Antibodies*. Berlin, Heidelberg: Springer, 2008:183–219.
55. Kainer M, et al. Correlation between CD16a binding and immuno effector functionality of an antigen specific immunoglobulin Fc fragment (Fcab). Arch Biochem Biophys 2012;**526**:154–158.
56. Woisetschläger M, et al. In vivo and in vitro activity of an immunoglobulin Fc fragment (Fcab) with engineered Her-2/neu binding sites. Biotechnol J 2014;**9**:844–851.
57. Jez J, et al. Significant impact of single N-glycan residues on the biological activity of Fc-based antibody-like fragments. J Biol Chem 2012;**287**:24313–24319.
58. Leung KM, et al. A HER2-specific modified Fc fragment (Fcab) induces antitumor effects through degradation of HER2 and apoptosis. Mol Ther 2015; in press.
59. Chaparro-Riggers J, et al. Increasing serum half-life and extending cholesterol lowering in vivo by engineering antibody with pH-sensitive binding to PCSK9. J Biol Chem 2012;**287**:11090–11097.
60. Igawa T, et al. Antibody recycling by engineered pH-dependent antigen binding improves the duration of antigen neutralization. Nat Biotechnol 2010;**28**:1203–1207.
61. Traxlmayr MW, et al. Construction of pH-sensitive Her2-binding IgG1-Fc by directed evolution. Biotechnol J 2014;**9**:1013–1022.
62. Bonvin P, et al. De novo isolation of antibodies with pH-dependent binding properties. MAbs 2015;**7**:294–302.
63. Lazar GA, et al. Engineered antibody Fc variants with enhanced effector function. Proc Natl Acad Sci USA 2006;**103**:4005–4010.
64. Heiss MM, et al. The trifunctional antibody catumaxomab for the treatment of malignant ascites due to epithelial cancer: results of a prospective randomized phase II/III trial. Int J Cancer 2010;**127**:2209–2221.
65. Kienast Y, et al. Ang-2-VEGF-A CrossMab, a novel bispecific human IgG1 antibody blocking VEGF-A and Ang-2 functions simultaneously, mediates potent antitumor, antiangiogenic, and antimetastatic efficacy. Clin Cancer Res 2013;**19**:6730–6740.
66. Kontermann RE, Brinkmann U. Bispecific antibodies. Drug Discov Today 2015;**20**:838–847.
67. Lewis SM, et al. Generation of bispecific IgG antibodies by structure-based design of an orthogonal Fab interface. Nat Biotechnol 2014;**32**:191–198.
68. Weidle UH, Kontermann RE, Brinkmann U. Tumor-antigen-binding bispecific antibodies for cancer treatment. Semin Oncol 2014;**41**:653–660.
69. Schaefer W, et al. Immunoglobulin domain crossover as a generic approach for the production of bispecific IgG antibodies. Proc Natl Acad Sci USA 2011;**108**:11187–11192.
70. Ridgway JB, Presta LG, Carter P. 'Knobs-into-holes' engineering of antibody CH3 domains for heavy chain heterodimerization. Protein Eng 1996;**9**:617–621.
71. Atwell S, Ridgway JB, Wells JA, Carter P. Stable heterodimers from remodeling the domain interface of a homodimer using a phage display library. J Mol Biol 1997;**270**:26–35.
72. Merchant AM, et al. An efficient route to human bispecific IgG. Nat Biotechnol 1998;**16**:677–681.
73. Davis JH, et al. SEEDbodies: fusion proteins based on strand-exchange engineered domain (SEED) CH3 heterodimers in an Fc analogue platform for asymmetric binders or immunofusions and bispecific antibodies. Protein Eng Des Sel 2010;**23**:195–202.
74. Gunasekaran K, et al. Enhancing antibody Fc heterodimer formation through electrostatic steering effects: applications to bispecific molecules and monovalent IgG. J Biol Chem 2010;**285**:19637–19646.
75. Strop P, et al. Generating bispecific human IgG1 and IgG2 antibodies from any antibody pair. J Mol Biol 2012;**420**:204–219.
76. Moore GL, et al. A novel bispecific antibody format enables simultaneous bivalent and monovalent co-engagement of distinct target antigens. MAbs 2011;**3**:546–557.
77. Von Kreudenstein TS, et al. Improving biophysical properties of a bispecific antibody scaffold to aid developability: quality by molecular design. MAbs 2013;**5**:646–654.
78. Choi HJ, Kim YJ, Lee S, Kim YS. A heterodimeric Fc-based bispecific antibody simultaneously targeting VEGFR-2 and Met exhibits potent antitumor activity. Mol Cancer Ther 2013;**12**:2748–2759.
79. Choi HJ, Seok SH, Kim YJ, Seo MD, Kim YS. Crystal structures of immunoglobulin Fc heterodimers reveal the molecular basis for heterodimer formation. Mol Immunol 2015;**65**:377–383.
80. Traxlmayr MW, Wozniak-Knopp G, Antes B, Stadlmayr G, Ruker F, Obinger C. Integrin binding human antibody constant domains–probing the C-terminal structural loops for grafting the RGD motif. J Biotechnol 2011;**155**:193–202.
81. Willuda J, et al. High thermal stability is essential for tumor targeting of antibody fragments: engineering of a humanized anti-epithelial glycoprotein-2 (epithelial cell adhesion molecule) single-chain Fv fragment. Cancer Res 1999;**59**:5758–5767.
82. Shi L, et al. De novo selection of high-affinity antibodies from synthetic fab libraries displayed on phage as pIX fusion proteins. J Mol Biol 2010;**397**:385–396.
83. Kehoe JW, et al. Isolation and optimization for affinity and biophysical characteristics of anti-CCL17 antibodies from the VH1-69 germline gene. Protein Eng Des Sel 2014;**27**:199–206.
84. Buchanan A, et al. Engineering a therapeutic IgG molecule to address cysteinylation, aggregation and enhance thermal stability and expression. MAbs 2013;**5**:255–262.

85. Traxlmayr MW, et al. Directed evolution of stabilized IgG1-Fc scaffolds by application of strong heat shock to libraries displayed on yeast. Biochim Biophys Acta 2012;**1824**:542–549.
86. Traxlmayr MW, et al. Construction of a stability landscape of the CH3 domain of human IgG1 by combining directed evolution with high throughput sequencing. J Mol Biol 2012;**423**:397–412.
87. Traxlmayr MW, et al. Directed evolution of Her2/neu-binding IgG1-Fc for improved stability and resistance to aggregation by using yeast surface display. Protein Eng Des Sel 2013;**26**:255–265.
88. Schaefer JV, Pluckthun A. Engineering aggregation resistance in IgG by two independent mechanisms: lessons from comparison of Pichia pastoris and mammalian cell expression. J Mol Biol 2012;**417**:309–335.
89. Wozniak-Knopp G, Stadlmann J, Ruker F. Stabilisation of the Fc fragment of human IgG1 by engineered intradomain disulfide bonds. PLoS ONE 2012;**7**:e30083.
90. Wozniak-Knopp G, Ruker F. A C-terminal interdomain disulfide bond significantly stabilizes the Fc fragment of IgG. Arch Biochem Biophys 2012;**526**:181–187.
91. Gong R, et al. Engineered human antibody constant domains with increased stability. J Biol Chem 2009;**284**:14203–14210.
92. Bloom JD, Labthavikul ST, Otey CR, Arnold FH. Protein stability promotes evolvability. Proc Natl Acad Sci USA 2006;**103**:5869–5874.
93. Ponsel D, Neugebauer J, Ladetzki-Baehs K, Tissot K. High affinity, developability and functional size: the holy grail of combinatorial antibody library generation. Molecules 2011;**16**:3675–3700.
94. Hasenhindl C, et al. Stability assessment on a library scale: a rapid method for the evaluation of the commutability and insertion of residues in C-terminal loops of the CH3 domains of IgG1-Fc. Protein Eng Des Sel 2013;**26**:675–682.
95. Koide A, Jordan MR, Horner SR, Batori V, Koide S. Stabilization of a fibronectin type III domain by the removal of unfavorable electrostatic interactions on the protein surface. Biochemistry 2001;**40**:10326–10333.
96. Xu L, et al. Directed evolution of high-affinity antibody mimics using mRNA display. Chem Biol 2002;**9**:933–942.
97. Parker MH, et al. Antibody mimics based on human fibronectin type three domain engineered for thermostability and high-affinity binding to vascular endothelial growth factor receptor two. Protein Eng Des Sel 2005;**18**:435–444.
98. Lipovsek D, et al. Evolution of an interloop disulfide bond in high-affinity antibody mimics based on fibronectin type III domain and selected by yeast surface display: molecular convergence with single-domain camelid and shark antibodies. J Mol Biol 2007;**368**:1024–1041.
99. Gong R, Wang Y, Feng Y, Zhao Q, Dimitrov DS. Shortened engineered human antibody CH2 domains: increased stability and binding to the human neonatal Fc receptor. J Biol Chem 2011;**286**:27288–27293.
100. Gong R, et al. N-terminal truncation of an isolated human IgG1 CH2 domain significantly increases its stability and aggregation resistance. Mol Pharm 2013;**10**:2642–2652.
101. Gong R, Wang Y, Ying T, Dimitrov DS. Bispecific engineered antibody domains (nanoantibodies) that interact noncompetitively with an HIV-1 neutralizing epitope and FcRn. PLoS ONE 2012;**7**:e42288.
102. North B, Lehmann A, Dunbrack RL Jr. A new clustering of antibody CDR loop conformations. J Mol Biol 2011;**406**:228–256.
103. Desiderio SV, et al. Insertion of N regions into heavy-chain genes is correlated with expression of terminal deoxytransferase in B cells. Nature 1984;**311**:752–755.
104. Furukawa K, Shirai H, Azuma T, Nakamura H. A role of the third complementarity-determining region in the affinity maturation of an antibody. J Biol Chem 2001;**276**:27622–27628.
105. Hasenhindl C, et al. Creating stable stem regions for loop elongation in Fcabs – insights from combining yeast surface display, in silico loop reconstruction and molecular dynamics simulations. Biochim Biophys Acta 2014;**1844**:1530–1540.
106. Batori V, Koide A, Koide S. Exploring the potential of the monobody scaffold: effects of loop elongation on the stability of a fibronectin type III domain. Protein Eng 2002;**15**:1015–1020.
107. Hackel BJ, Kapila A, Wittrup KD. Picomolar affinity fibronectin domains engineered utilizing loop length diversity, recursive mutagenesis, and loop shuffling. J Mol Biol 2008;**381**:1238–1252.
108. Lloyd C, et al. Modelling the human immune response: performance of a 1011 human antibody repertoire against a broad panel of therapeutically relevant antigens. Protein Eng Des Sel 2009;**22**:159–168.
109. Vaughan TJ, et al. Human antibodies with sub-nanomolar affinities isolated from a large non-immunized phage display library. Nat Biotechnol 1996;**14**:309–314.
110. Knappik A, et al. Fully synthetic human combinatorial antibody libraries (HuCAL) based on modular consensus frameworks and CDRs randomized with trinucleotides. J Mol Biol 2000;**296**:57–86.
111. Prassler J, et al. HuCAL PLATINUM, a synthetic Fab library optimized for sequence diversity and superior performance in mammalian expression systems. J Mol Biol 2011;**413**:261–278.
112. Zemlin M, et al. Expressed murine and human CDR-H3 intervals of equal length exhibit distinct repertoires that differ in their amino acid composition and predicted range of structures. J Mol Biol 2003;**334**:733–749.
113. Fellouse FA, Barthelemy PA, Kelley RF, Sidhu SS. Tyrosine plays a dominant functional role in the paratope of a synthetic antibody derived from a four amino acid code. J Mol Biol 2006;**357**:100–114.
114. Fellouse FA, Li B, Compaan DM, Peden AA, Hymowitz SG, Sidhu SS. Molecular recognition by a binary code. J Mol Biol 2005;**348**:1153–1162.
115. Fellouse FA, Wiesmann C, Sidhu SS. Synthetic antibodies from a four-amino-acid code: a dominant role for tyrosine in antigen recognition. Proc Natl Acad Sci USA 2004;**101**:12467–12472.
116. Fellouse FA, et al. High-throughput generation of synthetic antibodies from highly functional minimalist phage-displayed libraries. J Mol Biol 2007;**373**:924–940.
117. Hackel BJ, Ackerman ME, Howland SW, Wittrup KD. Stability and CDR composition biases enrich binder functionality landscapes. J Mol Biol 2010;**401**:84–96.
118. Hackel BJ, Wittrup KD. The full amino acid repertoire is superior to serine/tyrosine for selection of high affinity immunoglobulin G binders from the fibronectin scaffold. Protein Eng Des Sel 2010;**23**:211–219.
119. Kiyoshi M, et al. Structural basis for binding of human IgG1 to its high-affinity human receptor FcγRI. Nat Commun 2015;**6**:6866.
120. James LC, Keeble AH, Khan Z, Rhodes DA, Trowsdale J. Structural basis for PRYSPRY-mediated tripartite motif (TRIM) protein function. Proc Natl Acad Sci USA 2007;**104**:6200–6205.
121. Schneider S, Zacharias M. Atomic resolution model of the antibody Fc interaction with the complement C1q component. Mol Immunol 2012;**51**:66–72.
122. Saphire EO, et al. Crystal structure of a neutralizing human IGG against HIV-1: a template for vaccine design. Science 2001;**293**:1155–1159.

Fcab–HER2 Interaction: a Ménage à Trois. Lessons from X-Ray and Solution Studies

Lobner E., Humm A., Göritzer K., Mylnek G., Puchinger M.G., Hasenhindl C., Rüker F., Traxlmayr M.W., Djinović-Carugo K. and Obinger C.

Research article

Structure (2017), 25(6): 878-889.e5. doi: 10.1016/j.str.2017.04.014.

Structure

Fcab-HER2 Interaction: a Ménage à Trois. Lessons from X-Ray and Solution Studies

Graphical Abstract

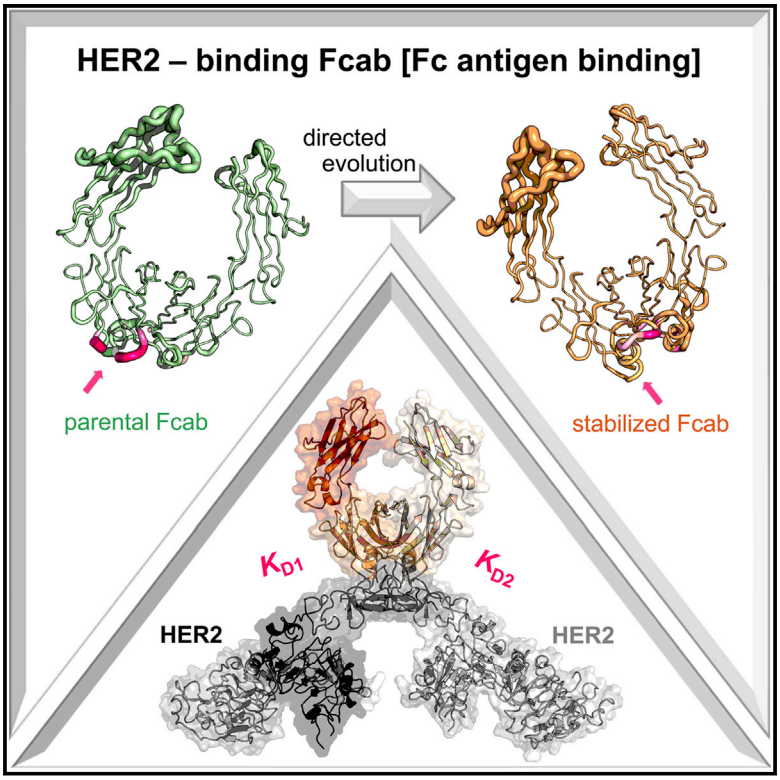

Authors

Elisabeth Lobner, Anne-Sophie Humm, Kathrin Göritzer, ..., Michael W. Traxlmayr, Kristina Djinović-Carugo, Christian Obinger

Correspondence

christian.obinger@boku.ac.at

In Brief

Lobner et al. determined the first crystal structures of two different Fcabs (Fc domain with antigen-binding sites) and their co-crystal structures together with HER2. Along with solution studies the authors show that one Fcab can bind two HER2 molecules in a negative cooperative binding mode.

Highlights

- The first X-ray structures of Fcabs (Fc antigen binding) confirm their intact fold
- Varieties in Fcab stability mainly arise from folding differences of binding loops
- The co-crystal structure shows that the Fcab interacts with two HER2 molecules
- Solution studies indicate a negative cooperative binding behavior of Fcab with HER2

Lobner et al., 2017, Structure *25*, 878–889
June 6, 2017
http://dx.doi.org/10.1016/j.str.2017.04.014

CellPress

Structure
Article

Fcab-HER2 Interaction: a Ménage à Trois. Lessons from X-Ray and Solution Studies

Elisabeth Lobner,[1,2] Anne-Sophie Humm,[1,3] Kathrin Göritzer,[1,2] Georg Mlynek,[3] Martin G. Puchinger,[3] Christoph Hasenhindl,[1,2] Florian Rüker,[4] Michael W. Traxlmayr,[1,2] Kristina Djinović-Carugo,[3,5] and Christian Obinger[1,2,6,*]

[1]Christian Doppler Laboratory for Antibody Engineering
[2]Department of Chemistry, Division of Biochemistry
BOKU – University of Natural Resources and Life Sciences, Muthgasse 18, 1190 Vienna, Austria
[3]Department for Structural and Computational Biology, Max F. Perutz Laboratories, University of Vienna, Dr. Bohr-Gasse 9, 1030 Vienna, Austria
[4]Department of Biotechnology, BOKU – University of Natural Resources and Life Sciences, Muthgasse 18, 1190 Vienna, Austria
[5]Department of Biochemistry, Faculty of Chemistry and Chemical Technology, University of Ljubljana, Večna pot 113, 1000 Ljubljana, Slovenia
[6]Lead Contact
*Correspondence: christian.obinger@boku.ac.at
http://dx.doi.org/10.1016/j.str.2017.04.014

SUMMARY

The crystallizable fragment (Fc) of the immunoglobulin class G (IgG) is an attractive scaffold for the design of novel therapeutics. Upon engineering the C-terminal loops in the CH3 domains, Fcabs (Fc domain with antigen-binding sites) can be designed. We present the first crystal structures of Fcabs, i.e., of the HER2-binding clone H10-03-6 having the AB and EF loop engineered and the stabilized version STAB19 derived by directed evolution. Comparison with the crystal structure of the Fc wild-type protein reveals conservation of the overall domain structures but significant differences in EF-loop conformations. Furthermore, we present the first Fcab-antigen complex structures demonstrating the interaction between the engineered Fcab loops with domain IV of HER2. The crystal structures of the STAB19-HER2 and H10-03-6-HER2 complexes together with analyses by isothermal titration calorimetry, SEC-MALS, and fluorescence correlation spectroscopy show that one homodimeric Fcab binds two HER2 molecules following a negative cooperative binding behavior.

INTRODUCTION

To date the antibody landscape counts 63 therapeutic products on the market, including three antibody-drug conjugates, two bispecific antibodies and three Fab fragments (antibodysociety.org, update: May 2017). Considering the high number of different antibodies and antibody formats that are currently being evaluated in the clinic together with the increasing demand for targeted therapies and the emerging sector of immuno-oncology, the number of approved antibodies on the market will rise significantly in coming years.

The first generation of antibody drugs simply mimicked the natural immunoglobulin class G1 (IgG1) topology with two antigen-binding fragments (Fabs) and one crystallizable fragment (Fc). The next generation focused on making smaller fragments of the full-size IgG (~150 kDa), including scFvs (~25 kDa), Fabs (~50 kDa), and minibodies (~80 kDa), and even smaller alternative binding domains have been engineered (e.g., DARPins or affibodies) (Holliger and Hudson, 2005; Spiess et al., 2015). However, most of these scaffolds lack the major asset of a full-size IgG, namely the crystallizable fragment (Fc), responsible for mediating effector functions such as antibody-dependent cellular cytotoxicity (ADCC), complement-dependent cytotoxicity, and the interaction with the neonatal Fc receptor (FcRn), which mediates the long in vivo half-life (Kubota et al., 2009).

One interesting development in the field is the use of the Fc fragment of IgG1 (50 kDa) for the design of Fc domains with antigen-binding sites (i.e., Fcabs). The starting scaffold for engineering is the dimeric Fc region with each chain (T225-K447, Eu numbering system [Edelman et al., 1969]) consisting of the (constant) CH2 and CH3 domains, with each domain being composed of two β-sheets adopting the typical immunoglobulin fold (Figure 1) (Halaby et al., 1999). Both chains are covalently linked by two disulfide bridges in the N-terminal hinge region and glycosylated at N297 (CH2 domain). This post-translational modification is key for modulating pharmacokinetics and effector functions (Higel et al., 2016; Quast et al., 2017) Each CH3 domain provides three C-terminal (structural) loops that can be engineered for the generation of novel antigen-binding sites: residues 355–362 (AB loop), residues 383–391 (CD loop), and residues 413–422 (EF loop) (Figure 1) (Edelman et al., 1969; Lobner et al., 2016). In 2010 the first generation of an Fcab with high affinity to the breast cancer-associated tumor antigen HER2 was reported (Wozniak-Knopp et al., 2010). This Fcab clone H10-03-6 was shown to trigger ADCC activity of natural killer cells against an HER2-positive cell line, and the in vivo half-life in mice was similar to that of wild-type IgG1-Fc (Fc-wt) (Wozniak-Knopp et al., 2010). Further studies described more elaborate investigations of the in vitro and in vivo activities of this HER2-binding Fcab, e.g., demonstrating that the Fcab H10-03-6 competes with the clinically approved antibody trastuzumab for HER2 binding (Jez et al., 2012; Woisetschläger et al.,

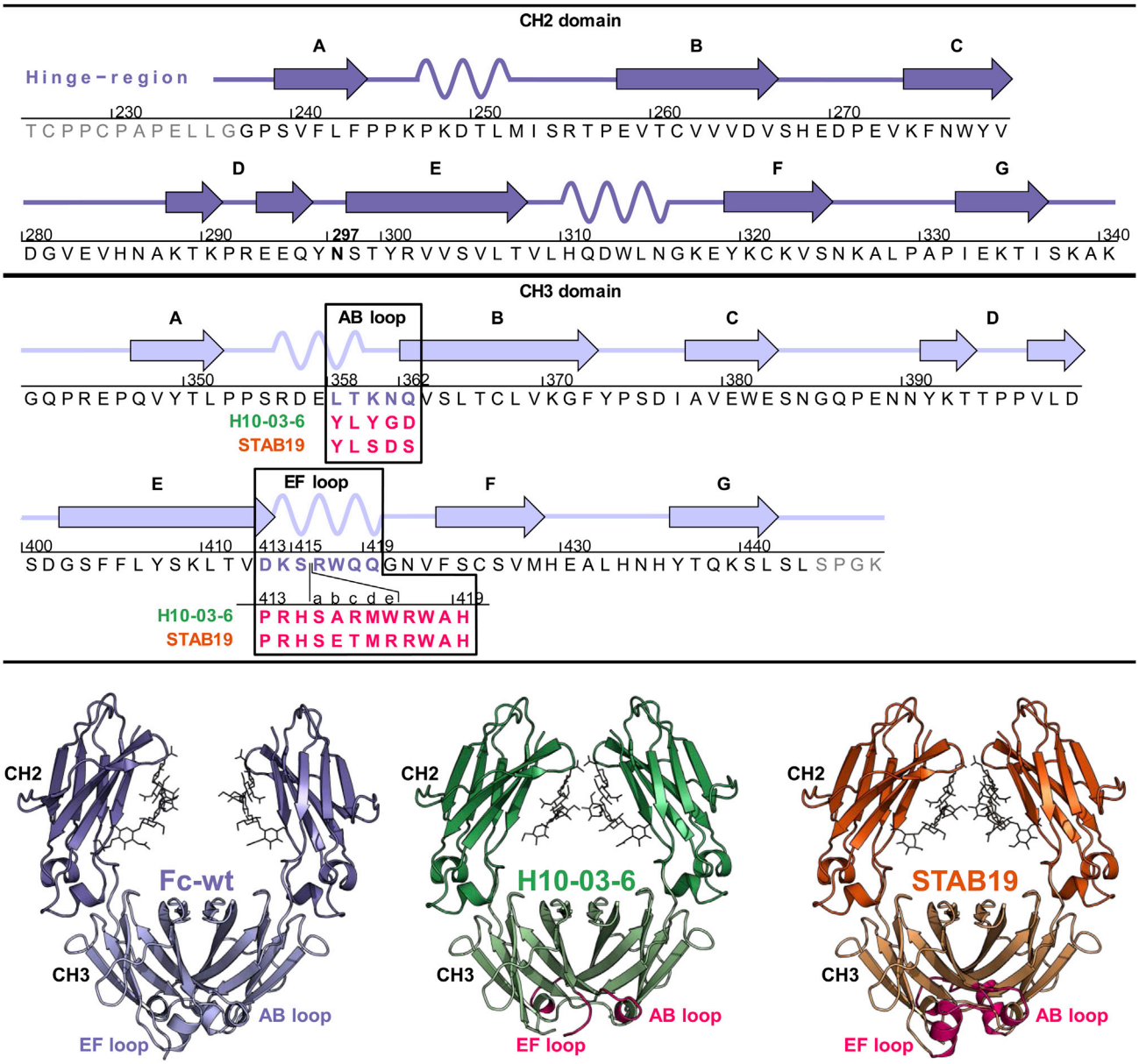

Figure 1. Structure and Amino Acid Sequence of Human IgG1-Fc and the Fcabs H10-03-6 and STAB19

Schematic representation of homodimeric human IgG1-Fc (Fc-wt) (violet, PDB: 5JII) as well as the Fcabs H10-03-6 (green, PDB: 5JIK) and STAB19 (orange, PDB: 5JIH), generated using PyMOL, with the corresponding amino acid sequence (Eu numbering system [Edelman et al., 1969]). Gray-colored residues at the N and C-termini are not resolved within all three structures. The engineered C-terminal AB and EF loops of the CH3 domains and the differences in length and sequence are depicted in pink. The asparagine at position 297 carries the glycan.

2014). Finally, a directed evolution protocol for increasing the conformational stability of H10-03-6 was developed and successfully applied. It included soft randomization of distinct loop regions of the parental binder, followed by heat incubation of the yeast displayed protein library and selection for retained HER2 binding (Traxlmayr et al., 2013).

Due to the great success of the HER2-specific Fcab FS102 in in vitro and in vivo studies, this Fcab is currently under evaluation in clinical phase I (Leung et al., 2015). FS102 binds HER2 with high affinity, comparable with that of the clinically approved HER2-specific antibodies trastuzumab and pertuzumab, but does not compete with either of those in binding to the receptor, indicating that it is targeting a different epitope. This Fcab induces profound HER2 internalization and degradation and, finally, tumor cell apoptosis.

Here we present the first crystal structures of Fcabs as well as of Fcab-antigen complexes. In detail we compare the crystal structures of Fc-wt with those of the parental HER2-binding clone H10-03-6 and its stability-engineered variant STAB19 (Traxlmayr et al., 2013), and discuss the impact of loop

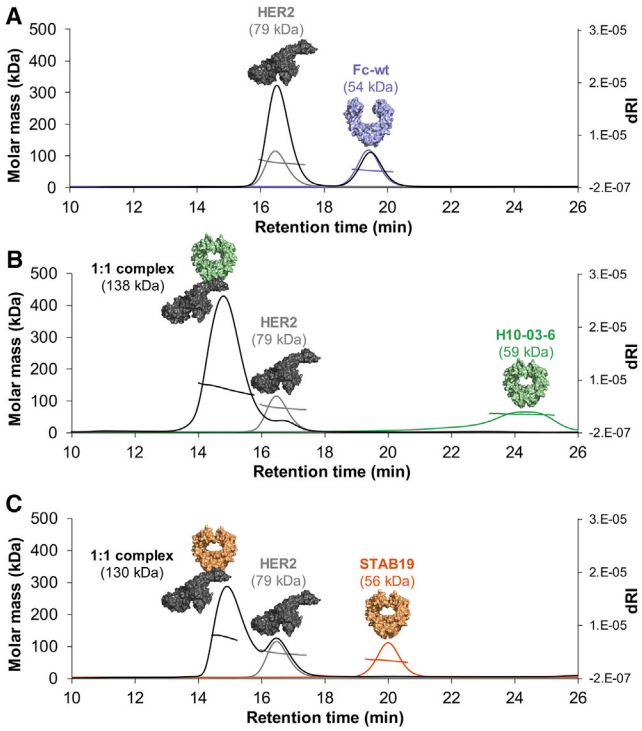

Figure 2. Size-Exclusion Chromatography Profiles and Molar Masses of Human IgG1-Fc, H10-03-6, STAB19, and Fcab-HER2 Complexes

Molar masses were determined by multi-angle light scattering and calculated using the ASTRA software.

(A) Overlay of the elution profile of Fc-wt (violet line), HER2 (gray line), and a mixture of Fc-wt and HER2 in a ratio of 1:2 (black line).

(B) Overlay of the elution profile of H10-03-6 (green line), HER2 (gray line), and a mixture of H10-03-6 and HER2 in a ratio of 1:2 (black line).

(C) Overlay of the elution profile of STAB19 (orange line), HER2 (gray line) and a mixture of STAB19 and HER2 in a ratio of 1:2 (black line). Note that the depicted molar masses are derived from MALS measurements and thus do not exactly match the exact molar masses.

engineering on the domain and loop structures with regard to Fc-wt. In addition, we show the crystal structures of the complexes of both Fcabs with the extracellular domain of HER2. Size-exclusion chromatography combined with multi-angle light scattering (SEC-MALS), isothermal titration calorimetry (ITC), and fluorescence correlation spectroscopy (FCS) were used to illuminate observed differences in binding stoichiometry of the respective complexes in solution and crystal structures. Finally, we discuss and compare the binding modes of the two Fcabs and the clinically applied humanized monoclonal antibodies trastuzumab and pertuzumab with the extracellular domain of HER2.

RESULTS

The HER2-binding Fcab H10-03-6 was selected from an IgG1-Fc library that was randomly mutated in the AB (positions 358–362) and EF loops (positions 412–415 [including five insertions] and 418–419) of the CH3 domains (Eu numbering system [Edelman et al., 1969], Figure 1) (Wozniak-Knopp et al., 2010). Upon titrating H10-03-6 on HER2-expressing SKBR-3 cells a K_D value of 23 nM was determined (Traxlmayr et al., 2013). Analysis by SEC demonstrated that the peak of H10-03-6 was markedly broadened and the retention time was longer compared with Fc-wt (Figures 2A and 2B). Moreover, the differential scanning calorimetry (DSC) profile of H10-03-6 only showed one broad transition at ~68°C suggesting that the CH3 domain was destabilized, confirming previously published data (Traxlmayr et al., 2013). Thermal unfolding of Fc-wt typically shows two endothermic transitions representing the unfolding of the less stable CH2 domains (T_{m1} = 70.4°C) followed by denaturation of the CH3 domains (T_{m2} = 82.6°C). Thus a directed evolution protocol was developed and a library of H10-03-6 variants was constructed by parsimonious mutagenesis of the same positions in the AB and EF loops, followed by heat incubation of the yeast displayed protein library and selection for retained HER2 binding (Traxlmayr et al., 2013). One of the selected Fcab clones that retained binding to HER2 but exhibited a significantly increased conformational stability and resistance to aggregation was STAB19 with T_{m1} and T_{m2} values of 70.6°C and 75.5°C, respectively. Moreover, its SEC profile was clearly improved and nearly identical to that of Fc-wt (Figure 2C). Compared with H10-03-6 in STAB19, the hydrophobicity of the AB and EF loops decreased (Figure 1) and the dissociation constant increased about 5-fold (K_D = 109 nM) (Traxlmayr et al., 2013).

The effects of loop engineering on the structure of the Fc protein was investigated by X-ray crystallography of the HEK293-produced Fcabs, H10-03-6 and STAB19.

Crystal Structures of Fcabs Unravel the Impact of Loop Engineering on Structure and Conformational Stability

Crystals of Fc-wt, H10-03-6, and STAB19 have the symmetry of space group $P2_12_12_1$ and contained one homodimeric protein in the asymmetric unit (Table 1). Comparison of the three structures shows a symmetric arrangement of the rigid CH3 domains, whereas the positions as well as the B factors of the respective CH2 domains vary among them (Figure 3). These variations result in an either more open or more closed structure of the horseshoe-shaped Fc. Potential reasons for this include altered crystal packing and qualitative and quantitative differences in the N297-linked glycans (Ahmed et al., 2014; Borrok et al., 2012). This movement of the CH2 domains relative to each other is also linked to a structural change of the highly conserved residues at the CH2-CH3 interface (Teplyakov et al., 2013). In contrast to the more closed structures of STAB19 and H10-03-6 determined by the distance of the C^{α} atoms at position P329 of each chain (23.0 Å and 24.7 Å, respectively), the observed tilt of the Fc-wt CH2 domain of chain A leads to a highly open structure with a distance of 37.5 Å.

The glycan structure at N297 of the Fc proteins recombinantly produced in HEK293-6E cells was analyzed. For each chain of all structures, a minimum of a pentasaccharide biantennary core composed of two N-acetylglucosamine and three mannose residues could be found. In addition, further sugar residues (β1,2-linked N-acetylglucosamine, α1,6-linked fucose, and β1,4-linked galactose) could be identified depending on the observed electron density. Figure S1 shows the model of the glycan structure at the CH2 domains of HEK produced Fc-wt. Furthermore, the relative amounts of different N-glycans were determined in a purified batch of Fc-wt by mass spectrometry analysis. From a total

Table 1. Crystallization Conditions, Data Collection, and Refinement Statistics for Fc-wt, H10-03-6, STAB19 and the Complexes H10-03-6-HER2 and STAB19-HER2

Structure	IgG1-Fc	H10-03-6	STAB19	H10-03-6-HER2	STAB19-HER2
PDB ID	5JII	5JIK	5JIH	5KWG	5K33
Crystallization conditions	0.05 M sodium phosphate, 16% (w/v) PEG 3350, pH 7.0, T = 22°C	0.05 M HEPES, 24% (w/v) PEG 3350, pH 7.0, T = 22°C	0.05 M Tris, 22% (w/v) PEG 3350, pH 7.5, T = 22°C	0.05 M citric acid, 18% (w/v) PEG 3350, pH 6.0, T = 22°C	0.05 M MES, 10% (w/v) PEG 3350, pH 6.0, T = 22°C
Data Collection					
X-ray source	ESRF ID23-2	ESRF ID23-1	ESRF ID29	ESRF ID30A-3	ESRF ID30A-3
Wavelength (Å)	0.8726	0.9763	0.9686	0.9677	0.9677
Space group	$P2_1\,2_1\,2_1$	$P2_1\,2_1\,2_1$	$P2_1\,2_1\,2_1$	$P3_2\,2\,1$	$P3_2\,2\,1$
Unit cell, a, b, c (Å)	49.4, 75.1, 149.4	49.7, 79.8, 140.9	49.7, 79.5, 140.5	109.8, 109.8, 176.1	108.6, 108.6, 174.3
Resolution range (Å)	46.89–1.79 (1.85–1.79)	42.21–1.82 (1.89–1.82)	46.82–1.66 (1.72–1.66)	47.53–4.30 (4.45–4.30)	47.03–3.30 (3.42–3.30)
Total reflections	243,812 (23,723)	329,822 (33,396)	238,194 (17,741)	55,512 (5,133)	121,881 (12,127)
Unique reflections	52,192 (5,021)	51,065 (5,002)	65,106 (5,746)	8,756 (853)	18,446 (1801)
Completeness (%)	98 (98)	100 (100)	98 (92)	100 (100)	100 (100)
Multiplicity	4.7 (4.6)	6.5 (6.7)	3.7 (3.0)	6.3 (6.0)	6.6 (6.7)
$CC_{1/2}$	99.9 (70.7)	99.9 (18.0)	99.7 (25.3)	99.8 (32.3)	99.8 (38.5)
R_{merge} (%)	4.7 (93.0)	7.2 (487.5)	5.8 (123.1)	19.0 (155.0)	14.2 (165.2)
$R_{meas.}$ (%)	5.3 (105)	7.8 (528)	6.8 (148)	20.7 (170)	15.4 (179)
$I/\sigma(I)$	15.87 (1.52)	11.72 (0.46)	8.87 (0.63)	6.48 (0.99)	9.99 (1.06)
Wilson B factor (Å^2)	28.83	44.38	35.03	174.26	112.08
Refinement Statistics					
R_{work}/R_{free} (%)	18.08/22.05	22.53/25.94	19.78/23.12	32.37/36.82	21.79/27.22
RMSD, bonds (Å)	0.013	0.006	0.013	0.002	0.004
RMSD, angles (°)	1.41	0.90	1.49	0.60	0.68
Ramachandran favored (%)	99	98	100	85	92
Ramachandran allowed (%)	0.97	1.76	0.24	13.27	7.21
Ramachandran outliers (%)	0.0	0.0	0.0	0.7	1.2
Average B factor	49.20	76.43	63.14	209.37	120.48

Values in parentheses represent the highest-resolution shell.

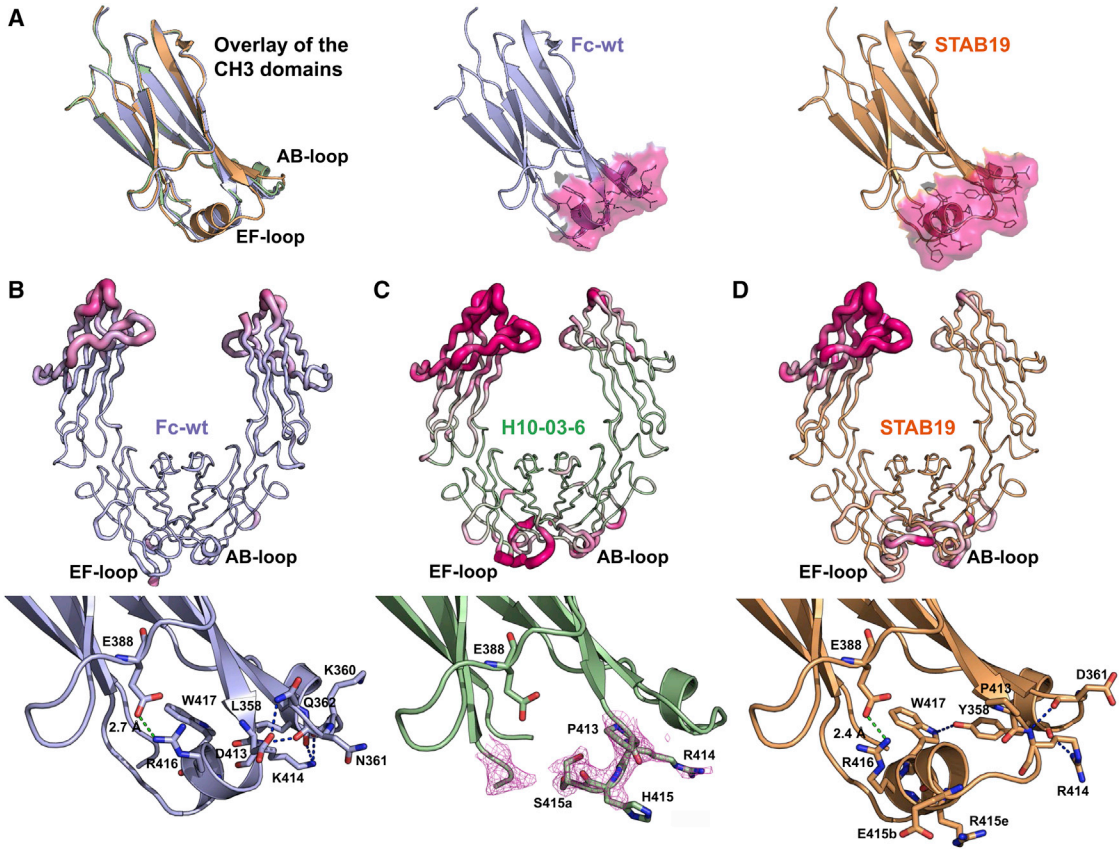

Figure 3. Crystal Structures of Human IgG1-Fc and the Fcabs H10-03-6 and STAB19

(A) Overlay of the CH3 domains of chain B of the three proteins (human IgG1-Fc [Fc-wt], violet; H10-03-6, green; STAB19, orange). Additionally a surface representation of the AB and EF loops (pink) of Fc-wt and STAB19 are shown.

(B) Structure and close-up view of the C-terminal loop region of chain B of Fc-wt.

(C) Structure and close-up view of the C-terminal loop region of chain B of H10-03-6 showing a gap of eight residues in the EF loop due to lack of electron density. Four residues of the EF loop could be modeled within the $2mF_o$-DF_c density map drawn at RMSD = 1 (pink mesh).

(D) Structure and close-up view of the C-terminal loop region of chain B of STAB19. In all Fc structures the B factors are shown as sausage representation, with higher values depicted by pink and thick tubes. Important stabilizing ionic interactions and H bonds between labeled residues are depicted in green and blue dashed lines, respectively, with distance values given for salt bridges only.

See also Figure S1 and Table S1.

of 73% of glycosylated peptides, the prevalent glycan species that could be found were core-fucosylated biantennary complex-type GnGnF (G0F) and its monogalactosylated variant AGnF (G1F) with over 80% incidence (Table S1).

In Fc-wt the three loops at the C-termini of the CH3 domains show clear electron density, and the AB and EF loop form a continuous surface (Figure 3A). Importantly, the EF loop comprises a short α-helical structure (K414-Q419) with the side chain of R416 forming a salt bridge with E388 of the CD loop and W417 being buried in the hydrophobic core of the CH3 domain (Figure 3B).

Superimposition of the β-strands of the CH3 domains of Fc-wt, H10-03-6, and STAB19 show a near perfect overlay (Figure 3A). B factor analysis reveals higher flexibility for the mutated loop regions of H10-03-6 and STAB19 compared with Fc-wt (Figures 3C and 3D). Despite the mutation in the AB loops of H10-03-6 and STAB19 (Figure 1), the loop structure in the two Fcabs is very similar to that of Fc-wt. By contrast, significant differences were seen in the structure of the respective EF loops. With H10-03-6, no electron density could be detected for 11 (chain A) and 8 (chain B) residues in the elongated EF loop, suggesting high flexibility and the absence of stable non-covalent interactions in this region (Figure 3C). By contrast, in STAB19 continuous electron density of the EF loop was observed, and the AB and EF loops form a continuous surface similar to Fc-wt (Figure 3A). The structure demonstrates the important role of P413 at the beginning of the EF loop (also present in H10-03-6). It turns the polypeptide chain to generate space for the five inserted residues that build up an α-helix (E415b-H419) similar to the Fc-wt structure (Figure 3D). For STAB19, residues R416 and W417 that were excluded from mutation are positioned very similarly to that in the Fc-wt structure. Additionally the formation of a novel salt bridge (Figure 3D, lower panel) between E415b and R415e (i + 3, distance 2.6 Å) is very likely, although the side chains of these two residues lack electron density.

In general, the crystal structures of Fc-wt and STAB19 show the presence of several stabilizing polar bonds between the

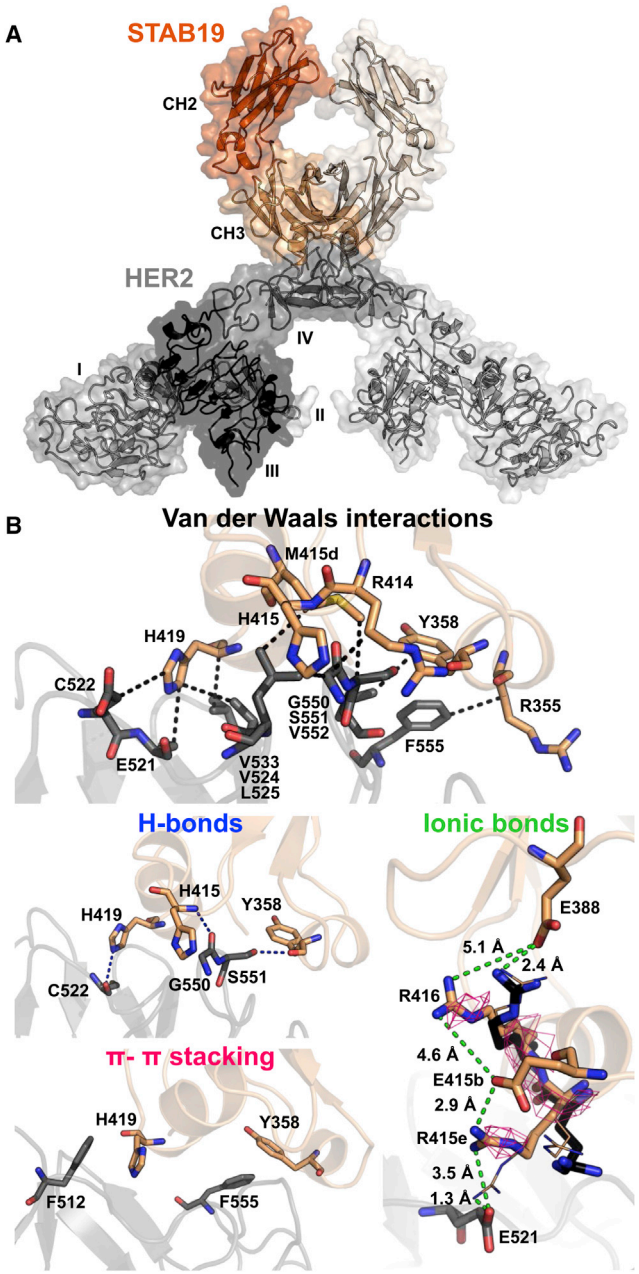

Figure 4. Crystal Structure of the STAB19-HER2 Complex at 3.30 Å Resolution; PDB: 5K33

(A) Surface representation of the STAB19-HER2 complex showing that each chain of the STAB19 molecule (CH2 and CH3 domains colored in shades of orange) binds to one HER2 molecule (domains I–IV colored in shades of gray). (B) Non-covalent interactions identified by using the RING 2.0 software tool (Piovesan et al., 2016) with van der Waals interactions (C-C, <4.0 Å, black), H bonds (NH-OC and OH-OC, <3.5 Å, blue) depicted as dashed lines, and π-π stacking (<5.5 Å). An ionic bond (green) can only be found between E415b and R415e (2.9 Å) of STAB19. Arginine residues at position 415e and 416 show weak electron density (pink mesh drawn at RMSD = 1). Upon changing rotamer configuration (orange lines), salt bridge distances between E521[HER2] and R415e as well as E388 and R416 can be reached. Side-chain orientations of R415e and R416 as found in the unbound STAB19 structure are depicted in black.

See also Figure S2.

respective AB and EF loops, namely Q362-D413, N361-K414, K360-K414, and L358-K414 in Fc-wt as well as Y358-R414, Y358-W417, and D361-R414 in STAB19 (blue dashed lines in Figures 3B and 3D).

Crystal Structures of Fcab-HER2 Complexes Reveal a Binding Stoichiometry of 1:2

Next, the crystal structures of the Fcab-HER2 complexes were determined. Therefore, mixtures of H10-03-6 and HER2 were analyzed by SEC-MALS. Figure 2 shows the elution profiles of Fc-wt, H10-03-6, STAB19, and HER2 (25 μg each) as well as of the mixtures Fc-wt-HER2 (Figure 2A), H10-03-6-HER2 (Figure 2B), and STAB19-HER2 (Figure 2C) in a ratio of Fc/HER2 of 1:2. Whereas Fc-wt cannot bind to HER2, both H10-03-6 and STAB19 form stable complexes with molar masses of about 138 and 130 kDa, respectively, which clearly indicates a binding stoichiometry of 1:1 (theoretical molar mass of the Fcab-HER2 complex is ~137 kDa). Importantly, the SEC profiles of the Fcab-HER2 mixtures show the absence of the respective unbound Fcabs and the presence of excess HER2 (Figures 2B and 2C, black lines).

Consequently, for crystallization of the Fcab-HER2 complexes HER2 was mixed with an excess of the respective Fcab and the complexes with 1:1 stoichiometry were isolated by preparative SEC. Fractions comprising the complex were concentrated and dialyzed, and crystallized using the sitting-drop vapor diffusion method. Crystals of the complexes had the symmetry of space group $P3_221$. Surprisingly, one unit cell contained six asymmetric units, one consisting of a monomeric Fcab chain and one HER2 molecule, meaning that each homodimeric Fcab molecule binds two molecules of HER2. The biological assembly is formed by two asymmetric units as depicted in Figures 4A and 5. Since STAB19 is a stabilized variant derived from H10-03-6, the paratopes of H10-03-6 and STAB19 bind to the same epitope on domain IV of HER2.

The resolutions of 3.30 Å (STAB19-HER2 complex) and 4.30 Å (H10-03-6-HER2 complex) are too low for assigning any water molecules, which can play a major role through bridging hydrogen bonds in protein-protein interfaces (Meenan et al., 2010). The RING 2.0 web server was used as a tool for analyzing the binding interface of the STAB19-HER2 complex by generating a residue interaction network based on all types of non-covalent interactions (Piovesan et al., 2016). The binding interface is stabilized by a combination of van der Waals interactions and hydrogen bonds, i.e., Y358[STAB19]-S551[HER2], H415[STAB19]-G550[HER2] and H419[STAB19]-C522[HER2], including residues from both the AB and the EF loop (Figure 4B). Additionally, Y358 and H419 of STAB19 establish π-π stacking interactions with a tilted edge-to-face and a parallel conformation with F555 and F512, respectively, of domain IV of HER2 with distances below 5.5 Å between the centers of mass of the respective aromatic rings (Figure 4B). Superimposition of the unbound STAB19 structure and the STAB19-HER2 complex revealed differences in the side-chain orientation of R415e and R416 (black sticks in Figure 4B). Interestingly, these two residues show weak electron density within the complex structure, suggesting high flexibility. They are in close proximity of glutamic acid residues E521[HER2], E388 (CD loop), and E415b (EF loop), and thus could form ionic bonds. By changing the rotamer

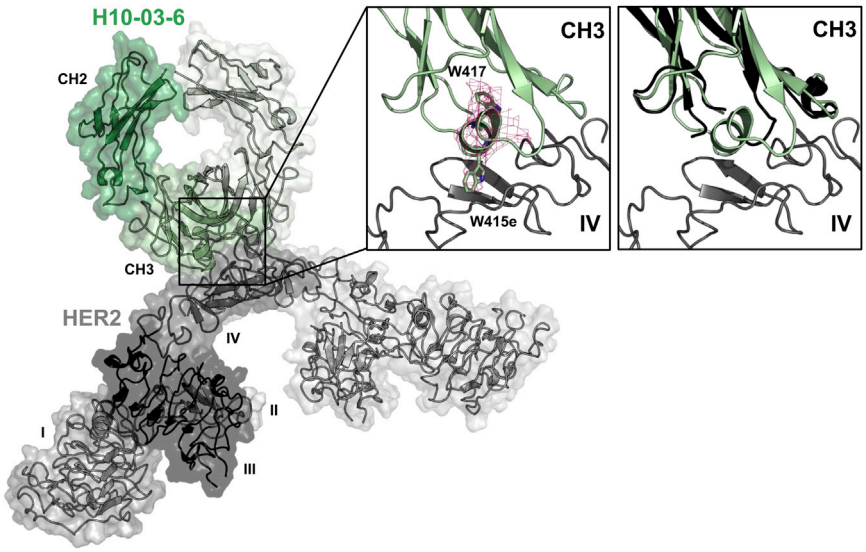

Figure 5. Crystal Structure of the H10-03-6-HER2 Complex at 4.30 Å Resolution; PDB: 5KWG

The surface representation of the H10-03-6-HER2 complex shows that each chain of the H10-03-6 molecule (CH2 and CH3 domains colored in shades of green) binds to one molecule of HER2 (domains I-IV colored in shades of gray). The close-up views focus on the CH3 domain bound to domain IV of HER2 showing the formed α-helix of the EF loop with electron density ($2mF_o$-DF_c) drawn at RMSD = 1 (pink mesh). Side-chain orientation of the tryptophan residues are depicted as green sticks. The CH3 domain of the unbound H10-03-6 structure (black) was superimposed with the H10-03-6-HER2 complex (window on the right).

conformations (orange lines in Figure 4B), salt bridge distances can be reached (green dashed lines in Figure 4B). However, due to the weak electron density, no stable salt bridges can be observed.

As a consequence of the low resolution, accurate fitting of the side-chain orientation of the H10-03-6-HER2 complex is difficult so that no reliable conclusions about the nature of the interaction can be made. Nevertheless, what can clearly be seen within the electron density is the backbone of the EF loop that forms an α-helix just like STAB19 (Figure 5). In addition, electron density is sufficient to see the two tryptophan side chains within the EF loop; W417 is buried within the hydrophobic core, whereas W415e is pointing toward the epitope on domain IV of HER2. Moreover, the overlay with the unbound structure of H10-03-6 clearly shows that the end of β-strand E as well as the start of β-strand F is lying farther apart, probably to create space for the formation of the α-helix (Figure 5).

An Fcab Binds Two HER2 Molecules in a Negative Cooperative Binding Mode

One possible explanation for the discrepancy in binding stoichiometry between the crystal structure (1:2) and SEC analysis (1:1) would be cooperative binding behavior. That is, binding of free Fcab to HER2 might show higher affinity than the interaction of the Fcab-HER2 complex with the second HER2 molecule.

To investigate whether this hypothesis is true, we performed ITC. Importantly, during an ITC experiment the protein samples are present in a sample cell at high concentration and therefore the ligand cannot be separated spatially from its receptor after dissociation, which, however, is possible during SEC. In contrast to the previously described light-scattering data after SEC, ITC analysis clearly revealed a binding stoichiometry of STAB19-HER2 of 1:2 (N = 0.533, Figure 6A). By having the HER2 displaying one binding site at high concentration (c = 80 μM) in the calorimetric cell, no cooperative binding behavior can be examined, since both binding sites of STAB19 are immediately occupied when titrated into the cell. For investigation of sequential binding behavior and determination of two different K_D values the setup must be inverted, having the STAB19 displaying two binding sites within the sample cell. However, the reverse application did not produce any reliable data.

Consequently, to examine the thermodynamics of interaction in more detail we performed FCS (Figures 6 and S3). By titrating HER2 to 31 nM of labeled STAB19, different diffusion times were measured. Assuming spherical shape of the molecules, molar masses were calculated as a function of HER2 concentration (Equation 1 and Figure 6B). The difference in the measured molar mass between very low and very high HER2 concentrations was ~170 kDa. Since one HER2 molecule has a molar mass of 79 kDa as measured by light scattering (Figure 2), the 170 kDa range confirms the 1:2 stoichiometry that was also observed by ITC and in the crystal structure. Moreover, in agreement with our hypothesis of negative cooperativity, the resulting data could be perfectly fitted with the Adair-Klotz equation describing two sequential transitions (Adair et al., 1925; Klotz, 1946, 2004) (Figure 6B, black line). For comparison, the data were additionally fitted with an equation describing a single transition (Hulme and Trevethick, 2010) (Figure 6B, gray line). An *F*-test was performed to compare the goodness of the fit between the two models (Motulsky and Ransnas, 1987). Using the residual sum of squares in consideration of the number of degrees of freedom, an *F*-value of 33.12 was calculated. The obtained *p*-value of <0.001 indicates that the Adair-Klotz equation fits the data significantly better than the one-set-of-sites model. Fitting the data with the more precise model yielded two K_D values of 0.07 μM (K_{D1}) and 1.1 μM (K_{D2}), describing negative cooperative binding behavior.

Remarkably, the fitted equation with two transitions yielded molar masses of 51 kDa for STAB19 and 87 kDa for HER2. These results are in perfect agreement with MALS measurements with calculated molar masses of 56 kDa (STAB19) and 79 kDa (HER2).

DISCUSSION

In this study the X-ray structures of the Fcab H10-03-6 and its stabilized variant STAB19, which was previously engineered by directed evolution (Traxlmayr et al., 2013), were determined. Superimposition of these two Fcab structures with Fc-wt clearly showed that the overall structure of these Fcabs was not

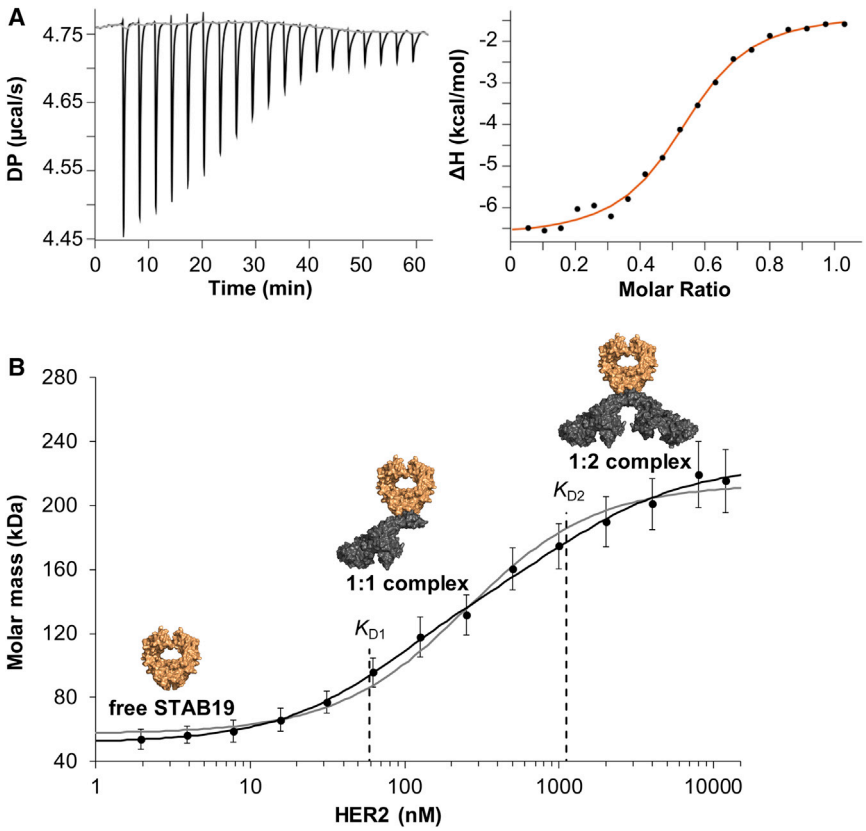

Figure 6. Unraveling the Binding Mode of HER2 to STAB19

(A) Isothermal titration calorimetry. The Microcal PEAQ-ITC system was used for the stepwise titration of 2 µL of STAB19 (400 µM) to 80 µM HER2. The left panel shows the raw data representing response to 19 injections at 25°C. The integrated data (right panel) fitted to one-set-of-sites interaction model clearly suggest a STAB19-HER2 binding stoichiometry of 1:2 (N = 0.533).

(B) Fluorescence correlation spectroscopy. Various concentrations of HER2 were titrated to 31 nM STAB19-DyLight 488 conjugate. Fluorescence fluctuations of labeled molecules through the confocal focus (pinhole size 35 µm) were monitored over 30 s and autocorrelated. From the obtained translational diffusion times the respective molar masses were calculated using the Stokes-Einstein relation assuming spherical shape of the molecules (n = 24; molar mass ± SD). HER2-binding isotherms were generated by fitting the data to a one-set-of-sites binding model (gray line) and to a cooperative binding model (black line) referring to the Adair-Klotz equation (Equation 2) (K_{D1} = 0.07 µM; K_{D2} = 1.1 µM). Significance for the cooperative binding model was evaluated by performing an *F*-test ($p < 0.001$).

See also Figure S3.

impaired by engineering the AB and EF loops of the CH3 domains. Apart from the engineered binding site in the CH3 domains, the only major deviation between the different structures was related to the distance between the two CH2 domains in the homodimeric proteins. Moreover, in all three structures the highly flexible hinge region (T225-L236) is not resolved, which is also true for the majority of the Fc structures published in the PDB. Importantly, as a consequence of the conservation of the overall structure of the Fc scaffold despite loop engineering, binding of the natural ligands such as FcγRI or FcRn is not or only slightly affected (Lobner et al., 2016; Traxlmayr et al., 2013; Wozniak-Knopp et al., 2010). Moreover, HER2-specific Fcabs, including H10-03-6, have been shown to trigger ADCC, demonstrating that the interaction with FcγRIII on natural killer cells is also maintained (Kainer et al., 2012; Wozniak-Knopp et al., 2010).

Interestingly, comparison of the structures of H10-03-6 and its stabilized version STAB19 mainly showed differences in the fold of the EF loop. While the EF loops of the stabilized variant STAB19 include an α-helical segment, no electron density could be seen for the major part of the EF loops of H10-03-6, suggesting high flexibility. Moreover, the distance between the C^{α} atoms of S415a and G420 flanking the non-resolved gap of the EF loop of H10-03-6 is only about half as long as in the STAB19 molecules, indicating that not enough space is available for the formation of the two-turn α-helical segment that is observed in the STAB19 structure. Together, these structural data strongly suggest that the EF loop is flexible and partially disordered in H10-03-6, but not in its stabilized variant STAB19. In line with these structural data, H10-03-6 migrates more slowly through SEC columns, probably explained by increased non-specific interaction between the unstructured EF loop and the column matrix. This flexible EF loop in H10-03-6, which could not be resolved in the unbound structure, becomes visible in the HER2-bound structure. Although the resolution of 4.30 Å is low, the tube-shaped electron density of the EF loop allows for perfect fitting of an α-helical segment. This means that the highly flexible EF loop of the unbound state of the H10-03-6 folds into a stable helical structure upon binding to HER2. This mechanism of molecular recognition resembles a disorder-to-order conformational transition that has also been reported for other proteins and peptides (Armstrong et al., 2013; Dyson et al., 1988; Wright and Dyson, 1999).

During in vitro evolution from H10-03-6 to STAB19, two mutations with opposite charges (E415b and R415e) emerged in the α-helical segment. Since these two residues are separated by approximately one turn ($i + 3$), it seems likely that they form a salt bridge that stabilizes this short secondary structural element. Interestingly, comparison of the STAB19 sequence with other engineered stabilized variants of H10-03-6 published by Traxlmayr et al. (2013) shows that the mutant STAB14 contains similar mutations (D415b and R415e), potentially enabling the formation of a similar salt bridge in STAB14. Intriguingly, the stabilities and SEC profiles of STAB14 and STAB19 are highly comparable, suggesting that this salt bridge is indeed an important factor for the stabilization of this Fcab family.

Previous studies indicated that the two residues R416 and W417 are important for the stability and proper folding of the CH3 domain, which can be structurally explained by the

formation of a salt bridge between R416 and E388 and the insertion of the side chain of W417 into the hydrophobic core within the Fc-wt structure (Hasenhindl et al., 2013; Traxlmayr et al., 2012b; Wozniak-Knopp et al., 2010). Therefore, this structurally important "RW" motif was not mutated in the course of engineering the binding site. Remarkably, both residues participate in the same interactions in the STAB19 structure as in the Fc-wt structure, despite excessive mutation and insertion in the EF loop.

Since an Fcab is a homodimeric protein containing two identical antigen-binding sites which are in close proximity, previously it was not clear whether one Fcab molecule is able to bind one or two HER2 molecules simultaneously. Not only the size and flexibility of the antigen but also the location of the binding epitope determines whether or not steric hindrance excludes binding of two antigen molecules. Moreover, it also seemed possible that after binding to the first antigen molecule, allosteric effects within the Fcab molecule could change the affinity of the second binding site, possibly resulting in stronger (positive cooperativity), weaker (negative cooperativity), or completely abolished binding, as was also seen with other dimeric proteins containing two binding sites (Macdonald and Pike, 2008).

Co-crystallization of Fcabs with HER2 identified a clear 1:2 binding stoichiometry. Importantly, since one asymmetric unit contains only one monomeric Fcab chain and one HER2 molecule, both binding sites are identical. Surprisingly, SEC-MALS measurements revealed a 1:1 stoichiometry, although Fcab and HER2 were mixed in a 1:2 ratio with an adequately high concentration of HER2 that should allow occupation of both STAB19 binding sites. To test whether the 1:2 complex is an artifact of the crystallization process, we analyzed the stoichiometry using ITC, which clearly showed a 1:2 stoichiometry that is consistent with the co-crystal structures. This unexpected discrepancy may be explained by the different experimental setups during SEC versus co-crystallization and ITC. Since SEC is a separation technology, the two interaction partners (i.e., Fcab and HER2) migrate differently after dissociation, whereas during ITC analysis and crystallization they are in equilibrium in a closed reaction chamber. Thus, based on our observation that after the SEC run the complex exists in a 1:1 stoichiometry, we hypothesized that one of the two interaction sites interacts with HER2 with lower affinity. Although the HER2 concentration in the loaded SEC-sample was about 10-fold above the low-affinity K_D determined by FCS, the sample is diluted immediately after injection. This dilution, together with the ability of SEC columns to separate proteins from each other, is expected to facilitate dissociation of the HER2 molecule that is associated with the low-affinity site. These dilution and separation effects are not present during ITC and crystallization, whereby the high concentrations of the interaction partners and the lack of a separation process facilitate binding to the low-affinity site as well. Thus, these results indicate a negative cooperative binding behavior, meaning that the binding affinity of the second binding site decreases after the Fcab has bound the first HER2 molecule. To test this hypothesis, we measured the interaction of STAB19 with HER2 using FCS, whereby HER2 was titrated to a fixed concentration of STAB19, facilitating fitting of two transitions with different affinities. The results clearly showed a 1:2 stoichiometry, confirming data from ITC and crystallography. Importantly, the resulting curve could not be appropriately fitted with a single transition, strongly suggesting that the two binding sites differ in affinity. The two apparent K_D values are in the low micromolar and intermediate nanomolar range, respectively, but do not differ sufficiently to reliably quantify them. Of note, the mean lifetime of a complex in the low micromolar range is dramatically shorter when compared with interactions within the lower nanomolar range for a given k_{on} value (Corzo, 2006), possibly explaining why a 1:1 complex was observed after SEC.

To investigate the structural reason for the observed negative cooperativity, we superimposed unbound STAB19 with HER2-bound STAB19 by aligning the two CH3 domains. In this superimposition no significant allosteric changes were observed in the engineered loop regions (Figure S2A). Moreover, analysis with the TM-align algorithm (Zhang and Skolnick, 2004) using the C^{α} atoms of residues located in the CH3 domains (G341-L441) resulted in a root-mean-square deviation (RMSD) value of 0.64 and a TM-score (template modeling score) of 0.9780, indicating very high congruency. Together, these data indicate that allosteric mechanisms within the STAB19 molecule are not responsible for the negative cooperativity.

Another potential explanation for negative cooperativity could be steric hindrance for the second HER2 molecule. Due to the high flexibility of the domain IV of HER2, a total of 55 residues on the C-terminus could not be resolved, which is also the case for other structures of HER2 (Franklin et al., 2004; Hu et al., 2015). However, the HER2 molecule of the trastuzumab Fab-HER2 complex structure (Cho et al., 2003), where the Fab fragment binds at the lower end of domain IV, shows more electron density in domain IV and therefore misses only 24 residues on the C-terminal part. By superimposition of this domain IV with the domain IV of the Fcab-HER2 complexes, the HER2 molecule can theoretically be extended on the C-terminus, showing a slight sterical clash with the second HER2 molecule (shown for the STAB19-HER2 complex structure, Figure S2B). Whereas in a crystal where the molecules are packed tightly together no differences between the two binding sites are observed, this sterical hindrance could be more pronounced in solution and may be the reason for the observed negative cooperativity.

While it is difficult to measure the stoichiometry between soluble Fcab and membrane-bound HER2, it seems possible that these Fcabs interact with two HER2 molecules simultaneously, especially at high expression densities of HER2 that are often observed on breast cancer cells (Kovacs et al., 2015).

Comparison of the H10-03-6- and STAB19-HER2 complexes with those of the clinically approved monoclonal antibodies trastuzumab and pertuzumab demonstrated that pertuzumab binds to the dimerization arm located in domain II (Franklin et al., 2004), whereas trastuzumab (Cho et al., 2003) and H10-03-6/STAB19 interact with the membrane-proximal domain IV. The epitopes of the Fcabs do not overlap with that of trastuzumab, but are in very close proximity (Figure 7A). This fact is inconsistent with the competition assays performed by Woisetschläger et al. (2014), which indicate that the epitopes partially overlap. But, indeed, the second non-binding chain of the Fcab, more precisely the CH3 domain, slightly sterically clashes with the variable domains of trastuzumab (Figure 7A), explaining the

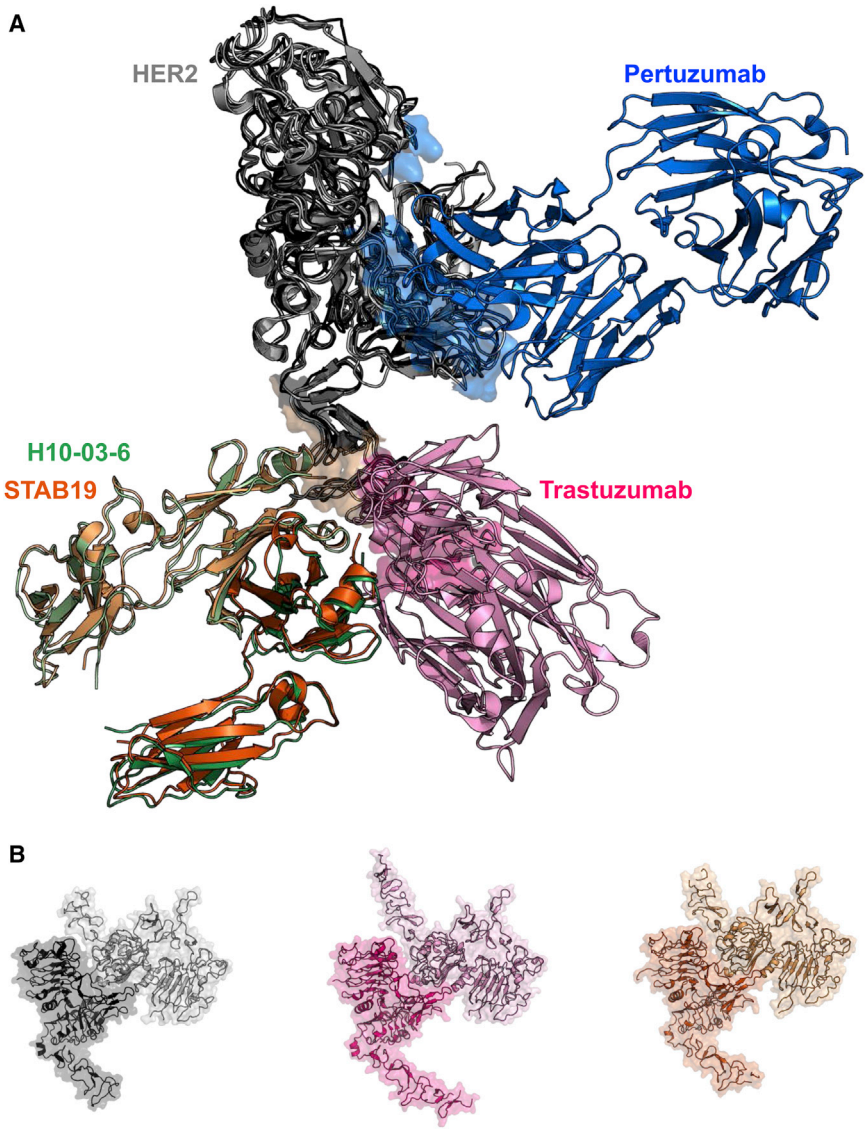

Figure 7. Superimposition of Antibody Fragment-HER2 Complexes and "Back-to-Head" Orientation of Putatively Dimeric HER2

(A) Superimposition of the H10-03-6 (green)-HER2 and STAB19 (orange)-HER2 complexes represented as one Fcab molecule bound to only one HER2 molecule with the trastuzumab Fab (pink)-HER2 (PDB: 1N8Z) and the pertuzumab Fab (blue)-HER2 (PDB: 1S78) complexes. Overlaying HER2 molecules are colored in shades of gray. Epitopes of pertuzumab, trastuzumab, and STAB19 are shown as surface representation.

(B) Structure of the "back-to-head" HER2 homodimer derived from the complex with an anti-domain I Fab fragment (PDB: 1WLW) (Hu et al., 2015) is shown in gray. Crystal packing of two neighboring HER2 molecules of the trastuzumab Fab-HER2 complex and the STAB19-HER2 complex generated by creating symmetry mates using PyMol are shown in pink and orange, respectively.

observed competition between these two molecules for HER2 binding.

Under certain conditions (e.g., HER2 overexpression on tumor cells) HER2 is known to homodimerize and/or to oligomerize (Kovacs et al., 2015). The exact mechanism of interaction in these dimers and oligomers is still poorly understood. Recently, Hu et al. (2015) reported the molecular architecture of a HER2 homodimer by crystallization of the extracellular domain of HER2 in complex with an anti-domain I Fab fragment not affecting the dimerization arm of domain II. In contrast to the "back-to-back" interactions in other homodimers and heterodimers of ERBB family members, the structure determined by Hu et al. suggests a novel "back-to-head" interaction in HER2 homodimers. In their crystal structure one asymmetric unit contains two HER2 molecules, where the dimerization arm of one HER2 molecule inserts into a C-shaped pocket formed by domains I–III of the second HER2 molecule. The same HER2 assembly was also present in the co-crystal structure of the trastuzumab Fab with HER2, but not in the structure containing the pertuzumab Fab, because this Fab binds to the dimerization arm and thereby prevents it from binding to the head of the second HER2 molecule. In line with these data, we also observed the same "back-to-head" architecture of HER2 dimerization (Figure 7B). The fact that this HER2 assembly was observed in complexes with completely different ligands suggests that this might indeed be the physiological interaction of HER2 dimerization instead of simply being a crystal contact.

Together, the data in this study show that Fcabs are capable of interacting with two antigens simultaneously. However, there may be differences in affinity between the two interaction sites for simultaneous binding. Moreover, our structural data clearly demonstrate that the overall fold of Fcabs is highly similar to that of Fc-wt, showing that the loop mutations are well tolerated, especially in the stabilized version STAB19.

STAR★METHODS

Detailed methods are provided in the online version of this paper and include the following:

- KEY RESOURCES TABLE
- CONTACT FOR REAGENT AND RESOURCE SHARING
- METHOD DETAILS
  - Expression and Purification of Fc Proteins
  - Expression and Purification of HER2
  - Differential Scanning Calorimetry
  - X-ray Crystallography and Data Collection
  - Structure Determination and Refinement
  - Validation of the Structures

SUPPLEMENTAL INFORMATION

Supplemental Information includes three figures and one table and can be found with this article online at http://dx.doi.org/10.1016/j.str.2017.04.014.

AUTHOR CONTRIBUTIONS

Conceptualization, E.L., C.O., C.H., and F.R.; Formal Analysis, E.L., A.-S.H., K.G., G.M., M.G.P., and M.W.T.; Investigation, E.L., A.-S.H., K.G., G.M., and M.G.P.; Writing – Original Draft, E.L., C.O., M.W.T., and A.-S.H.; Writing – Review & Editing, E.L., C.O., M.W.T., A.-S.H., K.G., G.M., and F.R.; Supervision, C.O. and K.D.-C.; Funding Acquisition, C.O.

ACKNOWLEDGMENTS

This work was supported by the Christian Doppler Research Association (Christian Doppler Laboratory for Antibody Engineering), the company F-star, the Austrian Science Foundation (FWF Project W1224 – Doctoral Program on Biomolecular Technology of Proteins – BioToP), as well as the Federal Ministry of Economy, Family and Youth through the initiative "Laura Bassi Centers of Expertise," funding the Center of Optimized Structural Studies, No. 253275. We thank Prof. Daniel J. Leahy from Johns Hopkins University (MD, USA) for giving permission to work with his hGH-HER2 expressing Lec1 cells and Dr. Josef Singer from Medical University Vienna (Austria) for providing the aforementioned cell line. We thank Dr. Mike R. Williams from Malvern Instruments Ltd. (UK) for assisting in ITC measurements and Prof. Sandro Keller from University of Kaiserslautern (Germany) for helping to interpret the ITC and FCS results. We acknowledge the European Synchrotron Radiation Facility (Grenoble, France) for provision of synchrotron radiation facilities and the Local Contacts for providing assistance in using beamlines ID23-2, ID29, and ID30A-3. We thank the DLS-CCP4 Data Collection and Structure Solution Workshop 2015 at Diamond Light Source (Oxfordshire, UK). F.R. holds stock in F-star.

Received: March 10, 2017
Revised: April 10, 2017
Accepted: April 28, 2017
Published: May 18, 2017

REFERENCES

Adair, G.S., Bock, A.V., and Field, H. (1925). The hemoglobin system: VI. The oxygen dissociation curve of hemoglobin. J. Biol. Chem. *63*, 529–545.

Adams, P.D., Afonine, P.V., Bunkoczi, G., Chen, V.B., Davis, I.W., Echols, N., Headd, J.J., Hung, L.W., Kapral, G.J., Grosse-Kunstleve, R.W., et al. (2010). PHENIX: a comprehensive Python-based system for macromolecular structure solution. Acta Crystallogr. D Biol. Crystallogr. *66*, 213–221.

Agirre, J., Iglesias-Fernandez, J., Rovira, C., Davies, G.J., Wilson, K.S., and Cowtan, K.D. (2015). Privateer: software for the conformational validation of carbohydrate structures. Nat. Struct. Mol. Biol. *22*, 833–834.

Ahmed, A.A., Giddens, J., Pincetic, A., Lomino, J.V., Ravetch, J.V., Wang, L.X., and Bjorkman, P.J. (2014). Structural characterization of anti-inflammatory immunoglobulin G Fc proteins. J. Mol. Biol. *426*, 3166–3179.

Armstrong, A., Hildreth, J.E., and Amzel, L.M. (2013). Structural and thermodynamic insights into the recognition of native proteins by anti-peptide antibodies. J. Mol. Biol. *425*, 2027–2038.

Borrok, M.J., Jung, S.T., Kang, T.H., Monzingo, A.F., and Georgiou, G. (2012). Revisiting the role of glycosylation in the structure of human IgG Fc. ACS Chem. Biol. *7*, 1596–1602.

Bouyain, S., Longo, P.A., Li, S., Ferguson, K.M., and Leahy, D.J. (2005). The extracellular region of ErbB4 adopts a tethered conformation in the absence of ligand. Proc. Natl. Acad. Sci. USA *102*, 15024–15029.

Chen, V.B., Arendall, W.B., 3rd, Headd, J.J., Keedy, D.A., Immormino, R.M., Kapral, G.J., Murray, L.W., Richardson, J.S., and Richardson, D.C. (2010). MolProbity: all-atom structure validation for macromolecular crystallography. Acta Crystallogr. D Biol. Crystallogr. *66*, 12–21.

Cho, H.S., Mason, K., Ramyar, K.X., Stanley, A.M., Gabelli, S.B., Denney, D.W., Jr., and Leahy, D.J. (2003). Structure of the extracellular region of HER2 alone and in complex with the Herceptin Fab. Nature *421*, 756–760.

Corzo, J. (2006). Time, the forgotten dimension of ligand binding teaching. Biochem. Mol. Biol. Educ. *34*, 413–416.

DiMaio, F., Echols, N., Headd, J.J., Terwilliger, T.C., Adams, P.D., and Baker, D. (2013). Improved low-resolution crystallographic refinement with Phenix and Rosetta. Nat. Methods *10*, 1102–1104.

Durocher, Y., Perret, S., and Kamen, A. (2002). High-level and high-throughput recombinant protein production by transient transfection of suspension-growing human 293-EBNA1 cells. Nucleic Acids Res. *30*, E9.

Dyson, H.J., Lerner, R.A., and Wright, P.E. (1988). The physical basis for induction of protein-reactive antipeptide antibodies. Annu. Rev. Biophys. Biophys. Chem. *17*, 305–324.

Edelman, G.M., Cunningham, B.A., Gall, W.E., Gottlieb, P.D., Rutishauser, U., and Waxdal, M.J. (1969). The covalent structure of an entire gammaG immunoglobulin molecule. Proc. Natl. Acad. Sci. USA *63*, 78–85.

Emsley, P., Lohkamp, B., Scott, W.G., and Cowtan, K. (2010). Features and development of Coot. Acta Crystallogr. D Biol. Crystallogr. *66*, 486–501.

Franklin, M.C., Carey, K.D., Vajdos, F.F., Leahy, D.J., de Vos, A.M., and Sliwkowski, M.X. (2004). Insights into ErbB signaling from the structure of the ErbB2-pertuzumab complex. Cancer Cell *5*, 317–328.

Halaby, D.M., Poupon, A., and Mornon, J. (1999). The immunoglobulin fold family: sequence analysis and 3D structure comparisons. Protein Eng. *12*, 563–571.

Harris, L.J., Skaletsky, E., and McPherson, A. (1995). Crystallization of intact monoclonal antibodies. Proteins *23*, 285–289.

Hasenhindl, C., Traxlmayr, M.W., Wozniak-Knopp, G., Jones, P.C., Stadlmayr, G., Ruker, F., and Obinger, C. (2013). Stability assessment on a library scale: a rapid method for the evaluation of the commutability and insertion of residues in C-terminal loops of the CH3 domains of IgG1-Fc. Protein Eng. Des. Sel. *26*, 675–682.

Higel, F., Seidl, A., Sorgel, F., and Friess, W. (2016). N-glycosylation heterogeneity and the influence on structure, function and pharmacokinetics of monoclonal antibodies and Fc fusion proteins. Eur. J. Pharm. Biopharm. *100*, 94–100.

Holliger, P., and Hudson, P.J. (2005). Engineered antibody fragments and the rise of single domains. Nat. Biotechnol. *23*, 1126–1136.

Hu, S., Sun, Y., Meng, Y., Wang, X., Yang, W., Fu, W., Guo, H., Qian, W., Hou, S., Li, B., et al. (2015). Molecular architecture of the ErbB2 extracellular domain homodimer. Oncotarget *6*, 1695–1706.

Hulme, E.C., and Trevethick, M.A. (2010). Ligand binding assays at equilibrium: validation and interpretation. Br. J. Pharmacol. *161*, 1219–1237.

Jez, J., Antes, B., Castilho, A., Kainer, M., Wiederkum, S., Grass, J., Ruker, F., Woisetschläger, M., and Steinkellner, H. (2012). Significant impact of single N-glycan residues on the biological activity of Fc-based antibody-like fragments. J. Biol. Chem. *287*, 24313–24319.

Joosten, R.P., Joosten, K., Murshudov, G.N., and Perrakis, A. (2012). PDB_REDO: constructive validation, more than just looking for errors. Acta Crystallogr. D Biol. Crystallogr. *68*, 484–496.

Joosten, R.P., Long, F., Murshudov, G.N., and Perrakis, A. (2014). The PDB_REDO server for macromolecular structure model optimization. IUCrJ *1*, 213–220.

Kabsch, W. (2010). XDS. Acta Crystallogr. D Biol. Crystallogr. *66*, 125–132.

Kainer, M., Antes, B., Wiederkum, S., Wozniak-Knopp, G., Bauer, A., Ruker, F., and Woisetschläger, M. (2012). Correlation between CD16a binding and immuno effector functionality of an antigen specific immunoglobulin Fc fragment (Fcab). Arch. Biochem. Biophys. *526*, 154–158.

Karplus, P.A., and Diederichs, K. (2012). Linking crystallographic model and data quality. Science *336*, 1030–1033.

Klotz, I.M. (1946). The application of the law of mass action to binding by proteins; interactions with calcium. Arch. Biochem. *9*, 109–117.

Klotz, I.M. (2004). Ligand-receptor complexes: origin and development of the concept. J. Biol. Chem. *279*, 1–12.

Kovacs, E., Zorn, J.A., Huang, Y., Barros, T., and Kuriyan, J. (2015). A structural perspective on the regulation of the epidermal growth factor receptor. Annu. Rev. Biochem. *84*, 739–764.

Kubota, T., Niwa, R., Satoh, M., Akinaga, S., Shitara, K., and Hanai, N. (2009). Engineered therapeutic antibodies with improved effector functions. Cancer Sci. *100*, 1566–1572.

Leahy, D.J., Dann, C.E., 3rd, Longo, P., Perman, B., and Ramyar, K.X. (2000). A mammalian expression vector for expression and purification of secreted proteins for structural studies. Protein Expr. Purif. *20*, 500–506.

Leung, K.M., Batey, S., Rowlands, R., Isaac, S.J., Jones, P., Drewett, V., Carvalho, J., Gaspar, M., Weller, S., Medcalf, M., et al. (2015). A HER2-specific modified Fc fragment (Fcab) induces antitumor effects through degradation of HER2 and apoptosis. Mol. Ther. *23*, 1722–1733.

Lobner, E., Traxlmayr, M.W., Obinger, C., and Hasenhindl, C. (2016). Engineered IgG1-Fc-one fragment to bind them all. Immunol. Rev. *270*, 113–131.

Lutteke, T., and von der Lieth, C.W. (2004). pdb-care (PDB carbohydrate residue check): a program to support annotation of complex carbohydrate structures in PDB files. BMC Bioinformatics *5*, 69.

Macdonald, J.L., and Pike, L.J. (2008). Heterogeneity in EGF-binding affinities arises from negative cooperativity in an aggregating system. Proc. Natl. Acad. Sci. USA *105*, 112–117.

McCoy, A.J., Grosse-Kunstleve, R.W., Adams, P.D., Winn, M.D., Storoni, L.C., and Read, R.J. (2007). Phaser crystallographic software. J. Appl. Crystallogr. *40*, 658–674.

Meenan, N.A., Sharma, A., Fleishman, S.J., Macdonald, C.J., Morel, B., Boetzel, R., Moore, G.R., Baker, D., and Kleanthous, C. (2010). The structural and energetic basis for high selectivity in a high-affinity protein-protein interaction. Proc. Natl. Acad. Sci. USA *107*, 10080–10085.

Motulsky, H.J., and Ransnas, L.A. (1987). Fitting curves to data using nonlinear regression: a practical and nonmathematical review. FASEB J. *1*, 365–374.

Murshudov, G.N., Vagin, A.A., and Dodson, E.J. (1997). Refinement of macromolecular structures by the maximum-likelihood method. Acta Crystallogr. D Biol. Crystallogr. *53*, 240–255.

Nicholls, R.A., Long, F., and Murshudov, G.N. (2012). Low-resolution refinement tools in REFMAC5. Acta Crystallogr. D Biol. Crystallogr. *68*, 404–417.

Piovesan, D., Minervini, G., and Tosatto, S.C. (2016). The RING 2.0 web server for high quality residue interaction networks. Nucleic Acids Res. *44*, W367–W374.

Quast, I., Peschke, B., and Lunemann, J.D. (2017). Regulation of antibody effector functions through IgG Fc N-glycosylation. Cell Mol. Life Sci. *74*, 837–847.

Rigler, R., and Elson, E.S., eds. (2001). Fluorescence Correlation Spectroscopy: Theory and Application, Springer Series in Chemical Physics (Springer-Verlag).

Smart, O.S., Womack, T.O., Flensburg, C., Keller, P., Paciorek, W., Sharff, A., Vonrhein, C., and Bricogne, G. (2012). Exploiting structure similarity in refinement: automated NCS and target-structure restraints in BUSTER. Acta Crystallogr. D Biol. Crystallogr. *68*, 368–380.

Spiess, C., Zhai, Q., and Carter, P.J. (2015). Alternative molecular formats and therapeutic applications for bispecific antibodies. Mol. Immunol. *67*, 95–106.

Teplyakov, A., Zhao, Y., Malia, T.J., Obmolova, G., and Gilliland, G.L. (2013). IgG2 Fc structure and the dynamic features of the IgG CH2-CH3 interface. Mol. Immunol. *56*, 131–139.

Traxlmayr, M.W., Faissner, M., Stadlmayr, G., Hasenhindl, C., Antes, B., Ruker, F., and Obinger, C. (2012a). Directed evolution of stabilized IgG1-Fc scaffolds by application of strong heat shock to libraries displayed on yeast. Biochim. Biophys. Acta *1824*, 542–549.

Traxlmayr, M.W., Hasenhindl, C., Hackl, M., Stadlmayr, G., Rybka, J.D., Borth, N., Grillari, J., Ruker, F., and Obinger, C. (2012b). Construction of a stability landscape of the CH3 domain of human IgG1 by combining directed evolution with high throughput sequencing. J. Mol. Biol. *423*, 397–412.

Traxlmayr, M.W., Lobner, E., Antes, B., Kainer, M., Wiederkum, S., Hasenhindl, C., Stadlmayr, G., Ruker, F., Woisetschläger, M., Moulder, K., et al. (2013). Directed evolution of Her2/neu-binding IgG1-Fc for improved stability and resistance to aggregation by using yeast surface display. Protein Eng. Des. Sel. *26*, 255–265.

Woisetschläger, M., Antes, B., Borrowdale, R., Wiederkum, S., Kainer, M., Steinkellner, H., Wozniak-Knopp, G., Moulder, K., Ruker, F., and Mudde, G.C. (2014). In vivo and in vitro activity of an immunoglobulin Fc fragment (Fcab) with engineered Her-2/neu binding sites. Biotechnol. J. *9*, 844–851.

Wozniak-Knopp, G., Bartl, S., Bauer, A., Mostageer, M., Woisetschläger, M., Antes, B., Ettl, K., Kainer, M., Weberhofer, G., Wiederkum, S., et al. (2010). Introducing antigen-binding sites in structural loops of immunoglobulin constant domains: Fc fragments with engineered HER2/neu-binding sites and antibody properties. Protein Eng. Des. Sel. *23*, 289–297.

Wright, P.E., and Dyson, H.J. (1999). Intrinsically unstructured proteins: re-assessing the protein structure-function paradigm. J. Mol. Biol. *293*, 321–331.

Zhang, Y., and Skolnick, J. (2004). Scoring function for automated assessment of protein structure template quality. Proteins *57*, 702–710.

STAR★METHODS

KEY RESOURCES TABLE

REAGENT or RESOURCE	SOURCE	IDENTIFIER
Deposited Data		
Complex between G0 version of an Fc bound to a minimized version of Protein A called Mini-Z	N/A	PDB: 1OQO
Crystal structure of extracellular domain of human HER2 complexed with Herceptin Fab	(Cho et al., 2003)	PDB: 1N8Z
Crystal structure of HER2 binding IgG1-Fc (Fcab STAB19)	This paper	PDB: 5JIH
Crystal structure of extracellular domain of HER2 in complex with Fcab STAB19	This paper	PDB: 5K33
Experimental Models: Cell Lines		
HEK293-6E	National Research Council Canada	http://www.nrc-cnrc.gc.ca/eng/; RRID: CVCL_HF20
CHO Lec1	Medical University Vienna (Josef Singer), Austria	(Cho et al., 2003; Leahy et al., 2000)
Recombinant DNA		
pTT5 vector	National Research Council Canada	http://www.nrc-cnrc.gc.ca/eng/
Software and Algorithms		
PyMOL Molecular Graphics System, Version 1.3	Schrödinger, LLC	https://www.pymol.org/; RRID: SCR_000305
Origin 7	OriginLab	http://www.originlab.com/; RRID: SCR_014212
PEAQ-ITC analysis software	Malvern Instruments, Ltd.	N/A
ASTRA 6	Wyatt Technology	http://wyatt-technology-astra.software.informer.com/6.0/
FCS ACCESS Fit	Carl Zeiss-Evotec	N/A
DataAnalysis Version 4.0 SP 5	Bruker Daltonik GmbH	N/A
XDS-suite	(Kabsch, 2010)	http://xds.mpimf-heidelberg.mpg.de/
Phaser-MR	(McCoy et al., 2007)	https://www.phenix-online.org/; RRID: SCR_014219
COOT	(Emsley et al., 2010)	http://www.ccp4.ac.uk/; RRID: SCR_014222
PHENIX-Refine	(Adams et al., 2010)	https://www.phenix-online.org/; RRID: SCR_014224
REFMAC5	(Murshudov et al., 1997)	http://www.ccp4.ac.uk/; RRID: SCR_014225
ProSMART	(Nicholls et al., 2012)	http://www.ccp4.ac.uk/
BUSTER	(Smart et al., 2012)	https://www.globalphasing.com/buster/
Rosetta-Refinement	(DiMaio et al., 2013)	https://www.phenix-online.org/
PDB_REDO	(Joosten et al., 2012; Joosten et al., 2014)	http://www.cmbi.ru.nl/pdb_redo/
MolProbity	(Chen et al., 2010)	https://www.phenix-online.org/; RRID: SCR_014226
pdb-care	(Lutteke and von der Lieth, 2004)	http://www.glycosciences.de/tools/pdbcare/; RRID: SCR_001562
Privateer	(Agirre et al., 2015)	http://www.ccp4.ac.uk/

CONTACT FOR REAGENT AND RESOURCE SHARING

Further information and requests for resources and reagents should be directed to and will be fulfilled by the Lead Contact, Christian Obinger (christian.obinger@boku.ac.at).

METHOD DETAILS

Expression and Purification of Fc Proteins

The HEK293-6E cell line constitutively expressing the Epstein-Barr virus nuclear antigen 1 of the Epstein-Barr virus was licensed from National Research Council (NRC) of Canada (Durocher et al., 2002). Cells were cultured and transfected according to the manufacturer's manual in chemically defined F17 medium supplemented with 0.1% pluronic F-68, 4 mM L-Glutamine (all from Life Technologies, Germany) and 0.05 mg mL^{-1} G418 (Biochrom, Germany). HEK293-6E cells were cultivated at 37°C in a humidified atmosphere with 5% CO_2 without exceeding 2 × 10^6 cells mL^{-1} during maintenance. High quality plasmid preparations of the pTT5 vector (NRC, Canada) containing the coding sequence for the heavy chain signal peptide "MELGLSWIFLLAILKGVQC" and either the Fc region (residues T225-K447) of Fc-wt or the Fcab clone H10-03-6 or STAB19 were prepared by using the NucleoBond Xtra Midi kit (Macherey Nagel, Germany) (Traxlmayr et al., 2013; Wozniak-Knopp et al., 2010). Transient transfection of the cells was performed at a cell density of around 1.7 × 10^6 cells mL^{-1}. A total of 1 μg plasmid-DNA and 2.5 μg linear polyethylenimine (PEI) (Polysciences, Inc., Germany) per mL culture volume were separately diluted in 1/10 volume of fresh medium. After adding the DNA/PEI mixture, the cells were incubated for 48 h, supplemented with 0.5% (w/v) tryptone N1 (Organotechnie, France) and further cultured for 72 h. Soluble protein was harvested by centrifugation (10 000 g, 30 min, 4°C), filtered (0.45 μm Durapore membrane filter, Merck Millipore, Germany) and purified by affinity chromatography using a 5 mL HiTrap Protein A HP column (GE Healthcare, USA) as reported previously including modifications of the loading buffer (20 mM phosphate buffer, 200 mM NaCl, pH 7.4) (Traxlmayr et al., 2012a). Highly concentrated fractions were pooled and dialyzed against Dulbecco's Phosphate Buffered Saline (PBS, pH 7.4) (Sigma-Aldrich, USA) supplemented with 200 mM NaCl at 4°C overnight (SnakeSkin Dialysis Tubing, 10 K MWCO, Thermo Fisher Scientific, USA). Protein samples were further concentrated using 30 kDa Amicon Ultra Centrifugal Filter (Merck Millipore, Germany) and subjected to size-exclusion chromatography (SEC) on a HiLoad 16/600 Superdex 200 pg (prep grade) column (GE Healthcare, USA) equilibrated with the same buffer used for dialysis.

Expression and Purification of HER2

The CHO Lec1 cell line expressing the extracellular domain of human HER2 (residues 1-631) as a fusion protein with human growth hormone via a poly-histidine tag and a tobacco etch virus (TEV) cleavage site (hGH-HER2) was a generous gift from Dr. Josef Singer (Medical University Vienna, Austria) with permission of Prof. Daniel J. Leahy (Johns Hopkins University, MD, USA) (Cho et al., 2003; Leahy et al., 2000). Cells were grown in roller bottles in DMEM/F-12 supplemented with 0.5-1% (v/v) fetal bovine serum (FBS), 2.5 mM L-glutamine (all from Life Technologies, Germany), 0.5 mg mL^{-1} G418 (Biochrom, Germany) and 100 nM methotrexate (Sigma-Aldrich, USA) in a humidified atmosphere containing 5% CO_2 at 37°C. Conditioned medium was harvested twice a week, stored at 4°C and prepared for metal chelate affinity chromatography as described previously (Bouyain et al., 2005). Solution was loaded onto a 5 mL HisTrap HP column (GE Healthcare, USA) and bound protein eluted applying a step gradient. Following rigorous washing with loading buffer (20 mM TRIS-HCl, 500 mM NaCl, 10 mM imidazole, pH 8.0), a large portion of impurities derived from FBS was removed using 27 mM imidazole. Finally, hGH-HER2 was eluted applying 500 mM imidazole. After TEV cleavage the sample was further purified by ion exchange chromatography using a 6 mL Resource Q column (GE Healthcare, USA) equilibrated with 20 mM TRIS-HCl (pH 8.0) and eluted using a gradient from 0 to 500 mM NaCl over 20 column volumes. Fractions containing HER2 were pooled, dialyzed (10 mM TRIS-HCl, 50 mM NaCl pH 7.5) and subjected to SEC as described before.

Differential Scanning Calorimetry

The thermal stabilities of Fcabs were measured by DSC. The proteins were diluted to 5 μM in PBS buffer (pH 7.4), followed by analysis on a MicroCal VP-Capillary DSC (Malvern Instruments, Ltd., UK). Samples were heated from 20 to 110°C with a heating rate of 1°C min^{-1}. After subtraction of buffer baselines, the data were normalized for protein concentration and fitted with a non-two-state thermal unfolding model using the software Origin 7.

X-ray Crystallography and Data Collection

To ensure optimal prerequisites for structural studies all protein samples were freshly produced and purified including SEC as final polishing step. Fc-wt, H10-03-6 and STAB19 in PBS buffer (pH 7.4) were concentrated using 30 kDa Amicon Ultra Centrifugal Filter to 8.0 mg mL^{-1}, 6.6 mg mL^{-1} and 4.7 mg mL^{-1}, respectively. Separation of the Fcab–antigen complexes was performed by mixing HER2 with an excess of Fcab and loading onto the HiLoad 16/600 Superdex 200 pg column (GE Healthcare, USA) pre-equilibrated with 10 mM TRIS-HCl and 50 mM NaCl (pH 7.5) buffer. Fractions comprising the complex were concentrated to 4 mg mL^{-1} for the STAB19-HER2 complex and 5 mg mL^{-1} for the H10-03-6-HER2 complex and dialyzed against 10 mM TRIS-HCl (pH 7.5). For crystallization of the H10-03-6-HER2 complex, HER2 was prior subjected to Endoglycosidase H (New England BioLabs Inc., Germany) digestion and re-chromatographed on the size-exclusion column.

Crystallization experiments were carried out using the sitting drop vapor diffusion method. Crystallization drops were set using a Phoenix HT robot (Art Robins Instruments, USA). The reservoir was filled with 40 μL precipitant solution. Ratios of 150:200 nL,

200:200 nL and 250:200 nL protein to precipitant were dispensed. Hits were only obtained in a slightly modified version of the Low Ionic Strength screen (Hampton Research, USA) based on Harris et al. (Harris et al., 1995). Crystallization plates were stored in a Minstrel DT UV imaging device (Rigaku, USA) at 22°C. Crystals were soaked with mother liquor supplemented with 20%-25% (v/v) glycerol, harvested using cryo-loops and flash-cooled in liquid nitrogen. Data sets were collected at the European Synchrotron Radiation Facility (ESRF, Grenoble, France) at 100 K on different DECTRIS PILATUS detectors according to the beamline used (Table 1).

Structure Determination and Refinement

Structure Determination and Refinement of Fc-wt, H10-03-6 and STAB19

Data sets were integrated and scaled with the XDS software-suite (Kabsch, 2010).The high-resolution cut-off was based on a CC1/2* criterion (Karplus and Diederichs, 2012). The phase problem was solved by molecular replacement using Phaser-MR (McCoy et al., 2007) taking the PDB structure 1OQO (Complex between G0 version of an Fc bound to a minimized version of Protein A called Mini-Z) as search model. The model was further improved by iterative cycles of manual model building using COOT (Emsley et al., 2010) and maximum likelihood refinement using PHENIX-Refine (Adams et al., 2010). Final stages of refinement included Translation Libration Screw (TLS) parameters (CH2 and CH3 domains of each chain were defined as TLS groups), isotropic B-factor model, automated correction of N/Q/H errors, automated addition of hydrogens and water molecules and optimization of X-ray/ADP- and X-ray/stereochemistry-weight. In the last refinement step, the occupancy of atoms of side chains in residues that were not clearly defined at an electron density higher than 1.0 RMSD (root-mean-square deviation) were set to zero. Modeling and refinement of H10-03-6 and STAB19 was done similar to Fc-wt. Details can be found in Table 1.

Structure Determination and Refinement of STAB19-HER2 and H10-03-6-HER2 Complexes

Data sets were integrated and scaled with the XDS software-suite (Kabsch, 2010). The high-resolution cut-off for the STAB19-HER2 complex was initially based on a CC1/2* criterion (3.00 Å) (Karplus and Diederichs, 2012) but for the last refinement run paired refinement was used to establish a new resolution cut-off at 3.30 Å. The structure of STAB19-HER2 was solved by several cycles of molecular replacement using the HER2 model of the PDB structure 1N8Z (Crystal structure of extracellular domain of human HER2 complexed with Herceptin Fab) (Cho et al., 2003) and STAB19 (PDB: 5JIH) as search model. This model was further improved by iterative cycles with COOT (Emsley et al., 2010) and refined using PHENIX-Refine (Adams et al., 2010), REFMAC5 (Murshudov et al., 1997) including ProSMART (Nicholls et al., 2012) restraints, BUSTER (Smart et al., 2012), TLS, Rosetta-Refinement (DiMaio et al., 2013) and a developed version of PDB_REDO (Joosten et al., 2012, 2014) that uses homology-based hydrogen bond restraints. Final stages of refinement included one TLS group per chain, isotropic B-factor model (based on the Hamilton R ratio test (Joosten et al., 2012, 2014)), automated correction of N/Q/H errors and optimization of X-ray/ADP- and X-ray/stereochemistry-weight. The structure of the H10-03-6-HER2 was processed and refined similar to the STAB19-HER2 structure using the latter as search model for molecular replacement (PDB: 5K33). Details can be found in Table 1.

Validation of the Structures

All models were validated with MolProbity (Chen et al., 2010) and PDB_REDO (Joosten et al., 2012, 2014). Carbohydrates were validated with pdb-care (Lutteke and von der Lieth, 2004) and Privateer (Agirre et al., 2015). Figures were prepared with PyMOL Molecular Graphics System (Version 1.3, Schrödinger, LLC). Atomic coordinates have been deposited in the Protein Data Bank under accession codes 5JII (Fc-wt), 5JIK (H10-03-6), 5JIH (STAB19), 5KWG (H10-03-6-HER2) and 5K33 (STAB19-HER2).

Size Exclusion Chromatography-Multi-Angle Light Scattering

Size-exclusion chromatography combined with multi-angle light scattering was performed to determine the molar mass of all proteins under study and the respective Fcab-HER2 complexes. HPLC (Shimadzu prominence LC20, Japan) was equipped with MALS (WYATT Heleos Dawn8+ plus QELS; software ASTRA 6), refractive index detector (RID-10A, Shimadzu) and a diode array detector (SPD-M20A, Shimadzu). The column (Superdex 200 10/300 GL, GE Healthcare, USA) was equilibrated with PBS plus 200 mM NaCl (pH 7.4) as running buffer. Experiments were performed at a flow rate of 0.75 mL min^{-1} at 25°C. The proper performance of molar mass calculation by MALS was verified by the determination of a sample of bovine serum albumin. Prior to analysis, all proteins were centrifuged (17 000 g, 10 min, 20°C) and filtered (0.1 μm Ultrafree-MC filter, Merck Millipore, Germany). Single protein measurements were performed by injection of a total amount of 25 μg. For the HER2 complex runs, Fc-wt, H10-03-6 and STAB19, respectively, were mixed with the antigen in a molar ratio of 1:2 starting from 25 μg of the respective Fc molecule prior to analysis. Concentrations of the interaction partners of the injected mixture amounted to 5 μM for the Fc proteins and 10 μM for the HER2.

Isothermal Titration Calorimetry

ITC measurements were performed on a MicroCal PEAQ-ITC (Malvern Instruments, Ltd., UK) to investigate the binding stoichiometry of the STAB19-HER2 complex in solution. All samples were prepared in PBS (pH 7.4), centrifuged (17 000 g, 10 min, 20°C) and filtered

(0.1 μm Ultrafree-MC filter, Merck Millipore, Germany) prior to measurements. Sample cell (V=200 μL) was filled with 80 μM HER2 and titrated with 400 μM STAB19. Titrations were conducted at 25°C using an initial injection of 0.1 μL followed by 19 successive injections of 2 μL with a 180 sec interval in between. Curve fitting was performed based on a one-site binding model to determine the binding stoichiometry (N) using the MicoCal PEAQ-ITC analysis software.

Fluorescence Correlation Spectroscopy

A ConfoCor 2 spectrofluorimeter (Carl Zeiss-Evotec, Germany) equipped with an air-cooled Argon-laser (LASOS Lasertech GmbH, Germany; intensity 70 μW) and a water immersion objective (C-Apochromat 63 ×/1.2 W Corr) was used for monitoring STAB19-HER2 interactions. The focus in the *z*-direction was set 150 μm over the cover glass of a 384-well plate (Greiner Bio-One, Germany) to record diffusion of fluorescent particles through the focal element. The diameter of the pinhole was set to 35 μm and the confocal volume was calibrated using DyLight 488 dye (D_{trans} = 4.0 × 10^{-10} m^2 s^{-1}). All FCS measurements were performed in a sample volume of 10 μL and at 20°C. Various concentrations from 12 000 nM to 2 nM HER2 were prepared in PBS buffer (pH 7.4) supplemented with 0.05% Tween (pH 7.4). To each dilution of HER2 a fixed concentration of 31 nM DyLight 488-labeled STAB19 was added. Intensity fluctuations were recorded by an avalanche photodiode (SPCM-CD 3017) in photon counting mode over a time period of 30 sec and autocorrelated with a hardware correlator (ALV 5000, ALV, Germany). Evaluation of the autocorrelated curves was performed with the FCS ACCESS Fit (Carl Zeiss-Evotec, Germany) software package using a Marquardt nonlinear least-squares algorithm for a one-component fitting model (Figure S3) (Rigler and Elson, 2001). The obtained translational diffusion times τ_D (s) are related to the translational diffusion coefficient D_{trans} (m^2 s^{-1}) and the radius ω_0 of the laser beam (2.38 × 10^{-7} m). The molar mass (kDa) was estimated from the Stokes-Einstein relation assuming spherical shape of the molecules

$$MW = \frac{4\rho N_A}{3\pi^2}\left(\frac{k_B T}{6\eta D_{trans}}\right)^3 \Bigg| D_{trans} = \frac{\omega_0^2}{4\tau_D} \qquad \text{[Equation 1]}$$

where ρ is the mean density of the molecules (1000 kg/m^3), N_A is the Avogadro's number (6.023 × 10^{23} mol^{-1}), k_B is the Boltzmann constant (1.38 × 10^{-23} J K^{-1}), T is the temperature (293 K) and η is the viscosity of the solvent (0.001 kg m^{-1} s^{-1}). Estimation of the two K_D values (nM) of negatively cooperative binding behavior was done by fitting the titration-isotherm in Figure 6B (black line) to the Adair-Klotz equation (Equation 2) for a two-site sequential binding model (Adair et al., 1925; Klotz, 1946, 2004)

$$MW = \frac{1}{2}\frac{\frac{[HER2]_0}{K_{D1}} + 2\frac{[HER2]_0^2}{K_{D1}K_{D2}}}{1 + \frac{[HER2]_0}{K_{D1}} + \frac{[HER2]_0^2}{K_{D1}K_{D2}}} MW_{HER2} + MW_{STAB19} \qquad \text{(Equation 2)}$$

where MW is the average molar mass (kDa), $[HER2]_0$ is the concentration of HER2 that was added (dilutions from 12 000 nM to 2 nM), K_{D1} and K_{D2} refer to the fitted association constants (nM) and MW_{HER2} and MW_{STAB19} are the fitted molar masses of unbound HER2 and STAB19 (kDa), respectively. This equation neglects the fact that the ligand (HER2) is partially consumed for complex formation, slightly changing its concentration. The gray line in Figure 6B shows the fit to a single class of sites (Hulme and Trevethick, 2010). Importantly, titration of the ligand was performed between 2 nM to 12 000 nM of HER2, covering 0.1 × K_D and 10 × K_D to reach over 90% occupancy (Hulme and Trevethick, 2010).

Liquid Chromatography-Electrospray Ionization-Mass Spectrometry

For glycopeptide profiling 20 μg of Fc-wt in PBS buffer (pH 7.4) were S-alkylated with iodoacetamide and further digested with sequencing grade modified trypsin (Promega, USA). 5 μg of the peptide mixture were analyzed using a Dionex Ultimate 3000 HPLC-system (Thermo Scientific, USA) directly linked to a QTOF instrument (maXis 4G ETD, Bruker, Germany) equipped with the standard ESI source in the positive ion, DDA mode (= switching to MSMS mode for eluting peaks). MS-scans were recorded (range: 150-2200 m/z, spectra rate: 0.5 Hz) and the three highest peaks were selected for fragmentation. Instrument calibration was performed using ESI tuning mix (Agilent, USA). For separation of the peptides a Thermo BioBasic C18 separation column (5 μm particle size, 150 × 0.320 mm) was used. A gradient from 96% solvent A and 4% solvent B (Solvent A: 65 mM ammonium formiate buffer, pH 3.0; Solvent B: 80% ACCN and 20% A) to 40% B in 35 min was applied, followed by a 15 min gradient from 40% B to 94% B, at a flow rate of 6 μL min^{-1} at 32°C. Manual glycopeptide searches were done using DataAnalysis 4.0 (Bruker, Germany). For the quantification of the different glycoforms the peak areas of EIC (Extracted Ion Chromatograms) of the first five isotopic peaks were summed. Different charge states and adduct formation were taken into account.

For the quantification of the amount of unglycosylated peptides the sample material was deglycosylated with PNGase A and re-measured using the same protocol and MS-tuning. True peak areas of coeluting unglycosylated and deamidated peptides were calculated using their theoretical isotopic pattern.

QUANTIFICATION AND STATISTICAL ANALYSIS

Evaluation of the Goodness of the Fit

Quoted error bars in FCS evaluation plot (Figure 6B) represent the standard deviation of a total of 24 (n) measurements performed in 3 independent experiments. Data points (N=14) were fitted to a one-state model (Hulme and Trevethick, 2010) with 3 parameters (V_1) to fit and to a two-state model (Equation 2) with 4 parameters (V_2) to fit. To compare the goodness of the fit between the two models an F-test was performed using the following equation

$$F = \frac{(SS1 - SS2)/(df1 - df2)}{SS2/\ df2}$$

where SS_1 and SS_2 refers to the sum of squares of each fit and df_1 and df_2 represent the respective number of degrees of freedom (N-V) (Motulsky and Ransnas, 1987). The calculated F-value together with (df_1-df_2) and df_2 was used to obtain a p value. Significance was declared by obtaining a p-value < 0.001. The small p-value indicates that the model with more parameters fits the data significantly better than model with less parameters.

DATA AND SOFTWARE AVAILABILITY

Atomic coordinates and structure factors have been deposited in the RCSB Protein Data Bank under ID codes 5JII (human IgG1-Fc), 5JIK (Fcab H10-03-6), 5JIH (Fcab STAB19), 5KWG (H10-03-6-HER2 complex) and 5K33 (STAB19-HER2 complex). All software described in the method details is available from the sites listed in the Key Resources Table.

Structure, Volume *25*

Supplemental Information

Fcab-HER2 Interaction: a Ménage à Trois.

Lessons from X-Ray and Solution Studies

Elisabeth Lobner, Anne-Sophie Humm, Kathrin Göritzer, Georg Mlynek, Martin G. Puchinger, Christoph Hasenhindl, Florian Rüker, Michael W. Traxlmayr, Kristina Djinović-Carugo, and Christian Obinger

Supplemental information

Table S1. Site-specific glycosylation profile of Fc-wt

	N-glycans	Rel. amount (%)
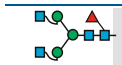	GnGnF	43.7
	GnAF	36.8
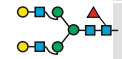	AAF	7.1
	GnAFbi	2.6
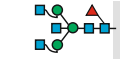	GnGnFbi	2.2
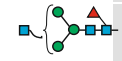	MGnF	1.5
	GnGn	0.8
	GnGnbi	0.8
	GnAbi	0.7
	MAF	0.7
	Man5	0.5
	ANaF	0.5
	UGnF	0.5
	GnNaF	< 0.5
	AAFbi	< 0.5
	MGn	< 0.5
	GnA	< 0.5
	NaNaF	< 0.5
	AA	< 0.5

Table S1. Related to Figure 3 and S1. Site-specific glycosylation profile of IgG1-Fc. The relative amounts of glycoforms for the peptide EEQYNSTYR are depicted. Site occupancy was quantified after PNGase A release (27% unglycosylated peptide, 73% glycopeptides). The composition of the six most abundant glycoforms is schematically represented. For glycan nomenclature, see www.proglycan.com.

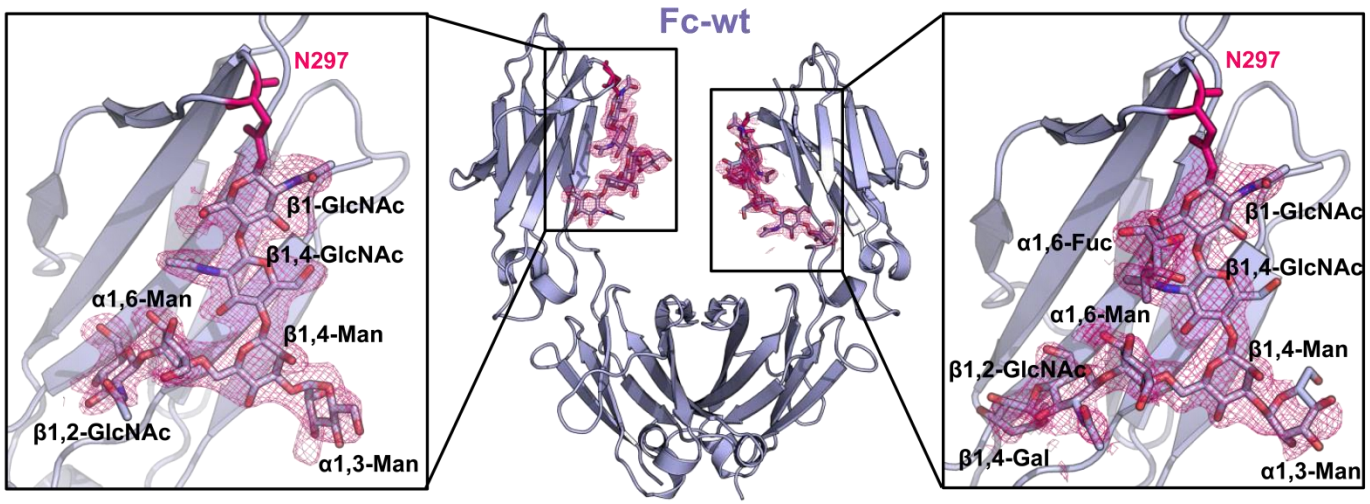

Figure S1. Related to Figure 3 and Table S1. N-glycosylation of the crystal structure of IgG1-Fc (Fc-wt). Close-up view of the biantennary N-linked glycan structure at N297 (pink) of both chains of Fc-wt. The $2mF_o$-DF_c electron density map is contoured at RMSD=1 and depicted in pink. Carbohydrates modelled in the electron density are shown as violet sticks.

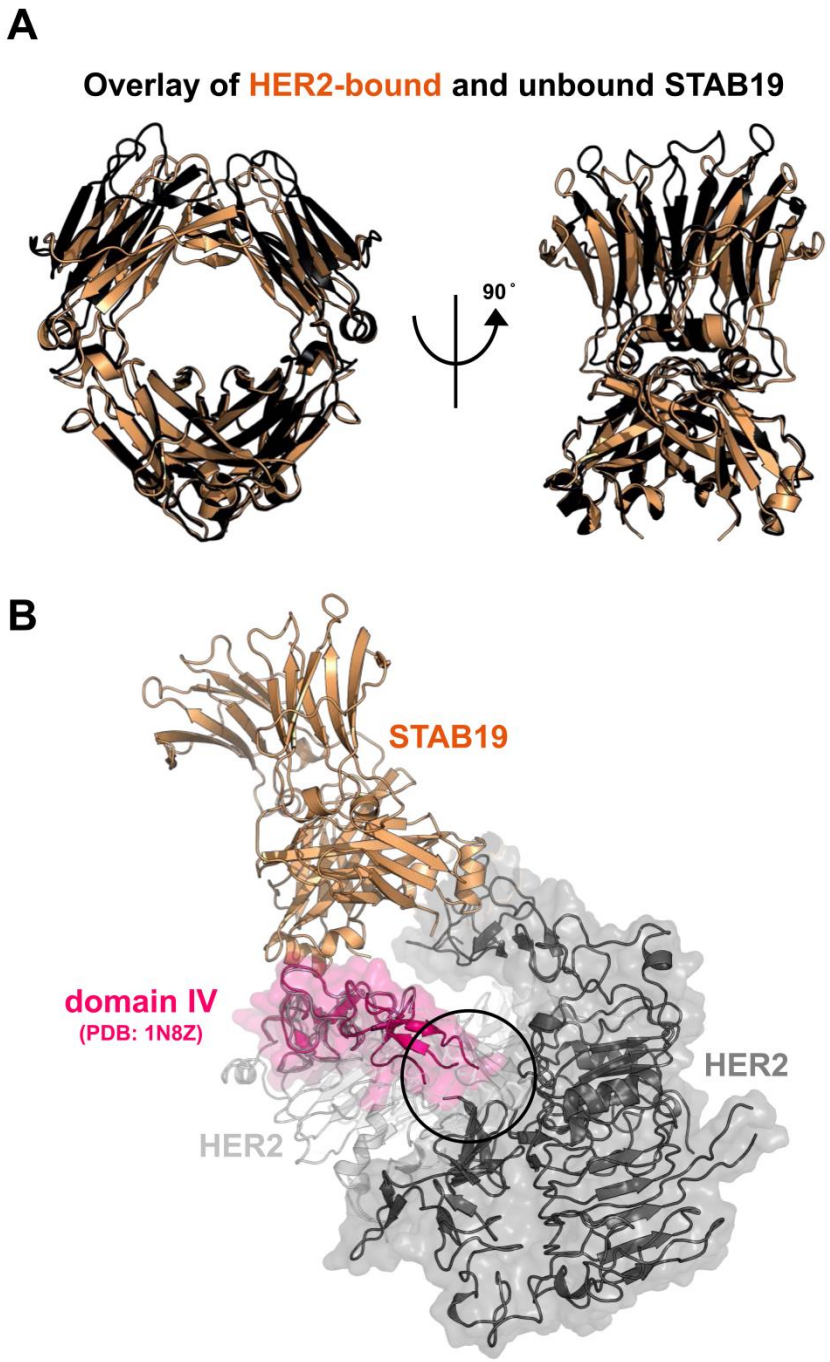

Figure S2. Related to Figure 4. Analysis of allosteric effects and sterical clashes. (A) Superimposition of the unbound STAB19 (black) and the HER2-bound STAB19 structure (orange) aligned on both CH3 domains. (B) Superimposition of domain IV (H490-A576) of the STAB19–HER2 complex and domain IV (H490-N607) of the trastuzumab Fab–HER2 complex (PDB: 1N8Z). For evaluation of sterical clashes the surfaces of domain IV of the trastuzumab Fab–HER2 complex (pink) and of one HER2 molecule of the STAB19–HER2 complex (dark gray) are depicted. Potential sterical clashes are indicated by a circle.

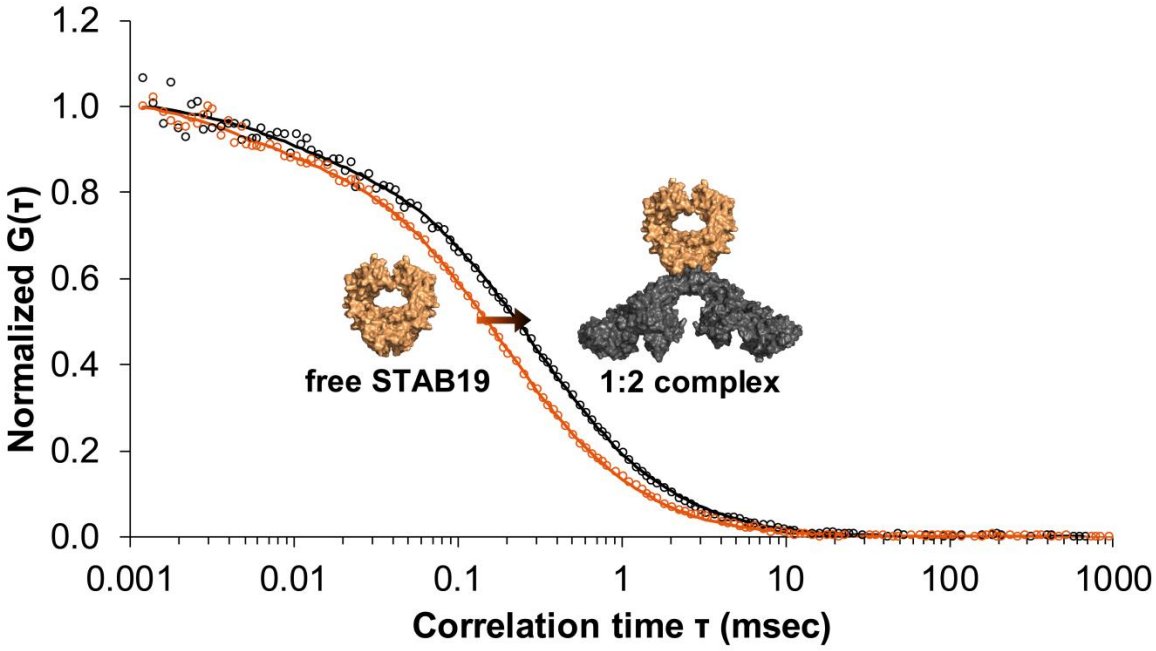

Figure S3. Related to Figure 6B. Autocorrelation analysis of STAB19-DyLight 488 in absence of and saturated with HER2. Fluorescence fluctuations of 31 nM of labeled STAB19 either unbound (orange) or bound to 12 µM HER2 (black) were recorded in triplicate over 30 sec using FCS and autocorrelated. The binding of HER2 to STAB19 results in an increase in molar mass and thus a shift of the autocorrelation curve to higher correlation times. Translational diffusion times were obtained from a one-component fitting routine (solid lines) of the autocorrelated dataset (circles) using the Marquardt nonlinear least-squares algorithm (Relative least-squares <0.0019).

Two-Faced Fcab Prevents Polymerization with VEGF and Reveals Thermodynamics and the 2.15 Å Crystal Structure of the Complex

Lobner E., Humm A., Mylnek G., Kubinger K., Kitzmüller M., Traxlmayr M.W., Djinović-Carugo K. and Obinger C.

Manuscript

Submitted to *MAbs* (June 2017)

Two-Faced Fcab Prevents Polymerization with VEGF and Reveals Thermodynamics and the 2.15 Å Crystal Structure of the Complex

Elisabeth Lobner[1,2], Anne-Sophie Humm[1,3], Georg Mlynek[3], Konstantin Kubinger[1,2], Michael Kitzmüller[1,2,§], Michael W. Traxlmayr[1,2], Kristina Djinović-Carugo[3,4], Christian Obinger[1,2,*]

[1]Christian Doppler Laboratory for Antibody Engineering, BOKU – University of Natural Resources and Life Sciences, Muthgasse 18, A-1190 Vienna, Austria
[2]Department of Chemistry, Division of Biochemistry, BOKU – University of Natural Resources and Life Sciences, Muthgasse 18, A-1190 Vienna, Austria
[3]Department for Structural and Computational Biology, Max F. Perutz Laboratories, University of Vienna, Dr. Bohr-Gasse 9, A-1030 Vienna, Austria
[4]Department of Biochemistry, Faculty of Chemistry and Chemical Technology, University of Ljubljana, Večna pot 113, 1000 Ljubljana, Slovenia
*Correspondence: christian.obinger@boku.ac.at
[§]Michael Kitzmüller passed away in October 2015.

Abbreviations: IgG, immunoglobulin class G; Fcab, Fc domain with antigen-binding sites; Fc-wt, Fc wild-type; 448 and CT6, VEGF-binding Fcabs; Janus448 and JanusCT6, heterodimeric VEGF-binding Fcabs; VEGF, vascular endothelial growth factor; SEC, size exclusion chromatography; MALS, multi-angle light scattering; DSC, differential scanning calorimetry; LC-ESI-MS, liquid chromatography-electrospray ionization-mass spectrometry; ITC, isothermal titration calorimetry.

Graphical abstract

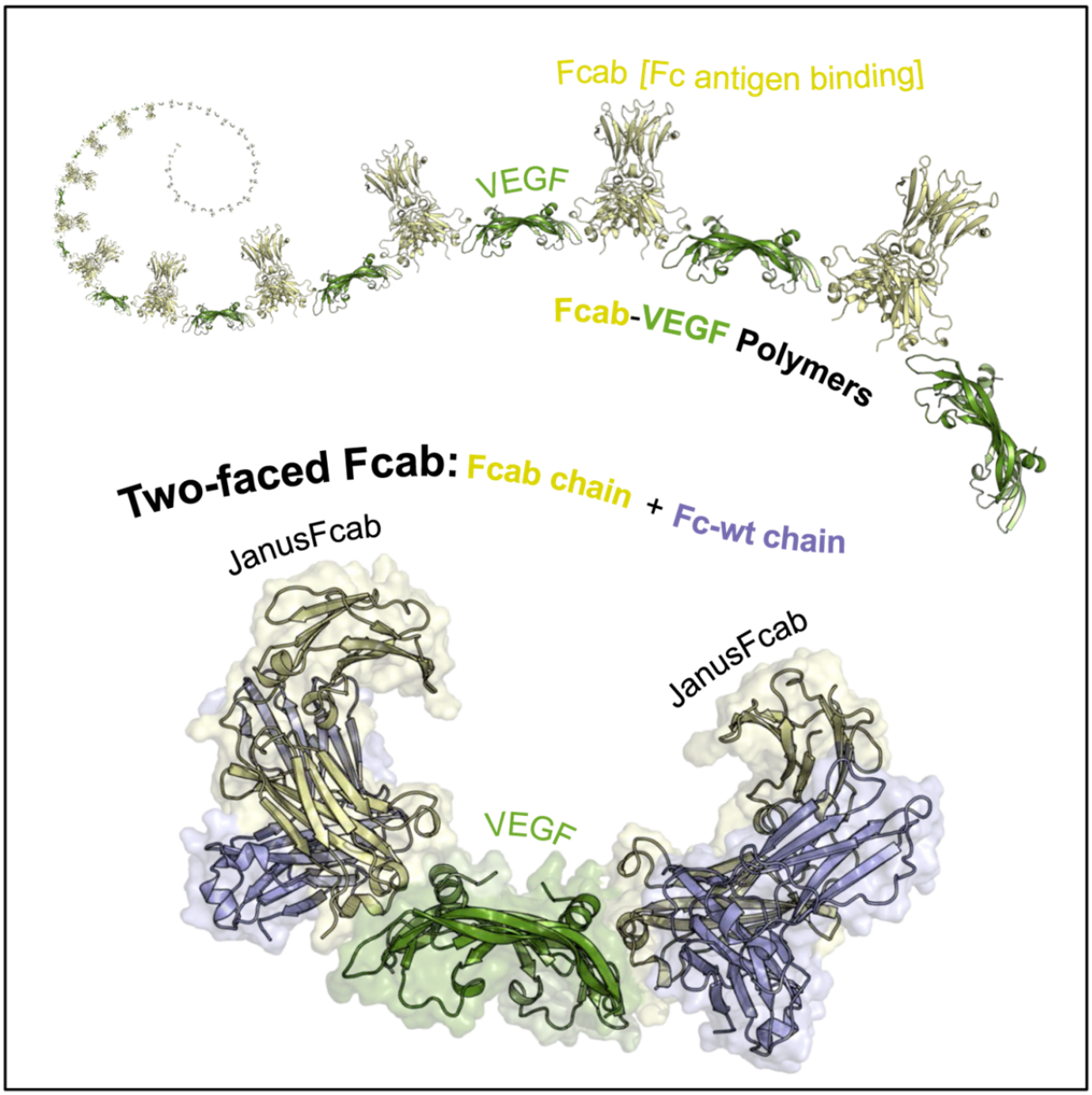

Keywords

Fcab, IgG1-Fc, X-ray crystallography, VEGF, heterodimeric Fcab, CH3 domain

ABSTRACT

Fcabs (Fc domain with antigen-binding sites) are promising novel therapeutics. By engineering of the C-terminal loops of the CH3 domains two antigen binding sites can be inserted in close proximity. In order to elucidate the binding mode(s) between homodimeric Fcabs and small homodimeric antigens, the interaction between the Fcabs 448 and CT6 (having the AB, CD and EF loops and the C-termini engineered) with homodimeric VEGF was investigated. The crystal structures of these Fcabs, which form polymers with the antigen VEGF in solution, were determined. However, construction of heterodimeric Fcabs (JanusFcabs: one chain Fc-wt, one chain VEGF-binding) results in formation of distinct JanusFcab–VEGF complexes (2:1) which allowed elucidation of the crystal structure of the JanusCT6–VEGF complex at 2.15 Å resolution. VEGF binding to Janus448 and JanusCT6 is shown to be entropically unfavorable but enthalpically favorable. Structure-function relationships are discussed with respect to Fcab design and engineering strategies.

INTRODUCTION

Since the mid-1980s more than 60 therapeutic antibodies or antibody-based products have granted approval (antibodysociety.org, update: June 2017). Approximately half of them gained market approval in the last six years demonstrating the substantial importance and commercial success of this fast growing class of biopharmaceutical drugs. Beside a considerable amount of chimeric, humanized and also human antibodies, to date, more than ten Fc-fusion proteins have been approved by the FDA (Jafari et al., 2017). The capability of this immunological protein to induce Fc-related effector functions such as antibody-dependent cellular cytotoxicity (ADCC), complement-dependent cytotoxicity (CDC) and the interaction with the neonatal Fc receptor (FcRn) responsible for the long *in vivo* half life (Beck and Reichert, 2011; Kubota et al., 2009; Rath et al., 2015) makes the Fc fragment to an indispensable feature for improvement of pharmacokinetics and achievement of clinical efficacy.

IgG1-Fc is a homodimeric protein with each chain (T225-K447, Eu numbering system (Edelman et al., 1969)) consisting of two domains (CH2 and CH3) and one N-linked glycosylation at position 297. The two chains are covalently connected via two disulfide bridges in the hinge region and non-covalently by extensive interactions between the two CH3 domains. This IgG1-Fc protein can serve as a starting scaffold for the design of Fc domains with antigen-binding sites (i.e. Fcabs). Each constant domain in IgG1-Fc is composed of two antiparallel β-sheets adopting the typical immunoglobulin fold which is known to tolerate variability in sequence and length in its loops connecting the β-strands, similar to the CDR-loops (Halaby et al., 1999). The CH3 domain exhibits three C-terminal structural loops that can be engineered for antigen-binding, namely the AB loop (R355-Q362), CD loop (S383-Y391) and EF loop (D413-V422). Incorporation of those artificial binding sites into an IgG1-Fc molecule results in Fcabs, which combine all antibody functions including antigen binding, at a size of only ~50 kDa. Moreover, by reunion of the Fcab with Fab arms of a different specificity a bispecific antibody (mAb^2) can be obtained (Lobner et al., 2016).

Proof of concept that it is possible to engineer binding sites in the CH3 domains of IgG1-Fc was demonstrated by generating the human epidermal growth factor receptor 2 (HER2)-binding Fcab H10-03-6. This Fcab was

engineered by randomly mutating the AB and EF loops in the CH3 domains, followed by selection for antigen binding using yeast surface display. Remarkable, this Fcab revealed *in vivo* half life in mice comparable to that of human wild type IgG1-Fc (Fc-wt) in addition to ADCC activation of natural killer cells against a HER2-positive cell line and significant retardation of tumor growth in mice xenograft models (Jez et al., 2012; Woisetschlager et al., 2014; Wozniak-Knopp et al., 2010). To improve the biophysical properties of this Fcab a directed evolution approach was developed resulting in Fcabs with increased conformational stability and retained binding affinity (STAB Fcabs) (Traxlmayr et al., 2013). Recently, the X-ray structures of the parental Fcab H10-03-6 and its stabilized version STAB19 were determined illuminating the impact of loop design on the fold and the stability of Fcabs. The complex structure representing one Fcab binding to two HER2 molecules together with elaborate solution studies unveiled a negative cooperative binding behavior (Lobner et al., 2017).

Moreover, the next generation Fcab FS102 targeting HER2 with high affinity was shown to surpass a combination of the two clinically approved antibodies trastuzumab and pertuzumab in *in vitro* and *in vivo* studies. This Fcab induces internalization and degradation of HER2 finally leading to tumor cell apoptosis (Leung et al., 2015). Due to this superior antitumor effect FS102 entered clinical phase I.

In order to investigate how a homodimeric Fcab, containing two independent binding sites, interacts with a soluble homodimeric antigen, the vascular endothelial growth factor (VEGF) was chosen as a homodimeric model protein. Depending on the steric constraints in the two interaction partners, 1:1, 1:2 or 2:1 complexes, or even the formation of polymers seemed to be possible. Detailed characterization of such an interaction yields valuable information for future engineering strategies using Fcabs or other bivalent binding molecules, such as antibodies. The present study aimed to investigate the interaction of the two Fcabs 448 and CT6 which were engineered for binding to VEGF-A. Both Fcabs carry the same mutations within the AB, CD and EF loops with CT6 having additionally the C-terminal part engineered for increased binding affinity (Figure 1). The biophysical and structural characterization of the two Fcabs and the exceptional circumstances that necessitated the generation of a heterodimeric Fcab molecule with only one binding site to finally obtain the 2.15 Å X-ray structure of a complex with VEGF-A are described.

RESULTS

This study aimed to investigate the interaction and binding stoichiometry between homodimeric Fcabs with their homodimeric antigen VEGF displaying two potential epitopes. Structural and thermodynamic studies would give interesting insights into the loop design, the overall structure of the engineered IgG1-Fc molecule, the binding mode and the interface residues that are involved in the interaction.

Homodimeric Fcabs derived from a mutated IgG1-Fc library displayed on the yeast cell surface (Boder and Wittrup, 1997). The library was sorted for binding to VEGF similar to previous studies (Traxlmayr et al., 2013; Wozniak-Knopp et al., 2010), resulting in the two Fcabs 448 and CT6. Both binders contain mutations in the AB (positions 359-361), CD (positions 388-389; including five insertions at positions 389a-389e) and EF loops (positions 413-422) of the CH3 domains (Eu numbering system (Edelman et al., 1969)). Finally, eight residues at the C-terminal end (position 440-447) of 448 were randomly mutated in order to improve its affinity, yielding the Fcab CT6. Thus, CT6 represents an affinity-matured version of 448 with the only sequence difference between these two Fcabs being seven C-terminal amino acids (Figure 1).

Biophysical and structural characterization of VEGF-binding Fcabs

To ensure that the HEK293-expressed Fcabs as well as *E. coli*-produced truncated VEGF are natively folded and stable, they were analyzed by size exclusion chromatography combined with multi-angle light scattering (SEC-MALS) and differential scanning calorimetry (DSC) (Figure 2). Evaluation by SEC-MALS revealed no high molecular weight aggregates. Only one symmetrical peak was observed for all proteins with molar masses of 54 kDa (Fc-wt), 58 kDa (448), 59 kDa (CT6) and 23 kDa (VEGF) (Figure 2A). Despite the higher molar masses of the two Fcabs, their retention times are slightly longer than that of Fc-wt indicating some nonspecific interaction with the column matrix. Moreover, DSC profiles present the thermal unfolding of the CH2 domains (T_{m1}) and the CH3 domains (T_{m2}) which show two distinct peaks in Fc-wt with a T_{m1} value of 70.4 °C and a T_{m2} value of 82.6 °C, which is consistent with previous studies (Figure 2B) (Lobner et al., 2017; Traxlmayr et al., 2013). The T_{m1} values of the Fcabs are wild-type like but due to the extensive mutations in the CH3 domains of the Fcabs

the T_{m2} values are shifted towards lower temperature. The Fcab 448 shows only one main transition with a fitted T_m value of 70.1°C. Interestingly, CT6, having also the C-terminal part mutated, exhibits an increased thermal stability. Its DSC profile clearly shows two thermal transitions with an increased T_{m2} value of 75.2 °C (Figure 2B). The determined T_m value of 110.5 °C of recombinant VEGF is in accordance with the published midterm transition value of VEGF measured by DSC (Muller et al., 2002).

Structural information on both Fcabs was obtained by crystallization using the sitting drop vapor diffusion method. Crystals of 448 and CT6 had the symmetry of space group $P12_11$ and $P22_12_1$, respectively (Table 1). The highly flexible hinge region of both structures could not be determined and each chain of the models encompasses residues G236-L443 (448) and G236-W445 (CT6). The electron density is of high quality throughout the structure, besides the loop regions of the CH2 domain of chain A of 448 and chain B of CT6. This is also reflected in higher B-factor values suggesting higher flexibility of the respective CH2 domain. The CH2 domain of chain B of 448 and chain A of CT6 is stabilized by crystal packing resulting in lower B-factors and electron density of higher quality. Superimposition of the two VEGF-binding Fcabs shows a continuous overlay of the protein backbone and side chain orientation for the CH2 and CH3 domains. Differences can only be seen at the C-terminus, which differs in sequence between these two Fcabs, as well as for the N-glycan content at position 297 in the CH2 domain. For each chain, electron density allowed fitting of the typical mammalian expressed N297-linked pentasaccharide biantennary core (MM) consisting of two N-acetylglucosamine and three mannose residues in addition to further residues such as β1,2-linked N-acetylglucosamine (GnM) and α1,6-linked fucose (GnMF) depending on the observed electron density. Comparison with the crystal structure of human Fc-wt (PDB: 5JII, (Lobner et al., 2017)) (Figure 3A) revealed differences in the arrangement of the flexible CH2 domains. In contrast to Fc-wt showing a highly open structure of the horseshoe shaped Fc, the CH2 domains of the Fcabs (Figure 3B and 3C) are positioned in a more closed arrangement. This fact could be attributed to quantitative and qualitative variations in the N-glycosylation as well as altered crystal packing (Ahmed et al., 2014; Borrok et al., 2012; Teplyakov et al., 2013).

After rotating the structures by 90° around the vertical axis (Figure 3A to 3C) the elongated CD loops of 448 and CT6 become very conspicuous by

protruding to the solvent. Although this loop seems very flexible, enough electron density allows for perfectly modelling of all residues in this region. This observation can be attributed to the certain crystal packing where the CD loops or parts of the CD loops make crystal contacts with the neighboring molecules (pink mesh in Figure 3D).

Beside the elongated CD loops the β-strands of the CH3 domains as well as the backbone of the mutated regions of AB and EF loops of the two Fcabs show perfect congruency when superimposed with Fc-wt (PDB: 5JII) (Figure 3E). Due to high structural similarity between the mutated loops of 448 and CT6, the CH3 domain of chain A of the latter was used for illustration of the following findings. Rigidity of the loops was shown to be supported by the formation of novel stabilizing polar bonds (NH-OC and OH-OC, < 3.5 Å) between non-mutated and mutated residues of the AB, EF and CD loops as well as the mutated C-terminus of CT6, namely Y361-Y414, N384-T421, N384-R422, I389-Q386, F389a-G389d, S416-T421, E442-Q444 and E442-R422 (blue dashed lines in Figure 3F). Moreover, an interesting network of aromatic rings contributing to π-π stacking (< 6.0 Å) that is not present in Fc-wt could be observed. Involved EF and CD loop residues include F389a, F423, W417 and Y443 (present in 448 and CT6) as well as W445 at the mutated C-terminus of CT6 (Figure 3I).

By focusing on the elongated CD loop of 448 and CT6 a right-handed one-turn α-helix stabilized by an H-bond between Q386 and F389a (*i*+4) can be recognized as indicated by the typical squarish assembly in Figure 3G (Fersht, 1999). The non-mutated proline at position P387 was found to be included in the α-helix. Generally, in the rare case where a proline is present within this structural motif it causes kinks of the α-helical structure (Barlow and Thornton, 1988; Hardy and Nelson, 2000). However, this is not observable in a one-turn helix. Moreover, another proline was selected at position 389b at the end of the short α-helix that is a common feature of this secondary structure motif. This proline is also part of a β-turn (F389a/ P389b/ N389c/ G389d) containing a stabilizing polar bond between F389a and G389d (*i*+3, yellow structure in Figure 3H) (Fu et al., 2009). Importantly, this hydrophobic side chain of the phenylalanine at position 389a points towards the hydrophobic core of the protein where it also takes part in π-π stacking as described above. A β-turn is also present in the CD loop of Fc-wt with the H-bond being located between S383 and Q386 (*i*+3, violet structure in Figure 3H).

These structural data suggest that the higher thermal stability of the CH3 domain of CT6 compared to 448 can be assigned to CT6-specific C-terminal residues that exhibit intradomain non-covalent interactions with both CT6-specific residues (E442-Q444, W445-Y443) and the EF-loop (E442-R422). This is also reflected by the fact that in the CT6 structure (but not in 448) residues 444 and 445 show distinct electron densities.

Formation of Fcab–VEGF polymers

To investigate how homodimeric Fcabs interact with homodimeric VEGF, the two proteins were mixed and analyzed by SEC-MALS. As expected, measurements of a 1:3 molar ratio mixture of Fc-wt and VEGF (Figure 4A) revealed two peaks that were highly similar to the elution profiles of individually analyzed proteins. Also the molar masses of 54 kDa (Fc-wt) and 23 kDa (VEGF) confirm absence of binding between Fc-wt and VEGF. In contrast, analysis of 1:1 molar ratio mixtures of Fcabs 448 or CT6 and VEGF revealed no remaining unbound protein but a tailing peak eluting just after the void volume (Figure 4B and 4C). Analysis of molar mass distribution across the eluted fraction shows descending masses of protein complexes starting with ~500 kDa (448–VEGF, Figure 4B, thick solid line) and ~760 kDa (CT6–VEGF, Figure 4C, thick solid line) indicating formation of Fcab–VEGF polymers varying in size. In agreement with the MALS signal, the CT6–VEGF polymers also start eluting around 15 sec earlier than 448–VEGF polymers, again suggesting that CT6 is able to form larger complexes (i.e. longer chains) with VEGF compared to 448. Together, these data demonstrate that mixing homodimeric Fcabs with homodimeric VEGF molecules results in the formation of polymeric chains, in which each homodimeric molecule binds to two homodimeric interaction partners as schematically represented in Figures 4B and 4C.

Generation and characterization of heterodimeric two-faced Fcabs (JanusFcabs)

The formation of these Fcab-VEGF polymers prevents isolation of a homogeneous protein fraction and thus X-ray crystallography studies. A solution to prevent polymerization is the heterodimerization of the Fcab molecule with a second chain encoding the wild-type sequences in the loop regions and at the C-terminus. For generation of a heterodimeric Fc protein many different strategies resulting in more or less stable proteins have been

developed so far. Here, the approach of Spreter Von Kreudenstein et al. (Spreter Von Kreudenstein et al., 2013) based on mutations within the CH3/CH3 interface was used for the generation of heterodimeric Fcabs (JanusFcab) composed of one VEGF-binding chain of 448 or CT6 and one Fc-wt chain lacking antigen binding sites.

The purity assessment of the heterodimeric samples was done by **liquid** chromatography-electrospray ionization-mass spectrometry (LC-ESI-MS). For evaluation, the predicted molar masses were determined using the ProtParam tool (http://web.expasy.org/protparam/) (Gasteiger et al., 2005) under consideration of hydrogen release due to disulfide bond formation and PNGaseF digest. Moreover, C-terminal lysine clipping by a carboxypeptidase that is a common modification in antibody processing was taken into account (Harris, 1995; van den Bremer et al., 2015). The theoretical values of 50481.5 Da and 50894.9 Da perfectly match the experimental determined values of 50481.2 Da (Janus448) and 50893.8 Da (JanusCT6) represented as main peaks in Figures 5A and 5B, respectively. No homodimeric species could be detected but several small peaks that could be assigned to different O-glycoforms on threonine at position 225 (Figure 5C). Around 10% of this very first amino acid of each Fc chain are occupied with this O-glycosylation. While O-glycosylations are known to be part of antibodies of other classes, IgGs are generally only occupied with N-glycans within the CH2 domains. However, Plomp et al. reported a partial O-glycosylation in the hinge region of human IgG3 samples derived from various sources. Moreover, O-glycans were also found on Fc constructs of IgG4 and IgG1 (Ahmed et al., 2014; Plomp et al., 2015). Whereas in a full-size IgG1 the accessibility for glycosyltransferases is limited, the HEK293-produced Fc proteins can be occupied more easily with an O-linked glycan in the N-terminal hinge region. The major O-glycan species found on T225 was a core 1 structure carrying either one or two additional *N*-acetylneuraminic acid residues (Figure 5C).

Additionally, evaluation by SEC-MALS revealed no high molecular weight aggregates but only one symmetric peak shifted to shorter retention times and slightly smaller molar masses of 56 kDa (Janus448) and 57 kDa (JanusCT6) compared with their respective homodimeric versions (compare Figure 2A Figure 6A). Analysis of the endothermic transitions showed an increase in thermostability despite the additional heterodimerization mutations that were introduced in the CH3 domains (Figure 6B). In contrast to 448 showing rather

one endothermic transition, its heterodimeric version Janus448 shows two distinct peaks with a significant increase of T_{m2} to 76.9 °C. In addition, the T_{m2} value of JanusCT6 was increased by 3 °C when compared to its homodimeric version CT6 (compare Figure 2B and 6B). Surprisingly, for both JanusFcabs the respective T_{m1} values, representing unfolding of the non-mutated CH2 domains, were also slightly increased, exceeding even the T_{m1} value of Fc-wt.

JanusFcabs enable biophysical and thermodynamic investigation of the interaction with VEGF

By mixing VEGF with the respective JanusFcab a binding stoichiometry of 1:2 should be obtained resulting from binding of two heterodimerc Fcabs (only containing one VEGF-binding site) to one homodimeric VEGF molecule (containing two epitopes). For investigation of the molar mass of the complex SEC-MALS measurements were performed mixing different molar ratios of VEGF and either Janus448 (Figure 7A) or JanusCT6 (Figure 7B). No protein fraction was detected right after the void volume but main peaks with molar masses between 104 kDa and 117 kDa for Janus448–VEGF mixtures and molar masses between 121 kDa and 124 kDa for JanusCT6–VEGF mixtures suggesting JanusFcab–VEGF complexes revealing mainly a 2:1 (theoretical molar mass of ~136 kDa) but also 1:1 (theoretical molar mass of ~80 kDa) binding stoichiometry. The overlay of single measurements of the respective amounts of the interaction partners that were mixed for the complex run fits to the remaining amount of the unbound interaction partner that was added in excess. For example the complex run of the 1:1 molar ratio mixtures reveals beside the JanusFcab–VEGF complex peak, no unbound JanusFcab but a small peak corresponding to unbound VEGF, consistent with the formation of 1:2 and 1:1 complexes, resulting in some unoccupied VEGF molecules. Moreover, mixing JanusFcabs and VEGF in molar ratios of 1:1 or 1:3 results in peak tailing, suggesting that in the absence of a molar excess of JanusFcab, a certain fraction of the formed complexes will show a molar ratio of 1:1. Of note, higher molar masses of the complex were observed with JanusCT6 as interaction partner (Figure 7B vs. 7A) suggesting that more complexes are fully saturated (i.e. 1:2) due to stronger binding affinity.

To pursue investigation towards binding affinity and mode of interaction isothermal titration calorimetry experiments were performed. By titrating VEGF to the heterodimeric Fcab in the calorimetric cell an N value of 0.5 clearly

indicates a binding stoichiometry of 2:1 for both JanusFcabs–VEGF complexes, confirming the SEC-MALS data (Figure 8). The steepness of the transition curves obtained by fitting the integrated data to a one-set-of-sites model yields binding affinities for Janus448 (K_D=26 nM, Figure 8A) and JanusCT6 (K_D=4 nM, Figure 8B). Both signature plots show a very similar mode of interaction. Binding of both heterodimeric Fcabs to VEGF is enthalpically favorable with ΔH values of -25 kcal mol^{-1} and -34 kcal mol^{-1} for Janus448 and JanusCT6, respectively, but entropically unfavorable with $-T\Delta S$ values of 15 kcal mol^{-1} (Janus448) and 23 kcal mol^{-1} (JanusCT6), respectively.

Crystal structure of the JanusCT6–VEGF complex at 2.15 Å resolution

For crystallization of the JanusCT6–VEGF complex the heterodimeric Fcab was mixed with an excess of VEGF and the complex was isolated using preparative SEC. The technique of microseeding was used to gain diffracting crystals with the best having the symmetry of space group $P2_12_12_1$ and a resolution of 2.15 Å. One asymmetric unit was composed of two JanusCT6 molecules (JanusCT6-A and JanusCT6-B) binding to one homodimeric VEGF molecule (Figure 9A). Due to crystal packing higher B-factors were observed for the CD loop of the VEGF-binding CT6 chain of JanusCT6-A and the CH2 domain of the non-binding Fc-wt chain of JanusCT6-B.

When comparing the eight heterodimer mutations within the interface of the CH3 domains of JanusCT6 with the original structure of the heterodimeric Fc (PDB: 4BSW) no major differences in side chain orientations can be observed (Figure 9B). Since the heterodimer mutations are located in the interior of the protein, they do not contribute to the crystallization behavior, thus one heterodimeric molecule can be incorporated into the crystal lattice in two different orientations (i.e. 0° and 180° rotated around its vertical axis). In short, crystal formation of the heterodimeric Fcab proceeded analogous to the homodimeric Fc-wt protein. As a consequence, both orientations are found to the same extent and therefore to every amino acid residue an occupancy of 0.5 is assigned. Figure 9B shows the relevant side chains of heterodimeric JanusCT6-A in comparison to one of the two orientations of heterodimeric Fc (PDB: 4BSW) (Spreter Von Kreudenstein et al., 2013) and to the respective residues found at the interface of homodimeric Fc-wt (PDB: 5JII, (Lobner et al., 2017)).

The CT6 chains of the two JanusCT6 molecules bind to opposite parts of the VEGF dimer. The epitope mainly comprises the helix α1 and the connecting loops of β-strands forming the characteristic cysteine knot motif of VEGF (Muller et al., 1997). Superimposition of homodimeric CT6 with JanusCT6-A and JanusCT6-B revealed no differences in the overall structure beside minor conformational changes in the flexible CD loop (Figure 10A).

Analysis of residues involved in the binding interface was performed by means of the RING 2.0 web server (Piovesan et al., 2016). This tool generates a residue interaction network based on different types of non-covalent interactions. The binding site of JanusCT6-A and JanusCT6-B is stabilized by a network of van der Waals interactions involving residues from all mutated loop regions and the C-terminus of JanusCT6 as well as both chains of VEGF (shown for the JanusCT6-A–VEGF complex, Figure 10B). Moreover, π-π stacking interaction between Y361 (AB loop of JanusCT6) and Y25 (VEGF) as well as Y414 (EF loop of JanusCT6) and Y21 (VEGF) contribute to the stabilization of the binding interface (Figure 10C).

The resolution of 2.15 Å of the JanusCT6-VEGF complex is high enough to determine several water molecules. Only one could be found to be conserved in both binding sites. This water molecule is responsible for bridging the backbone amide groups of L358 (AB loop) and N62 (VEGF) (Figures 10D and 10E). Interestingly, only in the binding site of JanusCT6-B, but not in that of JanusCT6-A, an H-bond between D388 (CD-loop) and K16 (VEGF) is formed via a bridging water molecule (Figure 10E). Since D388 is located in the CD loop, this H-bond might also account for the slightly different structures in the CD loops of JanusCT6-B vs. JanusCT6-A.

DISCUSSION

The Fcab is a promising protein scaffold for therapeutic applications, because it combines all antibody functions, including antigen binding, in a protein of only one third of the mass of a full size antibody. Recently the crystal structures of the HER2-binding Fcabs H10-03-6 and its stabilized version STAB19 both unbound and in complex with the extracellular domain of HER2 were described. These complex structures, as well as accompanying biochemical solution studies, revealed a stoichiometry of 1:2, with one Fcab binding to two antigen molecules following a negative cooperative binding mode (Lobner et al., 2017). That is, the second antigen molecule binds with lower affinity compared to the first molecule.

Given the close proximity of the two binding sites in the Fcab molecule, it was not guaranteed that both binding sites can be occupied simultaneously. In order to test if this is a more general property of Fcabs, we aimed at investigating the interaction between VEGF and its specific Fcabs 448 and CT6, which differs from the above mentioned HER2-Fcab interaction with regard to several properties: (i) in contrast to HER2, VEGF is a small, homodimeric molecule, potentially resulting in the formation of 1:1, 1:2 or 2:1 complexes, or even high molecular weight polymers; (ii) the potential binding surface at the C-terminal loops of the CH3 domains was increased by additionally mutating the CD loops (448 and CT6) and also the C-termini (CT6 only); (iii) the VEGF-binders in the present study were engineered to contain five insertions in the CD loops, whereas the HER2-binding Fcabs contain insertions in the EF loops. In more detail, three residues in the AB loop, seven residues in the CD loop (five of them being insertions) and ten residues in the EF loop were randomly mutated for selection of VEGF binding. The affinity-matured Fcab CT6 contains additional eight mutations at the C-terminal end.

The high level of mutations in the CH3 domain that had to be introduced to generate VEGF binding Fcabs has destabilized those domains in these molecules, as shown by DSC. Similar destabilizing effects have previously been observed with particular Fcabs containing a high content of mutations (Traxlmayr et al., 2013; Traxlmayr et al., 2014). Nevertheless, both Fcabs showed monomeric peaks when analyzed by SEC-MALS, demonstrating that they are natively folded and resistant to aggregation at the applied concentration.

Only the elution times were slightly extended compared to Fc-wt. This fact could be attributed to the higher flexibility of the elongated CD loop and the significantly higher content of hydrophobic residues in the mutated loop regions, potentially causing non-specific interactions with the column matrix.

In line with the SEC-MALS data, the crystal structures of both VEGF-binding Fcabs clearly show that these engineered molecules largely retain their native structure, as was also seen with the HER2-binding Fcabs H10-03-6 and STAB19 (Lobner et al., 2017), again confirming that the IgG1-Fc protein is highly tolerant to mutation in its C-terminal loop regions. Although the AB and EF loops of both Fcabs were mutated, the backbone structures in these loop regions were highly congruent with that of Fc-wt. Only the CD loops show an altered backbone conformation compared to Fc-wt. This observation is not surprising, because the CD loops contain an insertion of 5 amino acids. While the CD loops of Fc-wt only comprise one β-turn as a secondary structure element, the elongated CD loops of both VEGF-binding Fcabs contain a newly formed one-turn α-helix, followed by a newly formed β-turn. This is a striking similarity with the previously published structure of the HER2-binding Fcab STAB19, in which a pre-existing α-helix in the EF loops is elongated by the inserted mutations (Lobner et al., 2017). Together, these structural data indicate that in the case of insertions, the additional amino acids need to be incorporated by forming stable secondary structural motives in order to prevent unstructured regions that protrude into the solvent. At least for small insertions in loop regions an α-helix seems to be an appropriate option. This hypothesis is in line with a previous report, showing that insertions in AB, CD or EF loops strongly reduce the average thermostability of yeast displayed Fcab libraries (Hasenhindl et al., 2013). Thus, the formation of stable structural elements in the newly inserted regions seems to be one of the driving selection forces in the directed evolution experiment when using yeast surface display, which is known to simultaneously select not only for antigen binding, but also for expressibility and stability (Shusta et al., 2000; Traxlmayr and Obinger, 2012). In other words, parts of the randomly mutated Fcab libraries are probably misfolded, especially in the inserted regions, and the eukaryotic quality control machinery during protein expression in yeast ensures that only mutants with stabilized inserted regions are efficiently displayed on the surface and are therefore available for selection.

In addition, the interaction between Fcabs 448 and CT6 and their antigen VEGF was examined. SEC-MALS data clearly revealed polymer formation of Fcabs and VEGF, which can be explained by the homodimeric nature of both interaction partners (i.e. Fcab and VEGF). Consistent with the higher affinity of CT6, the molar masses of the CT6-containing polymers were higher compared with the 448-containing polymers. Thus, the higher affinity seems to enable the formation of longer polymer chains. These results again confirm that Fcabs can potentially bind two antigen molecules simultaneously, as has already been shown for the HER2-specific Fcabs (Lobner et al., 2017).

Since the formation of polymer prevented further investigation of the interaction with VEGF, heterodimeric Fcabs were constructed, which only contain one binding site. The design of heterodimeric Fcabs (Janus448 and JanusCT6) consisting of a non-binding Fc-wt chain and a VEGF-binding Fcab chain followed the procedure of heterodimeric Fc protein generation performed by Spreter Von Kreudenstein et al. (21). This strategy is based on a combination of negative design (prevention of Fc homodimers) and positive design (enhancement of stability of Fc heterodimers) using an *in silico* approach and *in vitro* analysis. While the negative mutations F405A and Y407V (chain A) combined with T366L and T394W (chain B) destroy important interface hotspots for homodimerization and promote heterodimerization, the positive mutations L351Y, T350V (chain A), K392L and T350V (chain B) significantly increase the T_m value of the CH3 domains. The final best performing candidate exhibited a T_{m2} value of 81.5 °C and heterodimer purity above 95% without detectable homodimeric contaminates but a small portion of unpaired monomeric chains (Spreter Von Kreudenstein et al., 2013). Consistent with these published results, similar purities of the heterodimeric Fcabs Janus448 and JanusCT6 with only minor monomeric contaminations were observed, which could be separated by SEC. Interestingly, while the heterodimerizing mutations slightly decreased the thermostability of the CH3 domains of Fc-wt by 0.6 °C (Spreter Von Kreudenstein et al., 2013), the stabilities of the CH3 domains of the JanusFcabs were markedly increased compared with their corresponding homodimeric versions. This strongly suggests that the two different CH3 domains do not denature independently at low and high temperatures, respectively, but together at an intermediate temperature in between the T_m values of Fc-wt and the respective Fcab.

SEC-MALS analysis of JanusFcab-VEGF mixtures confirmed the formation of 2:1 complexes. In general, higher affinities (CT6 vs. 448) and higher excess of JanusFcabs resulted in higher molar masses of the complex peaks, indicating that the complex peaks are composed of 1:1 and 2:1 complexes. ITC analysis of the interaction between both JanusFcabs and VEGF revealed thermodynamic parameters of the interactions in solution. CT6 (K_D=3.9 nM; ΔG = -11.5 kcal mol^{-1}) exhibits a more than 6-times higher affinity compared to 448 (K_D=25.5 nM; ΔG -10.4 kcal mol^{-1}). With both JanusFcabs binding to VEGF is enthalpically favorable. This effect is more pronounced with JanusCT6 reflecting a higher number of established non-covalent interactions of JanusCT6 or CT6 with VEGF. However, this is accompanied with an increased entropic penalty suggesting the presence of flexible structural regions in the unbound molecules, which become structurally more restricted in the JanusCT6-VEGF complex (Chodera and Mobley, 2013; Garbett and Chaires, 2012).

The increase in binding affinity of JanusCT6 can be attributed to the mutated C-terminal region, which represents the only difference in sequence between these two Fcabs. In line with ITC data, the X-ray structure of the JanusCT6–VEGF complex revealed contribution from van der Waals interaction and H-bonding in addition to π-π stacking. More electron density at the C-terminus of CT6 allowed for fitting of more residues within this region suggesting that especially the aromatic amino acids (Y443 and W445) not only contribute to overall stability (π-π stacking) but also to binding affinity. At least W445 was shown to be involved in van der Waals interactions with VEGF. In addition, the intramolecular □-□ stacking interaction of W445, which is only present in CT6 but not in 448, might also explain why CT6 is slightly more stable than 448.

Moreover, the complex structure revealed the location of the epitopes positioned at each pole of the homodimeric VEGF molecule. In general, hot spots on VEGF-A for binding to its natural receptor VEGFR-1 (PDB: 5T89) (Markovic-Mueller et al., 2017) and VEGFR-2 (PDB: 3V2A) (Brozzo et al., 2012) include β-strands connecting loops L1, L2 and L3 and the N-terminal helix α1. A similar but smaller epitope is occupied by the two clinically approved drugs, the antibody bevacizumab (PDB: 1BJ1) (Muller et al., 1998) and the Fab ranibizumab (PDB: 1CZ8) (Chen et al., 1999), which is an affinity-matured version of the first. JanusCT6 only marginally overlaps with the epitopes of bevacizumab and ranibizumab. All these crystal structures contain a truncated

version of VEGF-A encompassing only the important receptor binding domain (~residues 14-108). However, due to mRNA splicing eight isoforms of human VEGF-A are described comprising 121 to 206 amino acids in length (Harper and Bates, 2008). Since the epitope of JanusCT6 covers also residues at the C-terminal part of VEGF, binding to different isoforms could indeed lead to changes in affinity due to steric hindrance depending on the amino acid elongation in the respective isoform. Main contributions to VEGF binding derive from mutations within the AB and EF loops. Interestingly, the elongated CD loop is, beside its flexibility as shown when overlaying CT6 with JanusCT6-A and JanusCT6-B, only marginally involved in the interaction with VEGF. This becomes already obvious by looking at the cartoon representation of the entire JanusCT6–VEGF complex where it is located on top of the binding interface, but hardly interacts with the antigen (Figure 9A).

Together, this study demonstrates that homodimeric, bivalent Fcabs can simultaneously interact with two antigen molecules. In the case of homodimeric soluble antigens, also comprising two epitopes, this potentially leads to the formation of long polymers composed of alternating Fcab and antigen molecules. Since this effect prevented determination of the crystal structure of the Fcab–antigen complex, we established heterodimeric Fcabs which only contain one binding site. The present study, demonstrates that heterodimeric, monovalent Fcabs enable detailed structural and thermodynamic analysis of their interaction with homodimeric antigens, which is impossible with homodimeric, bivalent Fcabs, nicely demonstrating the great utility of heterodimeric, monovalent Fcabs or even other antibody constructs for structural and biochemical studies with their bivalent antigens.

MATERIAL AND METHODS

Recombinant expression and purification of Fc-wt, Fcabs (448, CT6) and heterodimeric Fcabs (Janus448, JanusCT6)

Expression and purification of Fc proteins was conducted as previously described (Lobner et al., 2017). In short, HEK293-6E suspension cells licensed from National Research Council (NRC) (Durocher et al., 2002) of Canada were transiently transfected with plasmid preparations of the pTT5 vector (NRC, Canada) containing the coding sequence for either the Fcab clone 448 or CT6 (generous gift of G. Wozniak-Knopp, University for Natural Resources and Life Sciences Vienna, Austria) or Fc-wt. For generation of the heterodimeric Fcabs (Janus448 and JanusCT6) mutations in the CH3 domain [448/CT6 (chain A): T350V/L351Y/F405A/Y407V and Fc-wt (chain B): T350V/T366L/K392L/T394W] were introduced via site-directed mutagenesis using the QuikChange Lightning kit (Agilent, USA) (Spreter Von Kreudenstein et al., 2013). For transient transfection a total of 1 µg of plasmid-DNA and 2.5 µg of linear *polyethylenimine* (Polysciences, Inc., Germany) per mL culture volume were used. For production of heterodimeric Fcabs the plasmid-DNA transfection ratio of 5:1 (chain A: chain B) has shown to perform best in terms of high protein yield. Harvesting and purification of the soluble protein was done exactly as described in Lobner et al. including purification steps with a HiTrap Protein A HP column (GE Healthcare, USA) and a HiLoad 16/600 Superdex 200 pg (prep grade) column (GE Healthcare, USA) (Lobner et al., 2017; Traxlmayr et al., 2012). Especially, the latter purification step was necessary for separation of heterodimeric Fcabs from the small portion of solitary monomeric Fc chains.

Recombinant expression and purification of VEGF

The gene encoding for residues 14-108 of human VEGF-A (UniProtKB: P15692) was synthesized and cloned into pJ414 vector, which carries the inducible T7 promotor (ATUM, USA). The plasmid was transformed into chemically competent *E. coli* BL21(DE3) cells (Agilent, USA). Expression in inclusion bodies, refolding and purification of the truncated version of VEGF was performed based on the protocol of Heiring and Muller (Christinger et al., 1996; Heiring and Muller, 2001). Fresh LB medium (8 × 500 mL) supplemented with ampicillin (100 µg mL^{-1}) was inoculated in shake flasks with 5 mL of an overnight culture,

respectively. After the culture has reached an optical density of 0.6 at 600 nm at 37 °C shaking, overexpression was induced by addition of 1 mM isopropyl-β-D-thiogalactopyranoside (IPTG) and the cells were incubated for another 4 h at 37 °C. Cells were harvested by centrifugation (5000 g, 20 min, 4 °C), resuspended in 8 × 20 mL of 20 mM TRIS-HCl buffer (pH 7.5) including 5 mM ethylenediaminetetraacetic acid (EDTA), incubated for 10 min and disrupted by ultrasonication with a Vibra-Cell 375 ultrasonic processor (Sonics & Materials, Inc., USA). Pellets obtained after centrifugation (39 000 g, 25 min, 4 °C) were pooled and washed twice using the same buffer as before. The resulting pellet was subsequently resuspended in 20 mL unfolding buffer (20 mM TRIS-HCl, 5 mM EDTA, 7.5 M urea, 4 mM dithiothreitol (DTT), pH 7.5), stirred for 2 h at room temperature followed by centrifugation (39 000 g, 25 min, 4°C). The supernatant containing the unfolded protein was diluted 10-fold into refolding buffer (20 mM TRIS-HCl, 7 µM $CuCl_2$, pH 8.4) and stirred overnight at room temperature. After dialysis against 20 mM TRIS-HCl (pH 8.0) the protein was loaded onto a 6 mL Resource Q column (GE Healthcare, USA). The protein was eluted by applying a linear gradient from 0 to 500 mM NaCl over 20 column volumes. Fractions containing VEGF were pooled, dialyzed in 50 mM sodium phosphate buffer (pH 7.0) containing 1.2 M $(NH_4)SO_4$ and purified using a 1 mL HiTrap Phenyl FF (Low Sub) column (GE Healthcare, USA). The protein was eluted by a linear decrease of the $(NH_4)_2SO_4$ concentration over 20 column volumes. Before purification with a HiLoad 16/600 Superdex 200 pg (prep grade) column (GE Healthcare, USA) the sample was concentrated and buffer-exchanged into Dulbecco's Phosphate Buffered Saline (PBS, pH 7.4) (Sigma-Aldrich, USA) supplemented with 200 mM NaCl using 10 kDa Amicon Ultra Centrifugal Filter (Merck Millipore, Germany).

Differential scanning calorimetry (DSC)

Analyses of thermal stabilities were performed on a MicroCal VP-Capillary DSC instrument (Malvern Instruments, Ltd., UK). All Fc proteins were diluted to a concentration of 5 µM in PBS buffer (pH 7.4) and heated from 20 to 110 °C. The highly thermostable VEGF was diluted to a concentration of 45 µM in PBS buffer (pH 7.4) and heated from 20 to 130 °C. All experiments were conducted at a constant heating rate of 1 °C min^{-1}. After subtraction of buffer baselines, the

data were normalized for protein concentration and fitted with a non-two-state thermal unfolding model using the software Origin 7.

Size exclusion chromatography–multi-angle light scattering (SEC–MALS)

Size-exclusion chromatography combined with multi-angle light scattering was used to determine the molar mass of all proteins and protein complexes under study. Analyses were performed on an LC20 prominence HPLC system equipped with the refractive index detector RID-10A, the photodiode array detector SPD-M20A (all from Shimadzu, Japan) and a MALS Heleos Dawn8+ plus QELS detector (Wyatt Technology, USA). The column (Superdex 200 10/300 GL, GE Healthcare, USA) was equilibrated with PBS plus 200 mM NaCl (pH 7.4) as running buffer. Experiments were carried out at a flow rate of 0.75 mL min^{-1} at 25 °C and analyzed using the ASTRA 6 software (Wyatt Technology, USA). Proper performance of molar mass calculation by MALS was verified by the determination of a sample of bovine serum albumin. All proteins were centrifuged (17 000 g, 10 min, 20 °C) and filtered (0.1 μm Ultrafree-MC filter, Merck Millipore, Germany) prior to analysis. A total amount of 25 µg was injected for all single protein measurements. For the complex runs consisting of 1:1 molar ratio mixtures of the respective Fc molecule and VEGF, 25 µg of the antigen were mixed with the appropriate amounts of Fc protein prior to analysis. For runs at molar ratios of 1:3 and 3:1 25 µg of the interaction partner present at lower molar concentration was used.

Protein identification using liquid chromatography–electrospray ionization–mass spectrometry (LC–ESI–MS)

For protein identification and quantification 30 µg of the respective SEC purified heterodimeric Fcab (Janus448 and JanusCT6) in PBS was treated with 1 U of N-Glycosidase F (Roche, Switzerland) to release N-linked glycans over night at 37 °C. A total of 2.5 µg of the sample was analyzed using a Dionex Ultimate 3000 HPLC-system (Thermo Scientific, USA) directly linked to a QTOF instrument (maXis 4G ETD, Bruker, Germany) equipped with the standard ESI source in the positive ion mode. MS-scans were recorded within a range of 400-3800 m/z. Instrument calibration was performed using ESIcalibration mixture (Agilent, USA). For separation of the proteins a Thermo ProSwift™ RP-4H Analytical separation column (250 * 0.200 mm) was used. A gradient from 80%

solvent A and 20% solvent B (Solvent A: 0.05% TFA (trifluoroacetic acid), B: 80.00% ACN (acetonitrile) and 20.00% A) to 62.5% B over 15 min was applied, followed by a 5 min gradient from 62.5% B to 95% B, at a flow rate of 8 µL min^{-1} and 65 °C. The analysis files were deconvoluted using DataAnalysis 4.0 (Bruker, Germany) (Maximum Entropy Method, low mass: 10000, high mass: 100000, instrument resolv. power: 10000) and manually annotated.

O-glycopeptide profiling of T225 using liquid chromatography-electrospray ionization-mass spectrometry (LC-ESI-MS)

For localization of the O-glycosylation site the same instruments were used as for protein identification. Therefore, a sample of 20 µg Fc-wt in PBS was S-alkylated with iodoacetamide and further digested with sequencing grade Glu-C (Roche, Switzerland). Measurements were performed as previously described (Lobner et al., 2017). In short, MS-scans were recorded within a range of 150-2200 m/z and the three highest peaks were selected for fragmentation in DDA mode. For peptide separation a Thermo BioBasic C18 separation column (Thermo Scientific, USA) was used. DataAnalysis 4.0 (Bruker, Germany) was used for glycopeptide evaluation. The site of glycosylation (T225) was determined by detection of the glycosylated peptide TCPPCPAPE that only contains a single threonine residue and no serine. Likewise, a tryptic digest with sequencing grade modified trypsin (Promega, USA) to confirm the findings resulted in the identically glycosylated peptide TCPPCPAPELLGGPSVFLFPPKPK (data not shown).

Isothermal titration calorimetry (ITC)

ITC measurements were conducted on a MicroCal PEAQ-ITC (Malvern Instruments, Ltd., UK) for determination of binding affinities and thermodynamics of the interaction between the heterodimeric Fcabs and VEGF. Prior to measurements, the samples were prepared in PBS (pH 7.4), centrifuged (17 000 g, 10 min, 20 °C) and filtered (0.1 µm Ultrafree-MC filter, Merck Millipore, Germany). The sample cell (V=200 µL) was washed several times with PBS (pH 7.4) before filling with 40 µM of either Janus448 or JanusCT6. Titrations with 200 µM VEGF were performed at 25 °C using an initial injection of 0.1 µL followed by 59 successive injections of 0.5 µL with a 120 sec interval in between. Curve fitting was performed based on a one-set-of-sites binding model using the MicoCal PEAQ-ITC analysis software.

X-ray crystallography and data collection

To provide best preconditions for X-ray crystallography studies, all proteins were freshly produced and purified with SEC as final polishing step. Fractions in PBS buffer (pH 7.4) containing either 448 or CT6 were pooled and concentrated using 30 kDa Amicon Ultra Centrifugal Filter (Merck Millipore, Germany) to 7.3 mg $mL^{-1}$and 4.9 mg mL^{-1}, respectively. Crystallization experiments were carried out using the sitting drop vapour diffusion method. Crystallization drops were set using a Phoenix HT robot (Art Robins Instruments, USA). The reservoir was filled with 40 µL precipitant solution. Ratios of 150:200 nL, 200:200 nL and 250:200 nL protein to precipitant were dispensed.

For isolation of the JanusCT6–VEGF complex the heterodimeric Fcab was mixed with an 3-fold molar excess of VEGF and loaded onto a HiLoad 16/600 Superdex 200 pg column (GE Healthcare, USA) equilibrated with 20 mM TRIS-HCl buffer (pH 7.5) including 50 mM NaCl. Fractions containing the complex were desalted and concentrated to 5.5 mg mL^{-1} using 30 kDa Amicon Ultra Centrifugal Filter (Merck Millipore, Germany). Growth of high quality complex crystals was achieved by applying the technique of microseeding which promotes growth of larger crystals in the metastable zone by providing nucleation seeds. Therefore, a seeding stock solution was prepared from tiny needle-shaped crystals of the JanusCT6–VEGF complex obtained from Morpheus® screen (condition F2) (Molecular Dimensions, UK) using the Seed Bead™ kit (Hampton Research, USA). The crystals were placed into 100 µL crystallization solution, crushed and transferred into a Seed Bead™ tube. The tube was vortexed 3 × 30 s cooling it on ice between the mixing steps. Drops were set using an Oryx8 crystallization robot (Douglas Instruments, Ltd, UK). The reservoir was filled with 40 µL precipitant solution. Ratios of 200:200:100 nL and 300:200:100 nL protein to precipitant to seeding stock were dispensed.

Crystallization plates were stored in a Minstrel DT UV imaging device (Rigaku, USA) at 22 °C. Diffracting crystals were grown in a slightly modified version of the Low Ionic Strength screen (Hampton Research, USA) based on Harris et al. (Harris et al., 1995) (448), the Morpheus® screen (CT6) and the JCSG-*plus*™ screen (JanusCT6–VEGF complex) (both from Molecular Dimensions, UK). Crystals of 448 were soaked with mother liquor supplemented with 20%-25% (v/v) glycerol as cryoprotectant. All crystals were harvested using cryo-loops and flash-cooled in liquid nitrogen. Data sets were collected at the

European Synchrotron Radiation Facility (ESRF, Grenoble, France) at 100 K on a DECTRIS PILATUS 2M detector (Table 1).

Structure determination and refinement of 448, CT6 and the JanusCT6–VEGF complex

Data sets were integrated and scaled with the XDS software-suite (Kabsch, 2010). The high-resolution cut-off was based on a CC1/2* criterion (Karplus and Diederichs, 2012). The structures of 448 and CT6 were determined by molecular replacement with the program Phaser-MR (McCoy et al., 2007) using an unpublished Fcab structure as search model for 448 and the structure of 448 as search model for CT6. For determination of the JanusCT6–VEGF complex structure, the phase problem was solved by molecular replacement applying *BALBES* using Fc-wt as sequence target (Long et al., 2008). The initial model was rebuilt using phenix.autobuild providing the sequence of VEGF and JanusCT6 (Terwilliger et al., 2008).

The models were improved by iterative cycles of manual model building using COOT (Emsley et al., 2010) and maximum likelihood refinement using PHENIX-Refine (Adams et al., 2010), REFMAC5 (Murshudov et al., 1997) and Rosetta-Refinement (DiMaio et al., 2013). Final stages of refinement included Translation Libration Screw (TLS) parameters, isotropic B-factor model, automated correction of N/Q/H errors, automated addition of hydrogens and water molecules and optimization of X-ray/ADP- and X-ray/stereochemistry-weight. Details can be found in Table 1.

Validation of the structures

All models were validated with MolProbity (Chen et al., 2010) and PDB_REDO (Joosten et al., 2012; Joosten et al., 2014). Carbohydrates were validated with pdb-care (Lutteke and von der Lieth, 2004) and Privateer (Agirre et al., 2015). Figures were prepared with PyMOL Molecular Graphics System (Version 1.3, Schrödinger, LLC). Atomic coordinates have been deposited in the Protein Data Bank under accession codes 5K64 (448), 5K65 (CT6) and 5O4E (JanusCT6–VEGF).

AUTHOR CONTRIBUTION

Conceptualization, E.L. and C.O.; Formal Analysis, E.L., A.H., G.M., K.K. and M.K.; Investigation, E.L., A.H., G.M., K.K. and M.K.; Writing – Original Draft, E.L., C.O., M.W.T., G.M. and A.H.; Writing – Review & Editing, E.L., C.O. and M.W.T.; Supervision, C.O. and K.D.-C.; Funding Acquisition, C.O.

Acknowledgements

This work was supported by the Christian Doppler Research Association (Christian Doppler Laboratory for Antibody Engineering), the Austrian Science Foundation (FWF Project W1224 – Doctoral Program on Biomolecular Technology of Proteins – BioToP) as well as the Federal Ministry of Economy, Family and Youth through the initiative "Laura Bassi Centres of Expertise", funding the Center of Optimized Structural Studies, No. 253275. We thank Dr. Gordana Wozniak-Knopp (University for Natural Resources and Life Sciences Vienna, Austria) for providing plasmid DNA of the Fcabs 448 and CT6. We thank Dr. Mike R. Williams from Malvern Instruments Ltd. (Malvern, UK) for assisting in ITC measurements. We acknowledge the European Synchrotron Radiation Facility (Grenoble, France) for provision of synchrotron radiation facilities and the Local Contacts for providing assistance in using beamline ID30A-3.

Figures

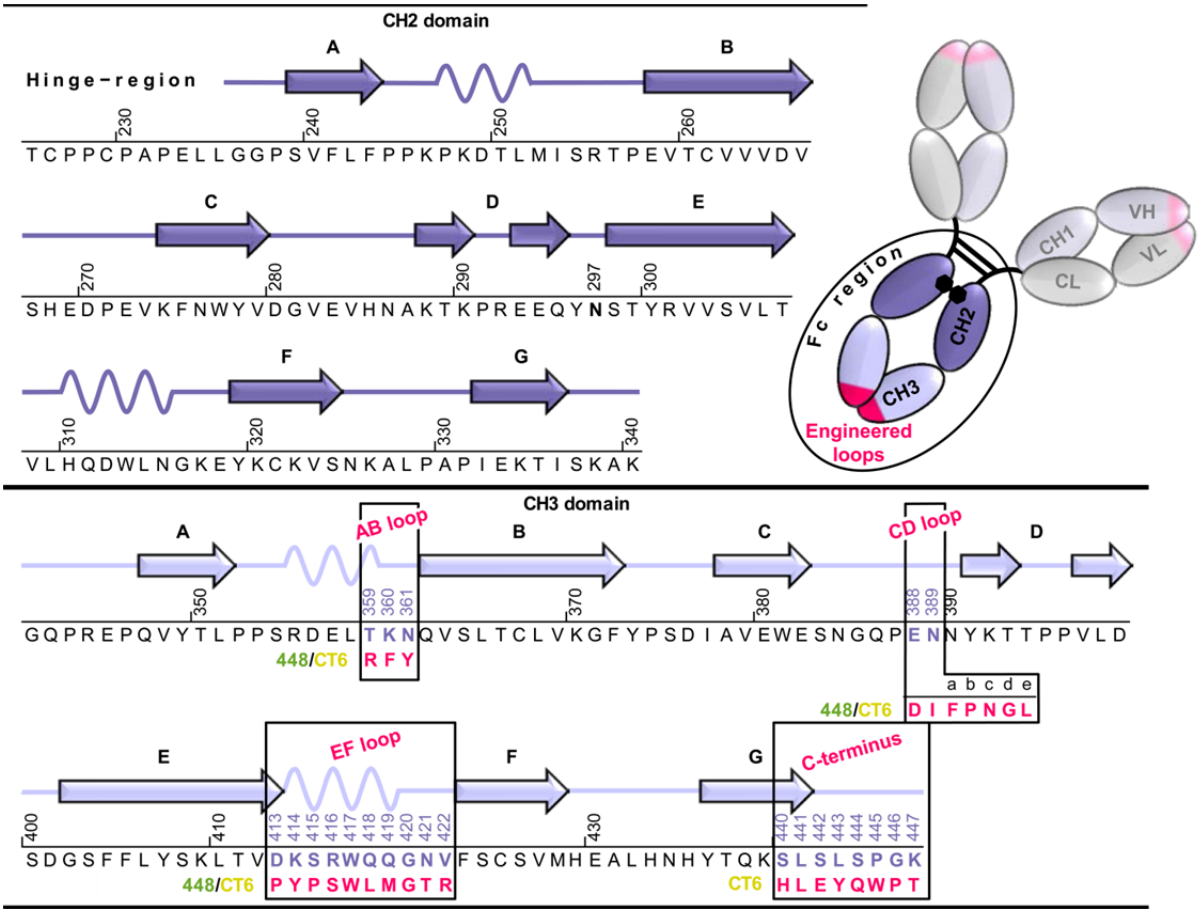

Figure 1. Amino acid sequence of human IgG1-Fc (Fc-wt) and the Fcabs 448 and CT6.

Schematic representation of full size IgG1 consisting of two heavy chains (VH, CH1, CH2 and CH3 domains) and two light chains (VL and CL domains) with the Fab fragment carrying the antigen-binding sites (pink). The secondary structure elements of one CH2 and CH3 domains (dark and light violet) are shown together with their corresponding amino acid sequence from residue T225 to K447 (Eu numbering system (Edelman et al., 1969)). The conserved N-linked glycosylation is located at position 297. The engineered loop regions (AB, CD and EF loops in the CH3 domains) of the Fcabs 448 and CT6 differing in length and sequence and the mutations at the C-terminus of CT6 are depicted in pink.

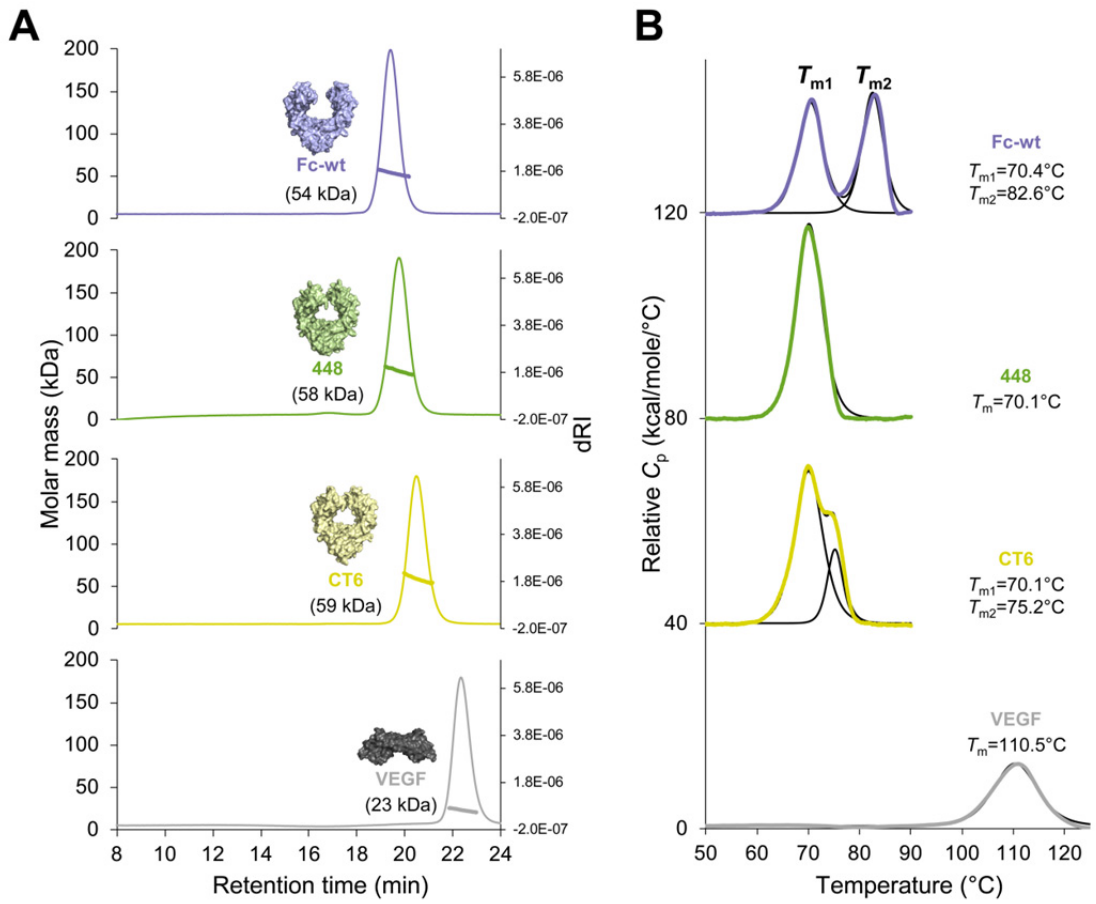

Figure 2. Size exclusion chromatography–multi-angle light scattering (SEC-MALS) and differential scanning calorimetry (DSC) analysis of human IgG1-Fc (Fc-wt), the Fcabs 448 and CT6 and VEGF.

(A) A Superdex 200 10/300 GL column (GE Healthcare, USA) pre-equilibrated with PBS plus 200 mM NaCl (pH 7.4) was loaded with 25 µg of Fc-wt (violet), 448 (green), CT6 (yellow) or VEGF (gray), respectively, upstream to MALS analysis. Molar masses were calculated using the ASTRA software. (B) For DSC measurements the Fc proteins and VEGF were diluted to 5 µM and 45 µM in PBS, respectively. The data were fitted to a non-two-state thermal unfolding model using the software Origin 7. The respective T_m values (average of n=2) are shown next to the graphs.

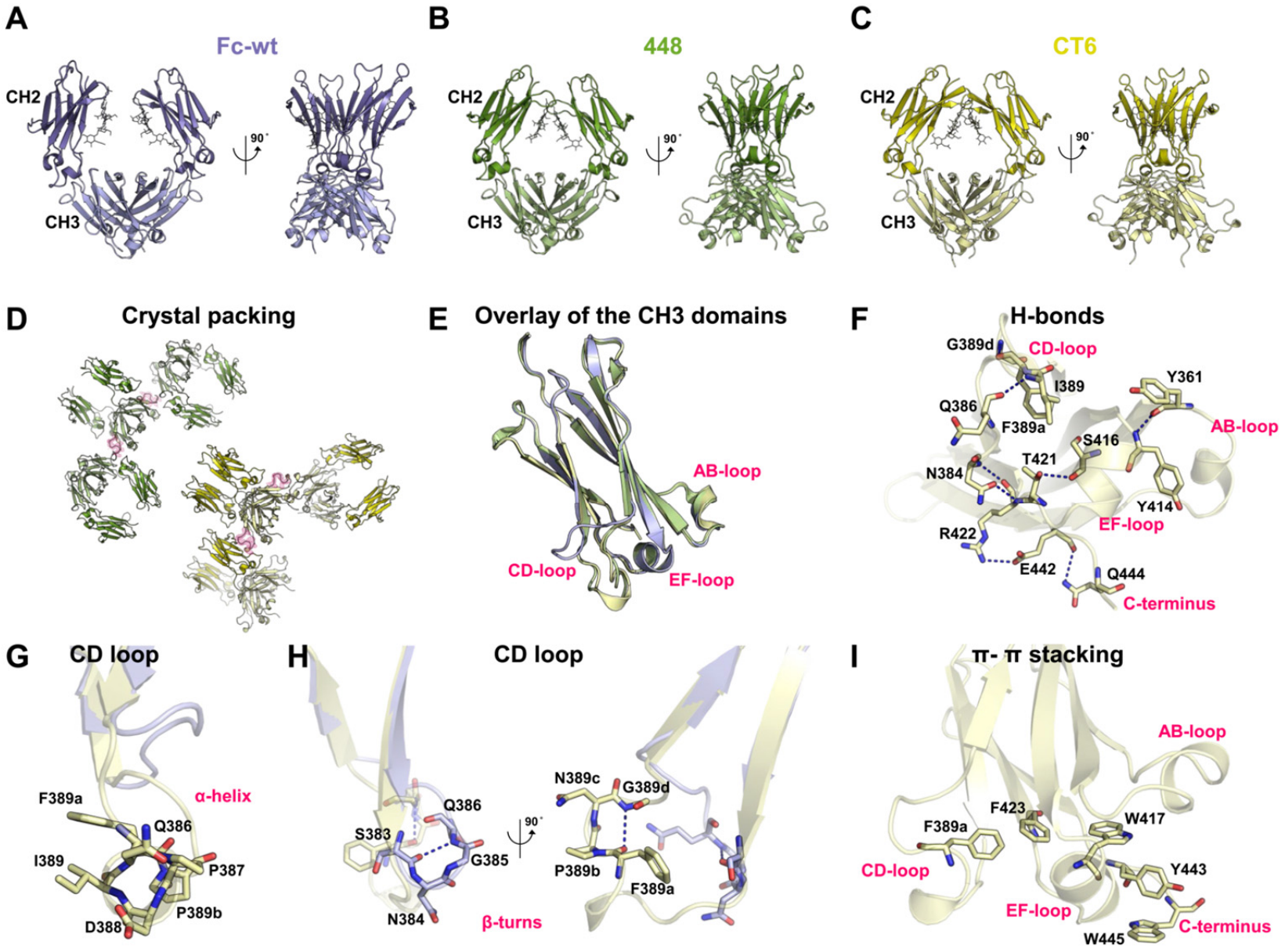
A
Fc-wt
CH2
CH3
90˚
B
448
CH2
CH3
90˚
C
CT6
CH2
CH3
90˚
D
Crystal packing
E
Overlay of the CH3 domains
AB-loop
CD-loop
EF-loop
F
H-bonds
G389d
CD-loop
I389
Y361
Q386
F389a
AB-loop
S416
T421
N384
Y414
EF-loop
R422
E442
Q444
C-terminus
G
CD loop
F389a
α-helix
Q386
I389
P387
P389b
D388
H
CD loop
Q386
S383
G385
90˚
N384
β-turns
N389c
G389d
P389b
F389a
I
π- π stacking
AB-loop
F423
F389a
W417
CD-loop
Y443
EF-loop
C-terminus
W445

Figure 3. Crystal structures of the Fcabs 448 (2.44 Å) and CT6 (2.50 Å) in comparison with human IgG1-Fc (Fc-wt).

Cartoon representation of the overall structure of (A) Fc-wt (violet; PDB: 5JII), (B) 448 (green) and (C) CT6 (yellow), each of them rotated by 90° around the vertical axis. (D) Crystal packing of 448 (green) and CT6 (yellow). The $2mF_o$-DF_c density map drawn at RMSD=1 of the mutated residues in the CD loops of the middle Fcab molecule are depicted as pink mesh. (E) Overlay of the CH3 domains (chain A) of Fc-wt, 448 and CT6. (F) H-bonds (NH-OC and OH-OC, < 3.5 Å) containing mutated regions of CT6 are shown as blue dashed lines. (G) Close-up view of the superimposed CD loop of Fc-wt (violet) and CT6 (yellow) with focus on selected (G) α-helix and (H) β-turns. Blue dashed lines represent important H-bonds (*i*+3) (I) Network of CT6 residues involved in π-π stacking (< 6.0 Å) is depicted.

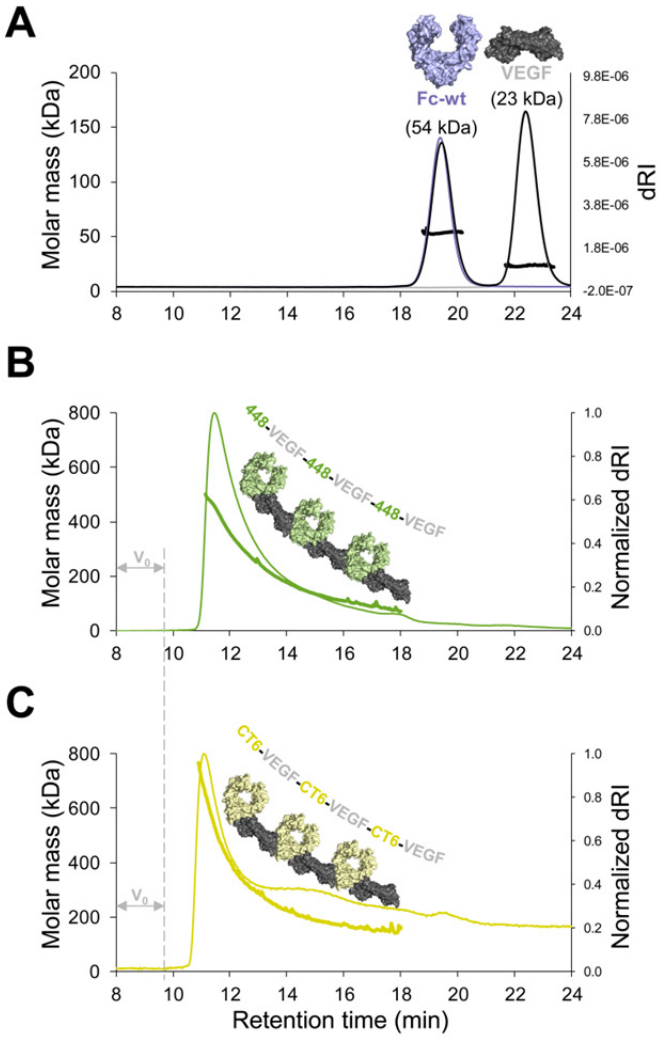

Figure 4. Polymerization of Fcab–VEGF complexes.

SEC-MALS analysis of Fc protein-VEGF mixtures. (A) Overlay of single measurements of the respective amounts of Fc-wt (violet) and VEGF (gray) that were used for a mixture of Fc-wt and VEGF in a 1:3 molar ratio (black). Calculated molar masses from the mixture run are depicted matching exactly values of the respective single runs. Analysis of 1:1 molar ratio mixtures of (B) 448–VEGF (green) and (C) CT6–VEGF (yellow). Samples elute just after the void volume (V_0), referring to high molar masses across the tailing peaks indicating polymerization of the Fcab–VEGF complexes. To facilitate comparison between (B) and (C) the differential refractive index signal (dRI) was normalized. Formation of Fcab–VEGF polymer chains is schematically represented.

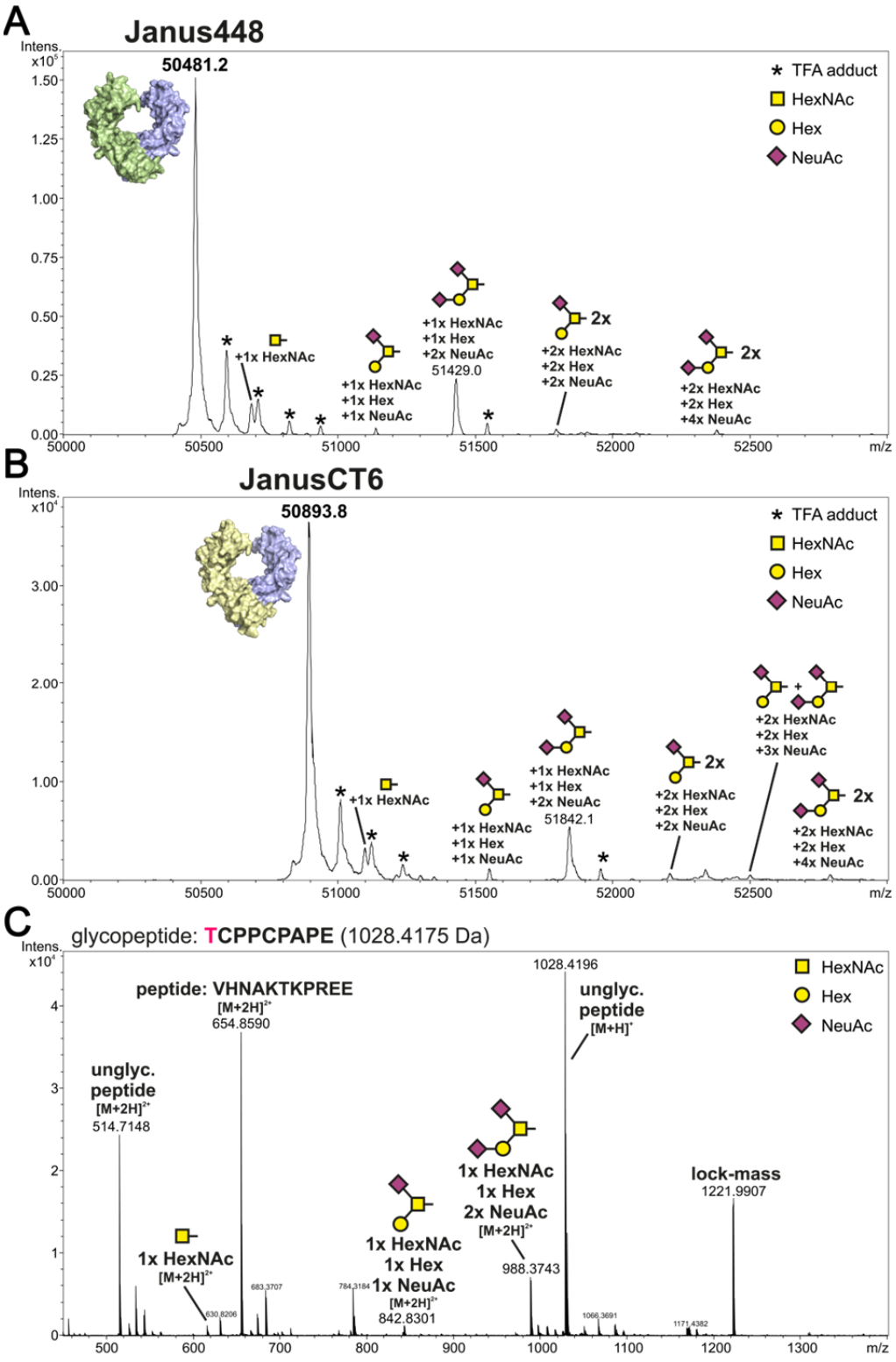
A
Janus448
Intens.
x10^5
50481.2
* TFA adduct
HexNAc
Hex
NeuAc
+1x HexNAc
+1x HexNAc
+1x Hex
+1x NeuAc
+1x HexNAc
+1x Hex
+2x NeuAc
51429.0
2x
+2x HexNAc
+2x Hex
+2x NeuAc
2x
+2x HexNAc
+2x Hex
+4x NeuAc
m/z
B
JanusCT6
Intens.
x10^4
50893.8
* TFA adduct
HexNAc
Hex
NeuAc
+1x HexNAc
+1x HexNAc
+1x Hex
+1x NeuAc
+1x HexNAc
+1x Hex
+2x NeuAc
51842.1
2x
+2x HexNAc
+2x Hex
+2x NeuAc
+2x HexNAc
+2x Hex
+3x NeuAc
2x
+2x HexNAc
+2x Hex
+4x NeuAc
m/z
C
glycopeptide: TCPPCPAPE (1028.4175 Da)
Intens.
x10^4
peptide: VHNAKTKPREE
[M+2H]2+
654.8590
1028.4196
unglyc. peptide
[M+H]+
HexNAc
Hex
NeuAc
unglyc. peptide
[M+2H]2+
514.7148
1x HexNAc
[M+2H]2+
1x HexNAc
1x Hex
2x NeuAc
[M+2H]2+
988.3743
1x HexNAc
1x Hex
1x NeuAc
[M+2H]2+
842.8301
lock-mass
1221.9907
m/z

Figure 5. Intact protein measurement of heterodimeric Fcabs and identification of O-glycosylation site using LC-ESI-MS.

The deconvoluted spectra of Janus488 (A) and JanusCT6 (B) after PNGaseF treatment are presented. The theoretical molar mass of the proteins (Janus448: 50481.5 Da; JanusCT6: 50894.9 Da) could be matched to the highest signal of the respective measurement. Several glycoforms of the proteins caused by O-glycosylation were identified and quantified to a relative amount of approximately 10%. The small portion of TFA (trifluoroacetic acid) adducts (marked with an asterisk) derives from the addition of 0.05% of TFA in solvent A. (C) Glycopeptide TCPPCPAPE was identified after endoproteinase Glu-C digestion of Fc-wt. The unglycosylated peptide in two different charge states and its observed glycoforms are depicted in the spectrum. The site of O-glycosylation is located on position T225. The signal of m/z = 654.86 could be assigned to a coeluting peptide. The peak of the lock-mass refers to an internal standard and was used for recalibration.

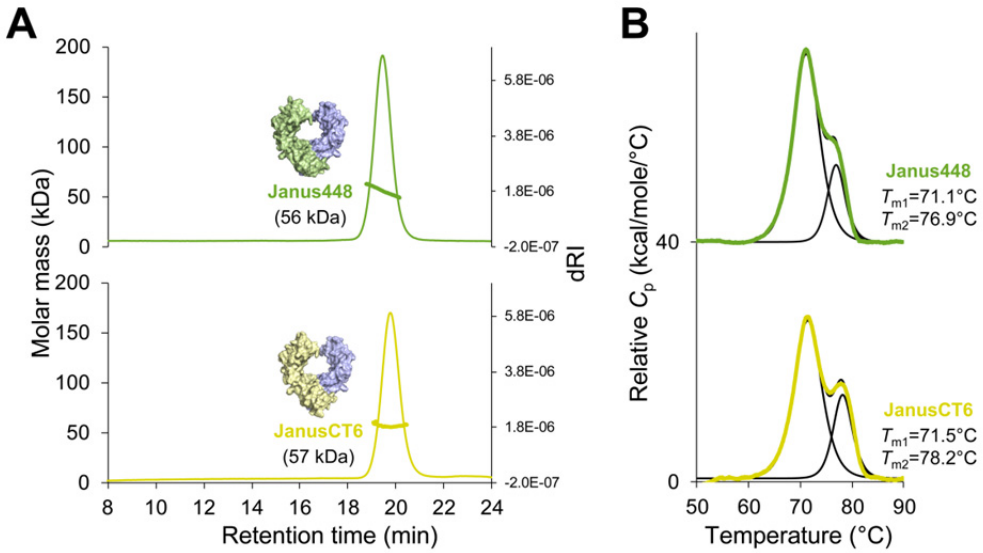

Figure 6. SEC-MALS and DSC analysis of the heterodimeric Fcabs Janus448 and JanusCT6.

(A) A total amount of 25 µg of Janus448 (green) and JanusCT6 (yellow) was analyzed on a Superdex 200 10/300 GL column (GE Healthcare, USA) pre-equilibrated with PBS plus 200 mM NaCl (pH 7.4) prior to MALS measurements. Molar masses were calculated using the ASTRA software. (B) For DSC measurements the heterodimeric Fcabs were diluted to 5 µM in PBS. The data were fitted to a non-two-state thermal unfolding model using the software Origin 7. The respective T_m values (average of n=2) are shown next to the graphs.

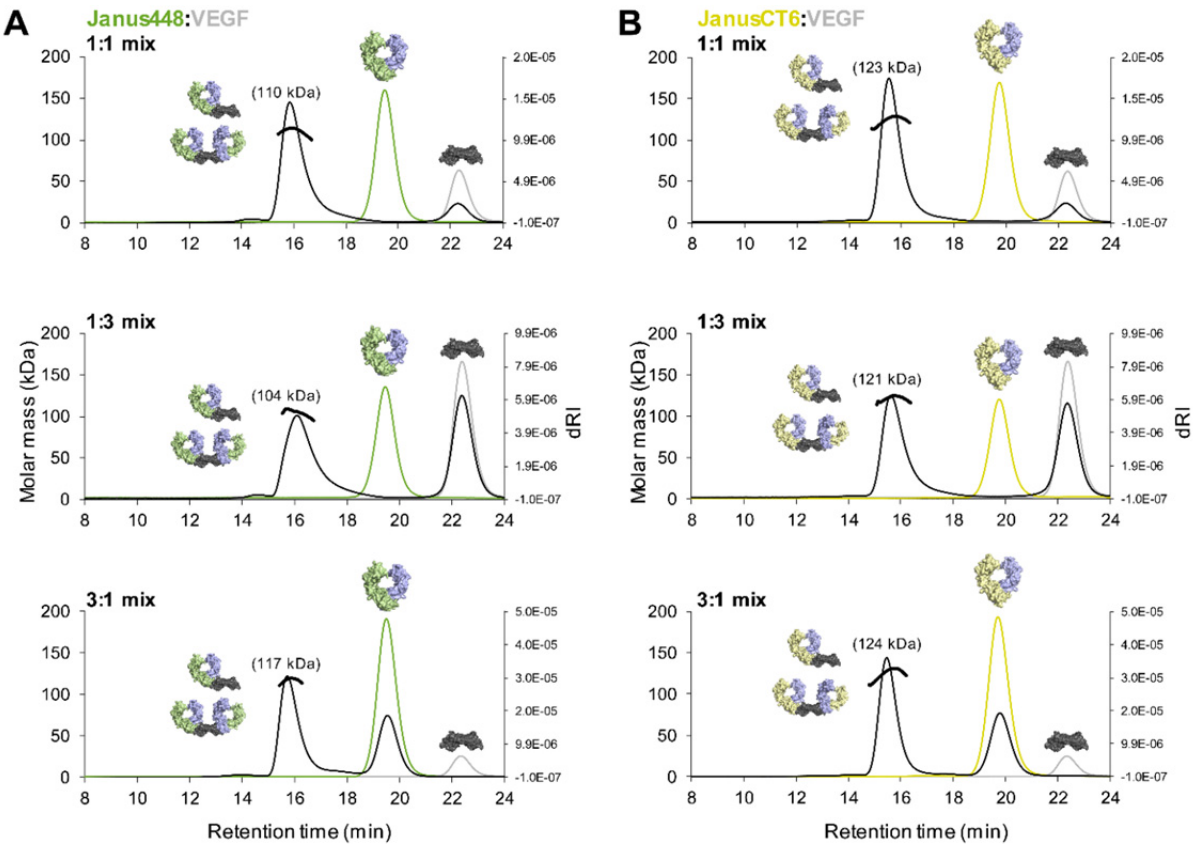

Figure 7. Preventing polymerization by application of heterodimeric Fcabs.

SEC-MALS analysis of heterodimeric Fcab-VEGF mixtures of different molar ratios (1:1/ 1:3/ 3:1) as indicated in the respective graphs. (A) Overlay of single measurements of the respective amounts of Janus448 (green) and VEGF (gray) that were used for the mixtures of the respective complex run (black). (B) Overlay of single measurements of the respective amounts of JanusCT6 (yellow) and VEGF (gray) that were used for the respective complex run (black). Molar masses of the main peaks of each complex run are depicted.

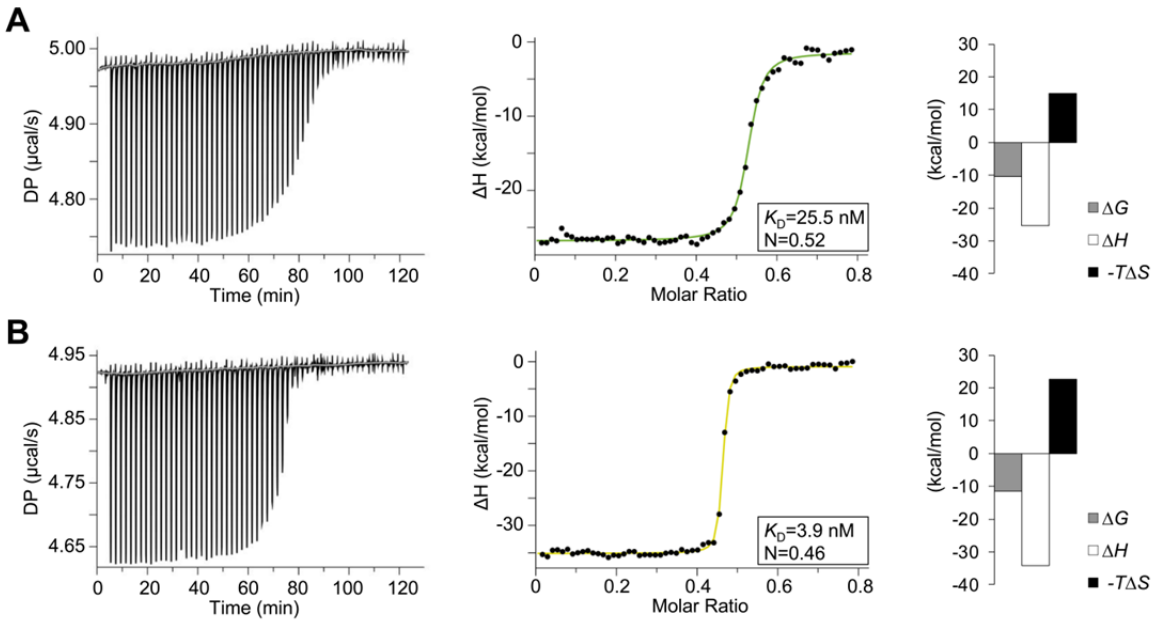

Figure 8. Thermodynamic analyses of the interactions between VEGF and Janus448 or JanusCT6.

Calorimetric experiments were performed on a MicroCal PEAQ-ITC instrument at 25°C. The sample cell (V=200 µL) was either filled with 40 µM Janus448 (A) or JanusCT6 (B) and titrated stepwise with 200 µM VEGF. The left panels show the raw ITC data representing the responses to 59 successive injections of 0.5 µL each. The integrated data were fitted to a one-set-of-sites interaction model (right panels). The insets and the binding signature plots show the fitted and thermodynamic parameters of the respective JanusFcab–VEGF interaction.

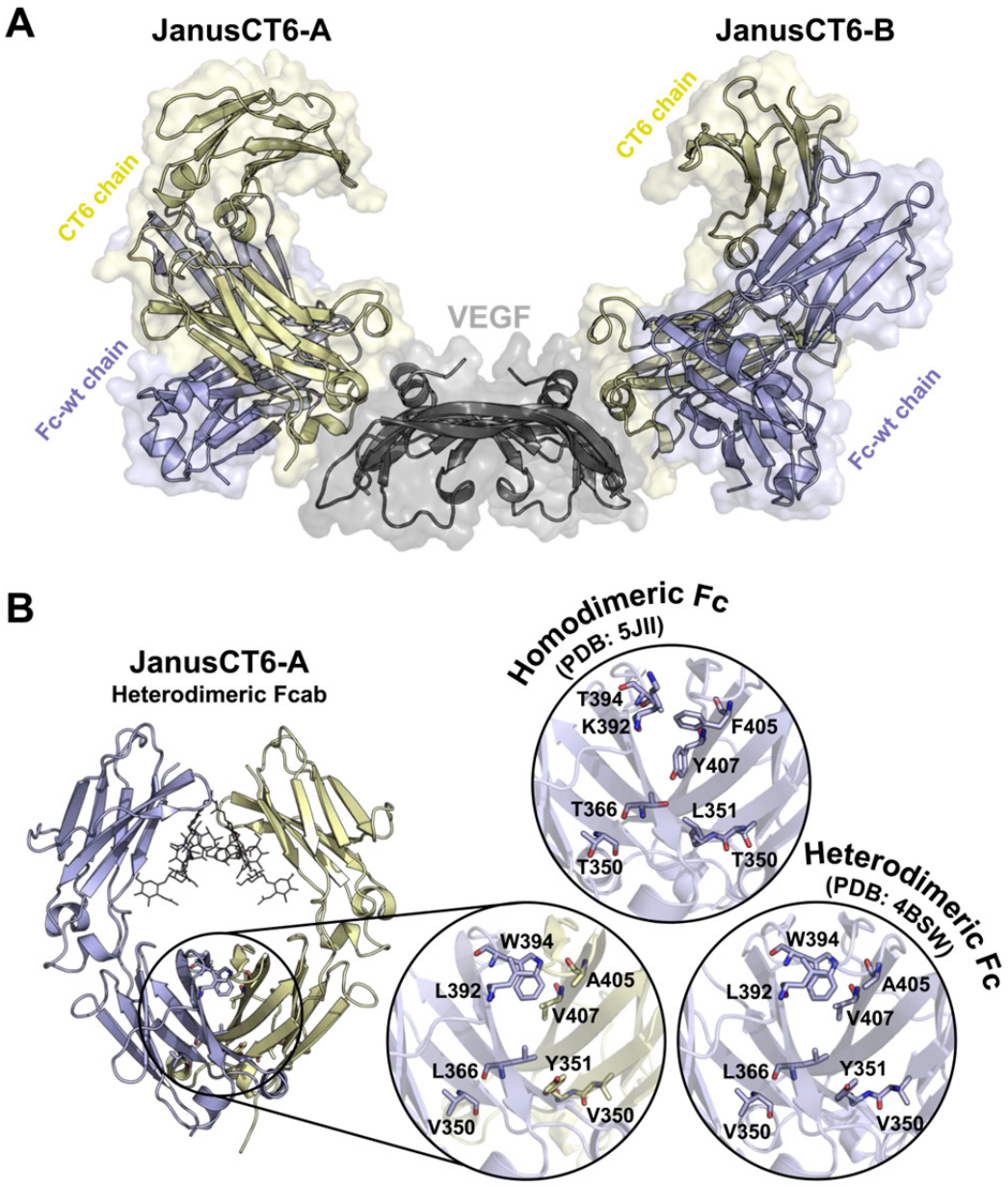

Figure 9. Crystal structure of the JanusCT6–VEGF complex at 2.15 Å resolution (PDB: 5O4E).

(A) Surface and cartoon representation of the JanusCT6–VEGF complex. Each of the two CT6 chains (yellow) of JanusCT6-A and JanusCT6-B is binding to the opposite poles of the homodimeric VEGF molecule (gray). The non-binding Fc-wt chains are colored in violet. (B) Close-up view on heterodimer mutations in the CH3 domains interface of JanusCT6 (yellow and violet) and the heterodimeric Fc variant (violet, PDB: 4BSW) (Spreter Von Kreudenstein et al., 2013) in comparison to the respective residues found at the interface of homodimeric Fc-wt (PDB: 5JII; (Lobner et al., 2017)).

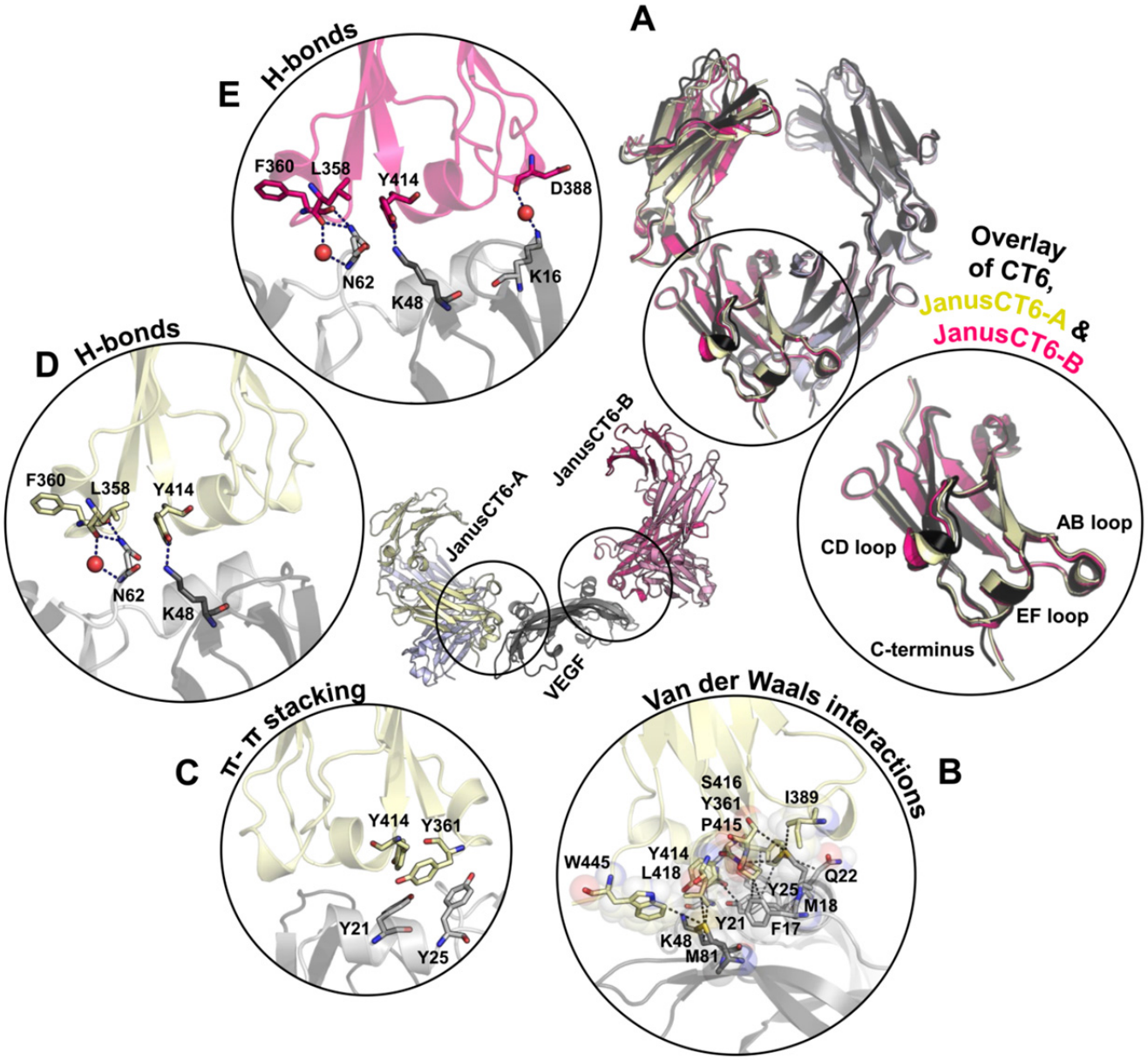
A
Overlay of CT6, JanusCT6-A & JanusCT6-B
AB loop
CD loop
EF loop
C-terminus
JanusCT6-A
JanusCT6-B
VEGF
B
Van der Waals interactions
S416
Y361
P415
I389
W445
Y414
L418
Q22
Y25
M18
Y21
F17
K48
M81
C
π- π stacking
Y414
Y361
Y21
Y25
D
H-bonds
F360
L358
Y414
N62
K48
E
H-bonds
F360
L358
Y414
D388
N62
K48
K16

Figure 10. Insights into JanusCT6–VEGF interaction.

(A) Superimposition of the backbone structure of CT6 (black), JanusCT6-A (yellow and violet) and JanusCT6-B (shades of pink) with close-up view on the CH3 domains of the VEGF-binding CT6 chains. (B, C) Non-covalent interactions between JanusCT6-A (yellow) and VEGF (gray) were identified by help of the RING 2.0 software tool using strict threshold options (Piovesan et al., 2016). (B) Van der Waals interactions identified by measuring the distance between the surface of atoms are depicted as black dashed lines. Surface of involved amino acids is represented as spheres. (C) Side chains of aromatic amino acids involved in π-π stacking evaluated below 6.5 Å between the center of mass are shown. H-bonds found between JanusCT6-A and VEGF (yellow and gray) (D) and JanusCT6-B and VEGF (pink and gray) (E) are depicted as blue dashed lines. Bridging water molecules are shown as red spheres.

4 CONCLUSION

This work focused on the profound clarification of differences in stability of various Fcabs as well as the interaction of these Fcabs with its respective antigen by means of X-ray crystallography and several biochemical methods. The Fcabs under study differ with regards to loop design, antigen specificity, affinities and thus biophysical properties. The loop design of the HER2-binding Fcabs H10-03-6 and its stabilized version STAB19 encompasses five mutations in the AB and EF loop. Additionally, five residues were inserted into the α-helical stretch of the EF loop (Traxlmayr et al., 2013; Wozniak-Knopp et al., 2010). Insertions of five residues are also part of the loop design of the VEGF-binding Fcabs 448 and its affinity matured version CT6. In these Fcabs the insertions are located in the CD loop together with two more mutations in the same loop. Moreover, three mutations in the AB loop and the ten mutations in the EF loop contribute to VEGF binding. To increase the affinity of 448 seven additional residues were mutated on the C-terminal part of the molecule yielding the Fcab CT6.

The crystal structures of all four Fcabs were determined and by superimposition with the determined Fc-wt structure a highly congruency and structural integrity of all horseshoe shaped molecules is observable. This fact is also reflected by the maintained binding of the natural Fc-ligands such as FcγRI or FcRn (Traxlmayr et al., 2013; Wozniak-Knopp et al., 2010). For all five structures the flexible hinge-region as well as few residues on the C-terminal end could not be resolved. Deviations among the Fcabs can be found in the mutated loop regions of the respective CH3 domain. The most destabilized Fcab H10-03-6 shows no electron density for the major part of the EF loops suggesting this loop to be highly flexible and partially disordered. In line with these structural data, the H10-03-6 shows a significant retarded SEC profile probably explained by the increased non-specific interactions with the column matrix through the unstructured EF loops. Remarkably, in the stabilized version of the parental binder STAB19 that differs in only three amino acids in this region, the elongated EF loop forms a stable α-helical segment as in the Fc-wt structure. This feature can also be observed for the elongated CD loop of 448 and CT6. Similar to the EF loop of the HER2 binders, the CD loop of the VEGF binders contains five additional residues that form a newly one-turn α-helix

followed by a β-turn. These interesting structural data suggest that in case of insertions the formation of stable secondary structural motives, especially α-helices, seems to be a driving force in the selection process during directed evolution. For the technique of yeast surface display, simultaneous selection for antigen binding as well as expressibility and stability has previously been shown (Shusta et al., 2000; Traxlmayr and Obinger, 2012). In other words, the quality control machinery in yeast ensures that mainly Fcabs, derived from a library, which encompass inserted regions that are stabilized by secondary structural motives, are displayed on the surface. Moreover, a common feature among all Fcab structures beside their significant increase in non-polar and aromatic residues correlating with the strength of the binding affinity is the selected proline on position 413 at the beginning of the EF loop. At least for STAB19 and for HER2-bound H10-03-6 it seems that this proline turns the polypeptide chain to generate space for the five inserted residues that form an α-helical segment. Another interesting feature of STAB19 is the ionic bond (*i*+3) in the EF loop that evolved during *in vitro* evolution. By comparing the STAB19 sequence with other engineered stabilized mutants, STAB14 contains similar mutations that would also allow the formation of a salt bridge in this region and behaves in terms of stability very similar to STAB19 (Traxlmayr et al., 2013). The backbone structure of the AB loop of all Fcabs under study remains despite mutations largely unchanged. The two VEGF-binding Fcabs differ only in their C-terminal amino acid content. Interestingly, the mutations of the C-terminus of CT6 significantly increase the thermostability of the CH3 domains. Moreover, the electron density of the mutated C-terminus of CT6 allowed for fitting of nearly all residues. In general, a certain rigidity of the respective mutated regions (AB, CD, EF loops and C-terminus) in STAB19, 448 and CT6 was shown to be supported by the formation of novel stabilizing polar bonds between mutated and non-mutated residues.

In the next step, the interaction of all Fcabs with its respective antigen HER2 or VEGF was investigated. In contrast to the 79 kDa large extracellular domain of the surface receptor HER2, the truncated version of the ligand VEGF-A is only 23 kDa in size and contains two identical monomeric chains. Since the Fcab is a homodimeric protein encompassing two identical binding sites in close proximity, the occupancy of each had to be determined. Factors that may influence if steric hindrance prevents occupation of both binding sites would be size and flexibility of the antigen and location of the binding epitope.

Analysis by SEC-MALS revealed a clear 1:1 (Fcab:HER2) binding stoichiometry in case of HER2-binding Fcabs but formation of large polymer chains in case of VEGF-binding Fcabs indicating occupancy of both binding sites. For the latter Fcab-antigen pairs further investigations such as co-crystallization would have been impossible. Therefore, one binding site was eliminated by the generation of heterodimeric Fcabs (JanusFcabs) following the design of Spreter Von Kreudenstein (WO2013063702A1) (Spreter Von Kreudenstein et al., 2013). This strategy is based on a combination of negative design (including mutations that prevent Fc homodimerization) and positive design (including mutations that enhance the stability of Fc heterodimers). Their final best performing heterodimeric Fc exhibited nearly wild-type like thermostability and very high purity. The JanusFcabs (Janus448 and JanusCT6) composed of one VEGF-binding Fcab chain and one non-binding Fc-wt chain showed increased thermostability and enabled further characterization of the antigen interaction as demonstrated by the formation of 2:1 (JanusFcab:VEGF) complexes using SEC-MALS.

As expected the structure of the JanausCT6-VEGF complex is composed of two heterodimeric Fcabs binding at each pole of the homodimeric VEGF molecule. Surprisingly, the co-crystal structures of Fcabs with HER2 identified a clear 1:2 binding stoichiometry with two identical binding sites. This discrepancy with the SEC-MALS measurements may be explained by the different experimental setups. SEC is a separation technology, meaning the two interaction partners (i.e. Fcab and HER2) migrate with different velocity after dissociation, whereas during the crystallization process they stay in equilibrium in a closed reaction chamber. These results indicate a negative cooperative binding process where binding of the first HER2 molecule decreases the affinity for the second binding event.

A similar equilibration setup as during crystallizations is also present during ITC measurements which confirmed the 1:2 (STAB19:HER2) binding stoichiometry. To investigate the negative cooperative binding behavior with an ITC experiment the binding partner displaying two binding sites (i.e. STAB19) has to be in the calorimetric cell. Since this experimental setup failed, the STAB19 encompassing two binding sites was titrated into the cell thereby immediately occupied with two HER2 molecules. ITC measurements were also performed for the JanusFcabs-VEGF interaction, again having the interaction partner with two binding sites (i.e. VEGF) in the syringe. However, in this case the epitopes are laying far apart as determined in the co-crystal structure. Thus,

the obtained thermodynamic parameters indicating enthalpically driven VEGF-binding can be used for evaluations. Moreover, the heterodimeric affinity-matured variant JanusCT6 exhibits a six times higher affinity (K_D=3.9 nM) than its parental version Janus448 (K_D=25.5 nM). The entropic penalty suggests the presence of flexible structural regions in the unbound JanusFcab molecules that get more restricted when bound to VEGF (Chodera and Mobley, 2013; Garbett and Chaires, 2012).

To confirm the hypothesis of negative cooperative binding behaviour of the HER2-binding Fcabs, fluorescence correlation spectroscopy (FCS) was performed. In this experimental setup HER2 is titrated to fixed concentration of STAB19 facilitating fitting of two transitions. The first obtained K_D value is in the intermediate nanomolar range that is high enough to allow the complex to survive a SEC run. The second K_D is in the low micromolar range that significantly shortens the lifespan of the 1:2 complex and thus this complex is not observable during SEC (Corzo, 2006).

A potential reason for this cooperative binding phenomenon could be allosteric effects. However, by comparing the unbound STAB19 with the HER2-bound structures no structural changes could be observed. A TM-score of 0.9780 obtained by comparing the C^{α} atoms of the CH3 domains indicates very high congruency. Therefore, steric hindrance for binding of the second HER2 molecules seems very likely. Whereas in a crystal where proteins are tightly packed no such effects were observed, steric hindrance could be more pronounced in solution and may be the explanation for the observed negative cooperativity. Interestingly, due to the high flexibility of the domain IV of HER2 around 55 residues on the C-terminal end could not be resolved. Theoretical extension of this domain by just superimposition with domain IV of the trastuzumab Fab-HER2 structure (PDB: 1N8Z) (Cho et al., 2003) reveals a slight steric clash with the second HER2 bound molecule. However, the trastuzumab bound HER2 molecule still misses around 24 residues on the C-terminal end, suggesting that steric hindrance in this region indeed can be responsible for the observed binding behaviour.

In addition, when comparing the contribution of mutated residues to antigen binding, for both Fcab-antigen pairs the main contribution derives from residues in the EF loop. Remarkably, the destabilized EF loop in H10-03-6, which could not be resolved in the unbound structure, becomes visible upon binding to HER2. Although the resolution is low, a tube-shaped electron density in the

H10-03-6-HER2 structure allows for perfectly fitting of an α-helical stretch as in the STAB19 molecule. Besides stabilizing bonds with the EF loop, the AB loop additionally contributes to antigen binding in both Fcab-antigen pairs. The CD loop, only mutated in the VEGF-binding Fcabs, is just marginally involved in antigen interaction. Obviously, mutating residues in the AB and EF loop seems to be sufficient for achieving specificity and high affinity. As demonstrated in the VEGF-Fcabs, insertion of additional residues in the EF loop is not necessary. If a stable α-helix is required for this region, then there can be anyway maximal two side chains involved in antigen binding in the case of an insertion of five residues. Thus, only mutating residues, which side chains are surface exposed in the α-helical stretch of the EF in addition to three to five residues in the AB loop, could be an interesting attempt in loop design to achieve antigen-binding as well as maintained stability. For increasing antigen affinity without necessarily negative consequences in stability a few residues on the C-terminal end could be included into the loop design as demonstrated for CT6.

Together, the data in this study demonstrate that the Fc molecule tolerates mutations in its C-terminal loops thereby conserving structural integrity of the overall fold as demonstrated for Fcabs comprising different loop designs. Although, the binding sites of the homodimeric Fcab molecule are in close proximity, binding of two antigen molecules is possible depending on the antigen size and location of the epitope. In contrast to the flexible Fab arms of a full-size IgG, the Fcab is able to bridge a rigid connection between two antigen molecules through the vicinity and rigidity of the two binding sites. This may lead to accelerated aggregation and internalization of tightly packed Fcab-antigen complexes (Leung et al., 2015).

Moreover, generation of heterodimeric Fcabs expands the design possibilities. Elimination of one binding site could be applicable if prevention of antigen cross-linking is required (Martens et al., 2006). Biparatopic or bispecific Fcabs could be designed for applications necessitating the incorporation of two different binding sites against different epitopes on the same or different targets (Baeuerle and Reinhardt, 2009; Heiss et al., 2010; Jost et al., 2013; Spangler et al., 2012). Furthermore, by connection of the Fcab with Fab arms a mAb^2 comprising multiple specificities could be generated.

5 REFERENCES

Adams, P.D., Afonine, P.V., Bunkoczi, G., Chen, V.B., Davis, I.W., Echols, N., Headd, J.J., Hung, L.W., Kapral, G.J., Grosse-Kunstleve, R.W., et al. (2010). PHENIX: a comprehensive Python-based system for macromolecular structure solution. Acta Crystallogr D Biol Crystallogr *66*, 213-221.

Agirre, J., Iglesias-Fernandez, J., Rovira, C., Davies, G.J., Wilson, K.S., and Cowtan, K.D. (2015). Privateer: software for the conformational validation of carbohydrate structures. Nat Struct Mol Biol *22*, 833-834.

Ahmed, A.A., Giddens, J., Pincetic, A., Lomino, J.V., Ravetch, J.V., Wang, L.X., and Bjorkman, P.J. (2014). Structural characterization of anti-inflammatory immunoglobulin G Fc proteins. Journal of molecular biology *426*, 3166-3179.

Baeuerle, P.A., and Reinhardt, C. (2009). Bispecific T-cell engaging antibodies for cancer therapy. Cancer Res *69*, 4941-4944.

Barlow, D.J., and Thornton, J.M. (1988). Helix geometry in proteins. Journal of molecular biology *201*, 601-619.

Beck, A., and Reichert, J.M. (2011). Therapeutic Fc-fusion proteins and peptides as successful alternatives to antibodies. MAbs *3*, 415-416.

Binz, H.K., Stumpp, M.T., Forrer, P., Amstutz, P., and Pluckthun, A. (2003). Designing repeat proteins: well-expressed, soluble and stable proteins from combinatorial libraries of consensus ankyrin repeat proteins. Journal of molecular biology *332*, 489-503.

Bird, R.E., Hardman, K.D., Jacobson, J.W., Johnson, S., Kaufman, B.M., Lee, S.M., Lee, T., Pope, S.H., Riordan, G.S., and Whitlow, M. (1988). Single-chain antigen-binding proteins. Science *242*, 423-426.

Boder, E.T., and Wittrup, K.D. (1997). Yeast surface display for screening combinatorial polypeptide libraries. Nat Biotechnol *15*, 553-557.

Borrok, M.J., Jung, S.T., Kang, T.H., Monzingo, A.F., and Georgiou, G. (2012). Revisiting the role of glycosylation in the structure of human IgG Fc. ACS Chem Biol *7*, 1596-1602.

Brozzo, M.S., Bjelic, S., Kisko, K., Schleier, T., Leppanen, V.M., Alitalo, K., Winkler, F.K., and Ballmer-Hofer, K. (2012). Thermodynamic and structural description of allosterically regulated VEGFR-2 dimerization. Blood *119*, 1781-1788.

Chen, V.B., Arendall, W.B., 3rd, Headd, J.J., Keedy, D.A., Immormino, R.M., Kapral, G.J., Murray, L.W., Richardson, J.S., and Richardson, D.C. (2010). MolProbity: all-atom structure validation for macromolecular crystallography. Acta Crystallogr D Biol Crystallogr *66*, 12-21.

Chen, Y., Wiesmann, C., Fuh, G., Li, B., Christinger, H.W., McKay, P., de Vos, A.M., and Lowman, H.B. (1999). Selection and analysis of an optimized anti-VEGF antibody: crystal structure of an affinity-matured Fab in complex with antigen. Journal of molecular biology *293*, 865-881.

Cho, H.S., Mason, K., Ramyar, K.X., Stanley, A.M., Gabelli, S.B., Denney, D.W., Jr., and Leahy, D.J. (2003). Structure of the extracellular region of HER2 alone and in complex with the Herceptin Fab. Nature *421*, 756-760.

Chodera, J.D., and Mobley, D.L. (2013). Entropy-enthalpy compensation: role and ramifications in biomolecular ligand recognition and design. Annu Rev Biophys *42*, 121-142.

Christinger, H.W., Muller, Y.A., Berleau, L.T., Keyt, B.A., Cunningham, B.C., Ferrara, N., and de Vos, A.M. (1996). Crystallization of the receptor binding domain of vascular endothelial growth factor. Proteins *26*, 353-357.

Corzo, J. (2006). Time, the forgotten dimension of ligand binding teaching. Biochem Mol Biol Educ *34*, 413-416.

Craik, D.J., Mylne, J.S., and Daly, N.L. (2010). Cyclotides: macrocyclic peptides with applications in drug design and agriculture. Cell Mol Life Sci *67*, 9-16.

Davis, J.H., Aperlo, C., Li, Y., Kurosawa, E., Lan, Y., Lo, K.M., and Huston, J.S. (2010). SEEDbodies: fusion proteins based on strand-exchange engineered domain (SEED) CH3 heterodimers in an Fc analogue platform for asymmetric binders or immunofusions and bispecific antibodies. Protein engineering, design & selection : PEDS *23*, 195-202.

de Picciotto, S., Dickson, P.M., Traxlmayr, M.W., Marques, B.S., Socher, E., Zhao, S., Cheung, S., Kiefer, J.D., Wand, A.J., Griffith, L.G., et al. (2016). Design Principles for SuCESsFul Biosensors: Specific Fluorophore/Analyte Binding and Minimization of Fluorophore/Scaffold Interactions. Journal of molecular biology *428*, 4228-4241.

Desmyter, A., Transue, T.R., Ghahroudi, M.A., Thi, M.H., Poortmans, F., Hamers, R., Muyldermans, S., and Wyns, L. (1996). Crystal structure of a camel single-domain VH antibody fragment in complex with lysozyme. Nat Struct Biol *3*, 803-811.

DiMaio, F., Echols, N., Headd, J.J., Terwilliger, T.C., Adams, P.D., and Baker, D. (2013). Improved low-resolution crystallographic refinement with Phenix and Rosetta. Nat Methods *10*, 1102-1104.

Durocher, Y., Perret, S., and Kamen, A. (2002). High-level and high-throughput recombinant protein production by transient transfection of suspension-growing human 293-EBNA1 cells. Nucleic Acids Res *30*, E9.

Edelman, G.M., Cunningham, B.A., Gall, W.E., Gottlieb, P.D., Rutishauser, U., and Waxdal, M.J. (1969). The covalent structure of an entire gammaG immunoglobulin molecule. Proc Natl Acad Sci U S A *63*, 78-85.

Edelman, G.M., and Poulik, M.D. (1961). Studies on structural units of the gamma-globulins. J Exp Med *113*, 861-884.

Emsley, P., Lohkamp, B., Scott, W.G., and Cowtan, K. (2010). Features and development of Coot. Acta Crystallogr D Biol Crystallogr *66*, 486-501.

Fersht, A. (1999). Structure and Mechanism in Protein Science: A Guide to Enzyme Catalysis and Protein Folding (W. H. Freeman).

Fu, H., Grimsley, G.R., Razvi, A., Scholtz, J.M., and Pace, C.N. (2009). Increasing protein stability by improving beta-turns. Proteins *77*, 491-498.

Gaboriaud, C., Juanhuix, J., Gruez, A., Lacroix, M., Darnault, C., Pignol, D., Verger, D., Fontecilla-Camps, J.C., and Arlaud, G.J. (2003). The crystal structure of the globular head of complement protein C1q provides a basis for its versatile recognition properties. J Biol Chem *278*, 46974-46982.

Garbett, N.C., and Chaires, J.B. (2012). Thermodynamic studies for drug design and screening. Expert Opin Drug Discov *7*, 299-314.

Gasteiger, E., Hoogland, C., Gattiker, A., Duvaud, S., Wilkins, M.R., Appel, R.D., and Bairoch, A., eds. (2005). Protein Identification and Analysis Tools on the ExPASy Server (Humana Press).

Gera, N., Hussain, M., Wright, R.C., and Rao, B.M. (2011). Highly stable binding proteins derived from the hyperthermophilic Sso7d scaffold. Journal of molecular biology *409*, 601-616.

Gille, H., Hulsmeyer, M., Trentmann, S., Matschiner, G., Christian, H.J., Meyer, T., Amirkhosravi, A., Audoly, L.P., Hohlbaum, A.M., and Skerra, A. (2016). Functional characterization of a VEGF-A-targeting Anticalin, prototype of a novel therapeutic human protein class. Angiogenesis *19*, 79-94.

Goebeler, M.E., Knop, S., Viardot, A., Kufer, P., Topp, M.S., Einsele, H., Noppeney, R., Hess, G., Kallert, S., Mackensen, A., et al. (2016). Bispecific T-Cell Engager (BiTE) Antibody Construct Blinatumomab for the Treatment of Patients With Relapsed/Refractory Non-Hodgkin Lymphoma: Final Results From a Phase I Study. J Clin Oncol *34*, 1104-1111.

Gunasekaran, K., Pentony, M., Shen, M., Garrett, L., Forte, C., Woodward, A., Ng, S.B., Born, T., Retter, M., Manchulenko, K., et al. (2010). Enhancing antibody Fc heterodimer formation through electrostatic steering effects: applications to bispecific molecules and monovalent IgG. J Biol Chem *285*, 19637-19646.

Halaby, D.M., Poupon, A., and Mornon, J. (1999). The immunoglobulin fold family: sequence analysis and 3D structure comparisons. Protein Eng *12*, 563-571.

Hardy, J.A., and Nelson, H.C. (2000). Proline in alpha-helical kink is required for folding kinetics but not for kinked structure, function, or stability of heat shock transcription factor. Protein Sci *9*, 2128-2141.

Harmsen, M.M., and De Haard, H.J. (2007). Properties, production, and applications of camelid single-domain antibody fragments. Appl Microbiol Biotechnol *77*, 13-22.

Harper, S.J., and Bates, D.O. (2008). VEGF-A splicing: the key to anti-angiogenic therapeutics? Nat Rev Cancer *8*, 880-887.

Harris, L.J., Larson, S.B., Hasel, K.W., and McPherson, A. (1997). Refined structure of an intact IgG2a monoclonal antibody. Biochemistry *36*, 1581-1597.

Harris, L.J., Skaletsky, E., and McPherson, A. (1995). Crystallization of intact monoclonal antibodies. Proteins *23*, 285-289.

Harris, R.J. (1995). Processing of C-terminal lysine and arginine residues of proteins isolated from mammalian cell culture. J Chromatogr A *705*, 129-134.

Hasenhindl, C., Traxlmayr, M.W., Wozniak-Knopp, G., Jones, P.C., Stadlmayr, G., Ruker, F., and Obinger, C. (2013). Stability assessment on a library scale: a rapid method for the evaluation of the commutability and insertion of residues in C-terminal loops of the CH3 domains of IgG1-Fc. Protein engineering, design & selection : PEDS *26*, 675-682.

Heiring, C., and Muller, Y.A. (2001). Folding screening assayed by proteolysis: application to various cystine deletion mutants of vascular endothelial growth factor. Protein Eng *14*, 183-188.

Heiss, M.M., Murawa, P., Koralewski, P., Kutarska, E., Kolesnik, O.O., Ivanchenko, V.V., Dudnichenko, A.S., Aleknaviciene, B., Razbadauskas, A., Gore, M., et al. (2010). The trifunctional antibody catumaxomab for the treatment of malignant ascites due to epithelial cancer: Results of a prospective randomized phase II/III trial. Int J Cancer *127*, 2209-2221.

Herrington-Symes, A.P., Farys, M., Khalili, H., and Brocchini, S. (2013). Antibody fragments: Prolonging circulation half-life special issue-antibody research. Advances in Bioscience and Biotechnology *4*, 689-698.

Holliger, P., and Hudson, P.J. (2005). Engineered antibody fragments and the rise of single domains. Nat Biotechnol *23*, 1126-1136.

Holliger, P., Prospero, T., and Winter, G. (1993). "Diabodies": small bivalent and bispecific antibody fragments. Proc Natl Acad Sci U S A *90*, 6444-6448.

Jafari, R., Zolbanin, N.M., Rafatpanah, H., Majidi, J., and Kazemi, T. (2017). Fc-fusion proteins in therapy: an updated view. Curr Med Chem.

James, L.C., Keeble, A.H., Khan, Z., Rhodes, D.A., and Trowsdale, J. (2007). Structural basis for PRYSPRY-mediated tripartite motif (TRIM) protein function. Proc Natl Acad Sci U S A *104*, 6200-6205.

Jefferis, R., Lund, J., and Pound, J. (1990). Molecular definition of interaction sites on human IgG for Fc receptors (huFc gamma R). Mol Immunol *27*, 1237-1240.

Jez, J., Antes, B., Castilho, A., Kainer, M., Wiederkum, S., Grass, J., Ruker, F., Woisetschlager, M., and Steinkellner, H. (2012). Significant impact of single N-glycan residues on the biological activity of Fc-based antibody-like fragments. J Biol Chem *287*, 24313-24319.

Joosten, R.P., Joosten, K., Murshudov, G.N., and Perrakis, A. (2012). PDB_REDO: constructive validation, more than just looking for errors. Acta Crystallogr D Biol Crystallogr *68*, 484-496.

Joosten, R.P., Long, F., Murshudov, G.N., and Perrakis, A. (2014). The PDB_REDO server for macromolecular structure model optimization. IUCrJ *1*, 213-220.

Jost, C., Schilling, J., Tamaskovic, R., Schwill, M., Honegger, A., and Pluckthun, A. (2013). Structural basis for eliciting a cytotoxic effect in HER2-overexpressing cancer cells via binding to the extracellular domain of HER2. Structure *21*, 1979-1991.

Kabsch, W. (2010). Xds. Acta Crystallogr D Biol Crystallogr *66*, 125-132.
Karplus, P.A., and Diederichs, K. (2012). Linking crystallographic model and data quality. Science *336*, 1030-1033.

Kipriyanov, S.M., Moldenhauer, G., Schuhmacher, J., Cochlovius, B., Von der Lieth, C.W., Matys, E.R., and Little, M. (1999). Bispecific tandem diabody for tumor therapy with improved antigen binding and pharmacokinetics. Journal of molecular biology *293*, 41-56.

Kiyoshi, M., Caaveiro, J.M., Kawai, T., Tashiro, S., Ide, T., Asaoka, Y., Hatayama, K., and Tsumoto, K. (2015). Structural basis for binding of human IgG1 to its high-affinity human receptor FcgammaRI. Nat Commun *6*, 6866.

Kontermann, R.E. (2009). Strategies to extend plasma half-lives of recombinant antibodies. BioDrugs *23*, 93-109.

Kontermann, R.E., and Brinkmann, U. (2015). Bispecific antibodies. Drug Discov Today *20*, 838-847.

Kubota, T., Niwa, R., Satoh, M., Akinaga, S., Shitara, K., and Hanai, N. (2009). Engineered therapeutic antibodies with improved effector functions. Cancer Sci *100*, 1566-1572.

Labrijn, A.F., Aalberse, R.C., and Schuurman, J. (2008). When binding is enough: nonactivating antibody formats. Curr Opin Immunol *20*, 479-485.

Layer, P., and Stanghellini, V. (2014). Review article: Linaclotide for the management of irritable bowel syndrome with constipation. Aliment Pharmacol Ther *39*, 371-384.

Leavy, O. (2010). Therapeutic antibodies: past, present and future. Nat Rev Immunol *10*, 297.

Leung, K.M., Batey, S., Rowlands, R., Isaac, S.J., Jones, P., Drewett, V., Carvalho, J., Gaspar, M., Weller, S., Medcalf, M., et al. (2015). A HER2-specific Modified Fc Fragment (Fcab) Induces Antitumor Effects Through Degradation of HER2 and Apoptosis. Mol Ther *23*, 1722-1733.

Levin, D., Golding, B., Strome, S.E., and Sauna, Z.E. (2015). Fc fusion as a platform technology: potential for modulating immunogenicity. Trends Biotechnol *33*, 27-34.

Lewis, S.M., Wu, X., Pustilnik, A., Sereno, A., Huang, F., Rick, H.L., Guntas, G., Leaver-Fay, A., Smith, E.M., Ho, C., et al. (2014). Generation of bispecific IgG antibodies by structure-based design of an orthogonal Fab interface. Nat Biotechnol *32*, 191-198.

Lindhofer, H., Mocikat, R., Steipe, B., and Thierfelder, S. (1995). Preferential species-restricted heavy/light chain pairing in rat/mouse quadromas. Implications for a single-step purification of bispecific antibodies. J Immunol *155*, 219-225.

Lobner, E., Humm, A.S., Goritzer, K., Mlynek, G., Puchinger, M.G., Hasenhindl, C., Ruker, F., Traxlmayr, M.W., Djinovic-Carugo, K., and Obinger, C. (2017). Fcab-HER2 Interaction: a Menage a Trois. Lessons from X-Ray and Solution Studies. Structure *25*, 878-889 e875.

Lobner, E., Traxlmayr, M.W., Obinger, C., and Hasenhindl, C. (2016). Engineered IgG1-Fc-one fragment to bind them all. Immunol Rev *270*, 113-131.

Long, F., Vagin, A.A., Young, P., and Murshudov, G.N. (2008). BALBES: a molecular-replacement pipeline. Acta Crystallogr D Biol Crystallogr *64*, 125-132.

Lutteke, T., and von der Lieth, C.W. (2004). pdb-care (PDB carbohydrate residue check): a program to support annotation of complex carbohydrate structures in PDB files. BMC Bioinformatics *5*, 69.

Madireddi, M., Malone, H., Kukral, D., Chimalakonda, A., Kozhich, A., Xiling, Y., Swain, J., Yamniuk, A., and Ahlijanian, M. (2016). BMS-986089 is a high affinity anti-myostatin adnectin that increases muscle volume in three preclinical species. Neuromuscular Disorders *26*, S94-S95.

Mallbris, L., Davies, J., Glasebrook, A., Tang, Y., Glaesner, W., and Nickoloff, B.J. (2016). Molecular Insights into Fully Human and Humanized Monoclonal Antibodies: What are the Differences and Should Dermatologists Care? J Clin Aesthet Dermatol *9*, 13-15.

Markovic-Mueller, S., Stuttfeld, E., Asthana, M., Weinert, T., Bliven, S., Goldie, K.N., Kisko, K., Capitani, G., and Ballmer-Hofer, K. (2017). Structure of the Full-length VEGFR-1 Extracellular Domain in Complex with VEGF-A. Structure *25*, 341-352.

Martens, T., Schmidt, N.O., Eckerich, C., Fillbrandt, R., Merchant, M., Schwall, R., Westphal, M., and Lamszus, K. (2006). A novel one-armed anti-c-Met antibody inhibits glioblastoma growth in vivo. Clin Cancer Res *12*, 6144-6152.

Martin, W.L., West, A.P., Jr., Gan, L., and Bjorkman, P.J. (2001). Crystal structure at 2.8 A of an FcRn/heterodimeric Fc complex: mechanism of pH-dependent binding. Mol Cell *7*, 867-877.

McCoy, A.J., Grosse-Kunstleve, R.W., Adams, P.D., Winn, M.D., Storoni, L.C., and Read, R.J. (2007). Phaser crystallographic software. J Appl Crystallogr *40*, 658-674.

Miller, E.A., Traxlmayr, M.W., Shen, J., and Sikes, H.D. (2016). Activity-based assessment of an engineered hyperthermophilic protein as a capture agent in paper-based diagnostic tests. Mol Syst Des Eng *1*, 377-381.

Moore, P.A., Zhang, W., Rainey, G.J., Burke, S., Li, H., Huang, L., Gorlatov, S., Veri, M.C., Aggarwal, S., Yang, Y., et al. (2011). Application of dual affinity retargeting molecules to achieve optimal redirected T-cell killing of B-cell lymphoma. Blood *117*, 4542-4551.

Muller, Y.A., Chen, Y., Christinger, H.W., Li, B., Cunningham, B.C., Lowman, H.B., and de Vos, A.M. (1998). VEGF and the Fab fragment of a humanized neutralizing antibody: crystal structure of the complex at 2.4 A resolution and mutational analysis of the interface. Structure *6*, 1153-1167.

Muller, Y.A., Heiring, C., Misselwitz, R., Welfle, K., and Welfle, H. (2002). The cystine knot promotes folding and not thermodynamic stability in vascular endothelial growth factor. J Biol Chem *277*, 43410-43416.

Muller, Y.A., Li, B., Christinger, H.W., Wells, J.A., Cunningham, B.C., and de Vos, A.M. (1997). Vascular endothelial growth factor: crystal structure and functional mapping of the kinase domain receptor binding site. Proc Natl Acad Sci U S A *94*, 7192-7197.

Murshudov, G.N., Vagin, A.A., and Dodson, E.J. (1997). Refinement of macromolecular structures by the maximum-likelihood method. Acta Crystallogr D Biol Crystallogr *53*, 240-255.

Nelson, A.L. (2010). Antibody fragments: hope and hype. MAbs *2*, 77-83.

Nygren, P.A. (2008). Alternative binding proteins: affibody binding proteins developed from a small three-helix bundle scaffold. FEBS J *275*, 2668-2676.

Piovesan, D., Minervini, G., and Tosatto, S.C. (2016). The RING 2.0 web server for high quality residue interaction networks. Nucleic Acids Res *44*, W367-374.

Plomp, R., Dekkers, G., Rombouts, Y., Visser, R., Koeleman, C.A., Kammeijer, G.S., Jansen, B.C., Rispens, T., Hensbergen, P.J., Vidarsson, G., et al. (2015). Hinge-Region O-Glycosylation of Human Immunoglobulin G3 (IgG3). Mol Cell Proteomics *14*, 1373-1384.

Pluckthun, A. (2015). Designed ankyrin repeat proteins (DARPins): binding proteins for research, diagnostics, and therapy. Annu Rev Pharmacol Toxicol *55*, 489-511.

Porter, R.R. (1959). The hydrolysis of rabbit y-globulin and antibodies with crystalline papain. Biochem J *73*, 119-126.

Ranganath, S., Bhandari, A., Avitahl-Curtis, N., McMahon, J., Wachtel, D., Zhang, J., Leitheiser, C., Bernier, S.G., Liu, G., Tran, T.T., et al. (2015). Discovery and Characterization of a Potent Interleukin-6 Binding Peptide with Neutralizing Activity In Vivo. PLoS One *10*, e0141330.

Rath, T., Baker, K., Dumont, J.A., Peters, R.T., Jiang, H., Qiao, S.W., Lencer, W.I., Pierce, G.F., and Blumberg, R.S. (2015). Fc-fusion proteins and FcRn: structural insights for longer-lasting and more effective therapeutics. Crit Rev Biotechnol *35*, 235-254.

Ribatti, D. (2015). Edelman's view on the discovery of antibodies. Immunol Lett *164*, 72-75.
Ridgway, J.B., Presta, L.G., and Carter, P. (1996). 'Knobs-into-holes' engineering of antibody CH3 domains for heavy chain heterodimerization. Protein Eng *9*, 617-621.

Saphire, E.O., Parren, P.W., Pantophlet, R., Zwick, M.B., Morris, G.M., Rudd, P.M., Dwek, R.A., Stanfield, R.L., Burton, D.R., and Wilson, I.A. (2001). Crystal structure of a neutralizing human IGG against HIV-1: a template for vaccine design. Science *293*, 1155-1159.

Sarma, V.R., Silverton, E.W., Davies, D.R., and Terry, W.D. (1971). The three-dimensional structure at 6 A resolution of a human gamma Gl immunoglobulin molecule. J Biol Chem *246*, 3753-3759.

Schaefer, W., Regula, J.T., Bahner, M., Schanzer, J., Croasdale, R., Durr, H., Gassner, C., Georges, G., Kettenberger, H., Imhof-Jung, S., et al. (2011). Immunoglobulin domain crossover as a generic approach for the production of bispecific IgG antibodies. Proc Natl Acad Sci U S A *108*, 11187-11192.

Schneider, L., Lumry, W., Vegh, A., Williams, A.H., and Schmalbach, T. (2007). Critical role of kallikrein in hereditary angioedema pathogenesis: a clinical trial of ecallantide, a novel kallikrein inhibitor. J Allergy Clin Immunol *120*, 416-422.

Schneider, S., and Zacharias, M. (2012). Atomic resolution model of the antibody Fc interaction with the complement C1q component. Mol Immunol *51*, 66-72.

Shusta, E.V., Holler, P.D., Kieke, M.C., Kranz, D.M., and Wittrup, K.D. (2000). Directed evolution of a stable scaffold for T-cell receptor engineering. Nat Biotechnol *18*, 754-759.

Silacci, M., Lembke, W., Woods, R., Attinger-Toller, I., Baenziger-Tobler, N., Batey, S., Santimaria, R., von der Bey, U., Koenig-Friedrich, S., Zha, W., et al. (2016). Discovery and characterization of COVA322, a clinical-stage bispecific TNF/IL-17A inhibitor for the treatment of inflammatory diseases. MAbs *8*, 141-149.

Silverman, J., Liu, Q., Bakker, A., To, W., Duguay, A., Alba, B.M., Smith, R., Rivas, A., Li, P., Le, H., et al. (2005). Multivalent avimer proteins evolved by exon shuffling of a family of human receptor domains. Nat Biotechnol *23*, 1556-1561.

Silverton, E.W., Navia, M.A., and Davies, D.R. (1977). Three-dimensional structure of an intact human immunoglobulin. Proc Natl Acad Sci U S A *74*, 5140-5144.

Simeon, R., and Chen, Z. (2017). In vitro-engineered non-antibody protein therapeutics. Protein Cell.
Skerra, A. (2008). Alternative binding proteins: anticalins - harnessing the structural plasticity of the lipocalin ligand pocket to engineer novel binding activities. FEBS J *275*, 2677-2683.

Skrlec, K., Strukelj, B., and Berlec, A. (2015). Non-immunoglobulin scaffolds: a focus on their targets. Trends Biotechnol *33*, 408-418.

Sorensen, J., Velikyan, I., Sandberg, D., Wennborg, A., Feldwisch, J., Tolmachev, V., Orlova, A., Sandstrom, M., Lubberink, M., Olofsson, H., et al. (2016). Measuring HER2-Receptor Expression In Metastatic Breast Cancer Using [68Ga]ABY-025 Affibody PET/CT. Theranostics *6*, 262-271.

Spangler, J.B., Manzari, M.T., Rosalia, E.K., Chen, T.F., and Wittrup, K.D. (2012). Triepitopic antibody fusions inhibit cetuximab-resistant BRAF and KRAS mutant tumors via EGFR signal repression. Journal of molecular biology *422*, 532-544.

Spreter Von Kreudenstein, T., Escobar-Carbrera, E., Lario, P.I., D'Angelo, I., Brault, K., Kelly, J., Durocher, Y., Baardsnes, J., Woods, R.J., Xie, M.H., et al. (2013). Improving biophysical properties of a bispecific antibody scaffold to aid developability: quality by molecular design. MAbs *5*, 646-654.

Teplyakov, A., Zhao, Y., Malia, T.J., Obmolova, G., and Gilliland, G.L. (2013). IgG2 Fc structure and the dynamic features of the IgG CH2-CH3 interface. Mol Immunol *56*, 131-139.

Terwilliger, T.C., Grosse-Kunstleve, R.W., Afonine, P.V., Moriarty, N.W., Zwart, P.H., Hung, L.W., Read, R.J., and Adams, P.D. (2008). Iterative model building, structure refinement and density modification with the PHENIX AutoBuild wizard. Acta Crystallogr D Biol Crystallogr *64*, 61-69.

Thell, K., Hellinger, R., Sahin, E., Michenthaler, P., Gold-Binder, M., Haider, T., Kuttke, M., Liutkevičiūtė, Z., Göransson, U., Gründemann, C., et al. (2016). Oral activity of a nature-derived cyclic peptide for the treatment of multiple sclerosis. Proceedings of the National Academy of Sciences *113*, 3960-3965.

Todorovska, A., Roovers, R.C., Dolezal, O., Kortt, A.A., Hoogenboom, H.R., and Hudson, P.J. (2001). Design and application of diabodies, triabodies and tetrabodies for cancer targeting. J Immunol Methods *248*, 47-66.

Traxlmayr, M.W., Faissner, M., Stadlmayr, G., Hasenhindl, C., Antes, B., Ruker, F., and Obinger, C. (2012). Directed evolution of stabilized IgG1-Fc scaffolds by application of strong heat shock to libraries displayed on yeast. Biochimica Et Biophysica Acta-Proteins and Proteomics *1824*, 542-549.

Traxlmayr, M.W., Kiefer, J.D., Srinivas, R.R., Lobner, E., Tisdale, A.W., Mehta, N.K., Yang, N.J., Tidor, B., and Wittrup, K.D. (2016). Strong Enrichment of Aromatic Residues in Binding Sites from a Charge-neutralized Hyperthermostable Sso7d Scaffold Library. J Biol Chem *291*, 22496-22508.

Traxlmayr, M.W., Lobner, E., Antes, B., Kainer, M., Wiederkum, S., Hasenhindl, C., Stadlmayr, G., Ruker, F., Woisetschlager, M., Moulder, K., et al. (2013). Directed evolution of Her2/neu-binding IgG1-Fc for improved stability and resistance to aggregation by using yeast surface display. Protein Engineering Design & Selection *26*, 255-265.

Traxlmayr, M.W., Lobner, E., Hasenhindl, C., Stadlmayr, G., Oostenbrink, C., Ruker, F., and Obinger, C. (2014). Construction of pH-sensitive Her2-binding IgG1-Fc by directed evolution. Biotechnol J *9*, 1013-1022.

Traxlmayr, M.W., and Obinger, C. (2012). Directed evolution of proteins for increased stability and expression using yeast display. Arch Biochem Biophys *526*, 174-180.

van den Bremer, E.T., Beurskens, F.J., Voorhorst, M., Engelberts, P.J., de Jong, R.N., van der Boom, B.G., Cook, E.M., Lindorfer, M.A., Taylor, R.P., van Berkel, P.H., et al. (2015). Human IgG is produced in a pro-form that requires clipping of C-terminal lysines for maximal complement activation. MAbs *7*, 672-680.

Weidle, U.H., Auer, J., Brinkmann, U., Georges, G., and Tiefenthaler, G. (2013). The emerging role of new protein scaffold-based agents for treatment of cancer. Cancer Genomics Proteomics *10*, 155-168.

Woisetschlager, M., Antes, B., Borrowdale, R., Wiederkum, S., Kainer, M., Steinkellner, H., Wozniak-Knopp, G., Moulder, K., Ruker, F., and Mudde, G.C. (2014). In vivo and in vitro activity of an immunoglobulin Fc fragment (Fcab) with engineered Her-2/neu binding sites. Biotechnol J *9*, 844-851.

Worn, A., and Pluckthun, A. (2001). Stability engineering of antibody single-chain Fv fragments. Journal of molecular biology *305*, 989-1010.

Wozniak-Knopp, G., Bartl, S., Bauer, A., Mostageer, M., Woisetschlager, M., Antes, B., Ettl, K., Kainer, M., Weberhofer, G., Wiederkum, S., et al. (2010). Introducing antigen-binding sites in structural loops of immunoglobulin constant domains: Fc fragments with engineered HER2/neu-binding sites and antibody properties. Protein engineering, design & selection : PEDS *23*, 289-297.

6 APPENDIX

Curriculum Vitae

Elisabeth Lobner

✉ elisabeth.lobner@boku.ac.at

BOKU – University of Natural Resources and Life Sciences, Vienna, Austria
Department of Chemistry – Division of Protein Biochemistry
CD Laboratory for Antibody Engineering
Muthgasse 18
1190 Vienna, Austria

Education

2013 – present **PhD**

University of Natural Resources and Life Sciences, Vienna, Austria

PhD program "BioToP– Biomolecular Technology of Proteins"
Doctoral thesis conducted at the CD Laboratory for Antibody Engineering, Department of Chemistry

2010 – 2013 **MSc**

University of Natural Resources and Life Sciences, Vienna, Austria

Master's degree in Biotechnology

2004 – 2010 **BSc**

University of Natural Resources and Life Sciences, Vienna, Austria

Bachelor's degree in Food- and Biotechnology

SCI-Publications

2017 **Lobner E.**, Humm A., Göritzer K., Mylnek G., Puchinger M.G., Hasenhindl C., Rüker F., Traxlmayr M.W., Djinović-Carugo K. & Obinger C. (2017) Fcab-HER2 interaction: A ménage à trois. Lessons from X-ray and solution studies. *Structure* 25(6), 878-889 e875

2016 Traxlmayr M.W., Kiefer J.D., Srinivas R.R., **Lobner E.**, Tisdale A.W., Mehta N.K., Yang N.J., Tidor B. & Wittrup K.D. (2016) Strong Enrichment of Aromatic Residues in Binding Sites from a Charge-neutralized Hyperthermostable Sso7d Scaffold Library. *J. Biol. Chem.* 291(43), 22496-22508

2016 **Lobner E.**, Traxlmayr M.W., Obinger C. & Hasenhindl C. (2016) Engineered IgG1-Fc - one fragment to bind them all. *Immunol. Rev.* 270(1), 113-131

2014 Traxlmayr M.W., **Lobner E.**, Hasenhindl C., Stadlmayr G., Oostenbrink C., Rüker F. & Obinger C. (2014) Construction of pH-sensitive Her2-binding IgG1-Fc by directed evolution. *Biotechnol. J.* 9(8), 1013-1022

2013 Traxlmayr M.W., **Lobner E.**, Antes B., Kainer M., Wiederkum S., Hasenhindl C., Stadlmayr G., Rüker F., Woisetschläger M., Moulder K. & Obinger C. (2013) Directed evolution of Her2/neu-binding IgG1-Fc for improved stability and resistance to aggregation by using yeast surface display. *Protein. Eng. Des. Sel.* 26(4), 255-265

Reseach Experience

Apr 2013 - present **PhD student**

University of Natural Resources and Life Sciences, Vienna, Austria
Department of Chemistry
CD Laboratory for Antibody Engineering in collaboration with F-star

Doctoral thesis title: "Structural and functional investigation of Fcab-antigen interaction"
Supervisor: Univ.Prof. Dr. Christian Obinger

Nov 2015 **PhD student**

Oak Ridge National Laboratory, Oak Ridge, USA

Spallation Neutron Source: Crystallography and neutron diffraction experiments

May 2011 – Dec 2011 **Master student**

University of Natural Resources and Life Sciences, Vienna, Austria
Department of Chemistry
CD Laboratory for Antibody Engineering in collaboration with F-star

Master thesis title: "Characterization of stabilized variants of a HER2-binding Fcab"
Supervisor: Univ.Prof. Dr. Christian Obinger

Oct 2007 – Dec 2007 **Bachelor student**

University of Technology, Vienna, Austria
Institute of Chemical Engineering

Bachelor thesis title: "The influence of biosynthesis of flavonoids on the defence reaction of apples against the germ of fire blight-*Erwinia amylovora*"
Supervisor: Ao.Univ.Prof. Dr. Karl Stich

Other Relevant Work Experience

Sep 2013 – present **Lecturer**

University of Natural Resources and Life Sciences, Vienna, Austria
Department of Chemistry

Organization and supervision of chemical and biochemical practical courses in both Bachelor and Master's programmes

Jan 2012 – Jul 2012 **Part Time Technician**

University of Natural Resources and Life Sciences, Vienna, Austria
Department of Chemistry
CD Laboratory for Antibody Engineering in collaboration with F-star

Nov 2008 – Feb 2011 **Part Time Technician**

Mondi Neusiedler GmbH, Hausmening, Austria
Division of Innovation and Product Development

Spallation Neutron Source: Crystallography and neutron diffraction experiments

Aug 2010– Sep 2010 **Internship**

Manipal University, Manipal, India
Department of Biotechnology

Isolation and Identification of bioactive compounds from *Catharanthus roseus*

Awards

2016 **Best Poster Presentation Award**

12th Protein Engineering Summit, Boston, USA

2014 **Best Poster Presentation Award**

The 16th European Congress on Biotechnology, Edinburgh, Scotland

Poster Presentations

2016 **Lobner E.**, Humm A., Mlynek G., Hasenhindl C., Kubinger K., Kitzmüller M., Rüker F., Traxlmayr M. W., Djinovic-Carugo K. & Obinger C. Complex between VEGF and heterodimeric Fcab: X-ray structure and thermodynamics of binding.

8th Protein & Antibody Engineering Summit, Lisbon, Portugal

2016 **Lobner E.**, Humm A., Goeritzer K., Mlynek G., Hasenhindl C., Traxlmayr M. W., Djinovic-Carugo K. & Obinger C. Structural characterization of HER2-binding Fcabs.

12th Protein Engineering Summit, Boston, USA

2015 **Lobner E.**, Humm A., Goeritzer K., Hasenhindl C., Djinovic-Carugo K. & Obinger C. (2015) Recombinant production and structural characterization of Fcabs.

8th Conference on Recombinant Protein Production, Palma de Mallorca, Spain

2014 **Lobner E.**, Traxlmayr M.W., Hasenhindl C., Stadlmayr G., Oostenbrink C., Rüker F. & Obinger C. Construction of pH-sensitive Her2 binding antibody fragment by directed evolution using yeast display.

The 16th European Congress on Biotechnology, Edinburgh, Scotland

2013 **Lobner E.**, Traxlmayr M.W., Hasenhindl C., Antes B., Kainer M., Wiederkum S., Stadlmayr G., Woisetschläger M., Moulder K., Rüker F. & Obinger C. Directed evolution of antibody fragments for improved stability and resistance to aggregation by using yeast surface display.

The 18th Human Antibody & Hybridoma Conference, Vienna, Austria

Miscellanous

Academic Service

Curriculum Committee

PhD program "BioToP- Biomolecular Technology of Proteins" University of Natural Resources and Life Sciences, Vienna, Austria

Member

Austrian Association of Molecular Life Sciences and Biotechnology (ÖGMBT)

Languages

German
Native language

English
Fluent in both written and spoken

French
Basic understanding